DRY DEPOSITION ONTO AERODYNAMIC SURFACES AND VEGETATION

Final Report

submitted to the California Air Resources Board

Contract A6-186-32

17 February 1989

Yee-Lin Wu and Cliff Davidson

Department of Civil Engineering
Carnegie Mellon University
Pittsburgh, PA 15213

Abstract

Aerodynamic surrogate surfaces employing Teflon plates and nylasorb filter paper have been used to measure dry deposition in three sets of field experiments. The first set involves sampling in Claremont during the Southern California Air Quality Study (SCAQS) in June and July 1988. Sampling was conducted at two locations : the Bernard Biological Station and Claremont McKenna College. The second set involves sampling at the same location during an extension of SCAQS in August and September 1988. Finally, the third set includes sampling at Emerald Lake in Sequoia National Park. Three species of vegetation (Waxleaf Privet, Canary Island Pine, and Japanese Privet) have also been used to assess dry deposition during the first set of field experiments.

For the first field program, measurable dry deposition fluxes have been obtained for nitrate, sulfate, lead, and calcium. The Teflon plates are shown to yield satisfactory results for sampling periods as short as four hours. The vegetation sampling is shown to yield satisfactory results for periods as short as four days, although it is likely that good results can be obtained for even shorter periods such as 1 - 2 days.

The fluxes of all four contaminants on the Teflon plates are highly variable. Values in ng/sec m^2 cover the following ranges: nitrate 7 - 213, sulfate 2 - 64, lead 0.035 - 0.46, and calcium 1.2 - 20.7. Results for the Teflon plates and vegetation are roughly comparable. In general, deposition on the Canary Island Pine shows the greatest values, exceeding those on the Teflon plates and nylasorb filter paper by factors of 2 - 3. Fluxes onto the Japanese Privet are only slightly lower than those onto Canary Island Pine, while fluxes onto the Waxleaf Privet are nearly the same as those on the Teflon plates and filter paper.

One of the findings of this study is the effect of exposure time on the observed deposition fluxes. Generally, short-term exposures yield greater deposition fluxes for both deposition to the Teflon plates and to vegetation. Resuspension of deposited particles is probably responsible for this phenomenon. Based on the assumed mechanism of resuspension of deposited particles, it is found that the resuspension rates of all four species from any surface are on the order of 10^{-6} sec^{-1}.

Only limited data are available from the second and third sets of field experiments. The results are generally consistent with the June - July SCAQS data, although nitrate fluxes are considerably smaller at Emerald Lake compared with Claremont. Sulfate fluxes at Emerald Lake are only slightly smaller than in Claremont.

ACKNOWLEDGMENTS

We would like to thank the staff of California Air Resources Board Laboratory at El Monte, especially Rose Papa, for assistance with use of the Ion Chromatograph there. We also want to thank Karen Mosher for her assistance with field work at the Bernard Biological Station. Thanks go also to Freeman Allen for his help in providing laboratory facilities at the Pomona College Chemistry Department, and to Samantha Alper for collecting samples during August and September in Claremont.

For the study at Emerald Lake, we wish to thank Jeff Harrington of Carnegie Mellon University and Paul Linaweaver of the Air Resources Board for their help in collecting samples.

Finally, the guidance offered by Lowell Ashbaugh and Kathy Tonnessen of the Air Resources Board throughout this study is greatly appreciated.

Disclaimer

The statements and conclusions in this report are those of the contractor and not necessarily those of the California Air Resources Board. The mention of commercial products, their source or their use in connection with material reported herein is not to be construed as either an actual or implied endorsement of such products.

Table of Contents

List of Figures

List of Tables

Summary and Conclusions

A passive aerodynamic surrogate surface for measuring dry deposition of airborne contaminants has been developed. The device is designed as a low-speed airfoil, symmetric with respect to a vertical axis through the center so that its characteristics are independent of wind direction. A deposition plate is positioned at the top of the airfoil. The leading edge is such that flow separation will not occur over the plate over a range of windspeeds (up to 15 m/sec) and angles of attack ($\pm 10^{o}$ relative to horizontal). The device offers the following advantages:

- The boundary layer characteristics are known, allowing studies of dry deposition mechanisms.
- Because a laminar boundary layer exists over the surface, particle deposition measured with the device is a reasonable lower limit to deposition on rough natural surfaces.
- When used with inert material (e.g. a Teflon plate), the unit can assess deposition of particulate species. When used with reactive material, the unit can assess deposition of reactive gases (e.g. nylon for nitric acid vapor, potassium carbonate-impregnated filter for sulfur dioxide).
- For chemical species associated with particles of a wide range of sizes, the device may be particularly useful in identifying mass deposition dominated by a small fraction of the largest particles.
- The device is inexpensive and easy to use for routine dry deposition monitoring. Trends in deposition onto the device are likely to be similar to trends in deposition on natural vegetation and other surfaces where measurement is more difficult.

Experimental Methods

A. Aerodynamic Surface

The aerodynamic surface is composed of a Teflon-coated solid aluminum airfoil and a deposition plate. The deposition plate, which can have any kind of surface characteristics, was put on the top of the airfoil. Teflon-coated aluminum plates and nylon filter papers were used as deposition surfaces in this study. After each exposure, the surface was removed from the airfoil and immediately washed using a TFE Teflon digestion vessel with 8 ml of distilled/deionized water. The vessel containing the plate was then shaken for three minutes to extract the pollutants, and the solution was poured into a polyethylene tube.

B. Vegetation

The plants that we used were Ligustrum japonicum texanum (Waxleaf Privet), Pinus canariensis (Canary Island Pine) and Ligustrum japonicum (Japanese Privet). The plants were placed at about the same height as the aerodynamic surfaces. Before the plants were put on-site, they were washed with distilled/deionized water. After being exposed for periods which ranged from 4 to 16 days, the leaves were harvested from the plants, put into 50 ml of distilled/deionized water and shaken for three minutes [Lindberg et al., 1984; John et al., 1985]. Because of the variation and complexity of dry deposition to vegetation, 2 to 4 samples consisting of ten leaves each with the same exposure time were collected

simultaneously from the same plant or different plants.

Both aerodynamic surface and foliar extraction samples were refrigerated until they were analyzed. Analyses were conducted by ion chromatography for sulfate and nitrate and by flameless atomic absorption spectrophotometry for lead and calcium.

Results and Discussion

The results of the field measurement data are summarized as:

A. Aerodynamic Surface

1. There is good agreement between conjugate samples: the difference in flux associated with co-located samplers is generally less than 20%. The difference between conjugate sample values is inversely proportional to the amount of pollutant collected. Nitrate, with the greatest fluxes, has the best agreement. The fluxes of lead, which are smallest, differ most. These differences are caused by natural variation, sampling artifacts and limitations of instruments used for analyses.

2. There is substantial variation in deposition rate from time to time. For each sampling experiment, the two deposition fluxes (i.e., pair of conjugate values) have been averaged to provide a single flux for that time period. The fluxes are shown in Table S.1 for the various species analyzed. The differences in fluxes among the various species are caused by variations in airborne concentration and in deposition velocity.

3. There is a strong diurnal variation in the deposition rate. Such variations are shown in all of the plots with greatest fluxes during the daytime hours. This may be due to both greater airborne concentrations and higher deposition velocities during the day.

4. There is a marked effect of exposure time on deposition rate. Comparing the 4 to 6-hour exposures with 24-hour exposures, it is found that the short-term fluxes generally yield higher deposition fluxes. Comparing 12-hour exposures with 2-day and 4-day exposures, we obtain the same results; the short-term exposures generally yield higher deposition fluxes.

B. Vegetation

1. Differences in fluxes measured with different sets of leaves exposed simultaneously average about 31%. These differences are caused by different orientations and shapes of leaves or needles, by the complex airflow patterns around the vegetation, and by sampling and analytical problems.

2. Substantial variation in deposition rate is observed from experiment to experiment and among the different plant species. Table S.1 shows ranges of deposition fluxes to the vegetation. In general, the fluxes to Canary Island Pine exceed those to the Privet by factors averaging 3.0 for nitrate, 2.3 for sulfate, 1.3 for lead, and 2.0 for calcium.

3. Short-term exposures generally yield greater deposition fluxes than longer exposures, as with the

	0.5 day	1 day	1.5 days	2 days	4 days
nitrate	56.8±29.1	40.6±17.0	53.7±9.4	41.7±14.6	24.0±5.1
sulfate	11.7±5.6	12.3±4.8	9.9±2.8	12.9±1.7	7.7±2.2
lead	0.072±0.043	0.112±0.041	0.070±0.027	0.082±0.026	0.079±0.026
calcium	5.4±2.5	5.7±1.6	7.2±1.5	9.0±2.2	6.5±2.9

A. Teflon plate

	4 days	8 days	12 days	16 days
nitrate	49.8±14.7	33.6±13.8	30.8±24.9	26.8±20.8
sulfate	11.0±3.5	7.7±3.8	7.2±3.9	5.0±3.7
lead	0.145±0.056	0.072±0.021	0.081±0.014	0.022
calcium	12.3±1.6	6.5±1.4	3.9	5.1

B. Waxleaf Privet

	4 days	8 days	12 days	16 days
nitrate	111.8±43.9	109.4±57.3	85.3±15.9	145.3
sulfate	23.1±8.7	11.4±13.9	11.2±1.5	22.1
lead	0.180±0.083	0.104±0.004	0.063±0.006	0.084
calcium	24.9±2.4	10.1±0.3	10.8±4.0	7.2

C. Canary Island Pine

	4 days	8 days	12 days	16 days
nitrate	51.5±36.2	43.2±1.2	31.3	38.7
sulfate	21.3±11.5	29.5±16.5	11.1	7.5
lead	0.227±0.144	0.068±0.036	0.064	0.036
calcium	18.4±6.8	12.3±0.2	7.9	9.2

D. Japanese Privet

Table S.1 Summary of deposition fluxes to surfaces used in this study. All values are expressed in units of ng/sec m^2

Teflon plates.

The greater fluxes for short-term exposures are also found in the study by John et al. [1986] for deposition to surrogate surfaces and vegetation. There are at least two possible processes responsible for this phenomenon in both the present study and that of John et al. : interactions between gaseous species and previously deposited particles, and resuspension of deposited particles. Thermodynamic equilibrium among ammonia, nitric acid and atmospheric aerosols is believed to be reached in the ambient environment [Hildemann et al.,1984; Stelson et al.,1984]. Unless a large fraction of the deposited particles is not from the atmosphere, such as local soil resuspension, the gas-particle interaction should not be significant. From the results for calcium, which is always in the form of solid particles in the ambient environment, it is likely that gas-solid interactions are not an important factor. Therefore, we assume that resuspension of deposited particles is the mechanism that causes the greater fluxes for short-term exposures

The parameters in a model for particle resuspension are obtained by fitting the observed data with an exponential curve. Results are shown in Table S.2. All the resuspension rates except for nitrate to Canary Island Pine are on the order of 10^{-6} sec^{-1}.

The Teflon plate results in this study suggest that the resuspension rate increases as particle size increases. This is consistent with the findings of Garland [1983] in his study of resuspension of particles from soil and grass. In wind speeds from 3 to 10 m/sec, Garland [1983] has reported that the resuspension rate varies from 10^{-9} to 10^{-5} sec^{-1} for particle sizes ranging from < 1 to 5 μm. Our results lie at the upper end of the data of Garland. Future work with the SCAQS data will consider the influence of windspeed on the observed resuspension rate.

Conclusions

- The aerodynamic surfaces with Teflon plates yield consistent, measurable dry deposition fluxes over periods as short as four hours for nitrate, sulfate, calcium, and lead in the Los Angeles Basin.
- The foliar extraction technique applied to Waxleaf Privet, Canary Island Pine, and Japanese Privet yields consistent, measurable dry deposition fluxes over periods as short as four days. However, it is likely that good results can be obtained for even shorter periods such as 1 - 2 days.
- Short-term exposures yield greater deposition fluxes than longer exposures for both the Teflon plates and the vegetation. This is probably due to increased resuspension as more particles accumulate on the surface.
- Based on the assumed mechanism of resuspension of deposited particles, the deposition flux data suggest that all four species have resuspension rates on the order of 10^{-6} sec^{-1} for any of the surfaces studied.

surface	resuspension fitting	nitrate	sulfate	lead	calcium
Teflon plate	average flux ng/sec m^2	70.2	15.7	0.092	16.7
	resuspension rate in 10^{-6} sec^{-1}	7.6	5.8	1.8	7.7
	max. exposure time, hours	3.8	5.0	16	3.7
Waxleaf Privet	average flux ng/sec m^2	53.5	14.9	0.18	
	resuspension rate in 10^{-6} sec^{-1}	1.1	1.8	1.8	
	max. exposure time, hours	26	16	16	
Canary Island Pine	average flux ng/sec m^2	99.0	22.1	0.33	
	resuspension rate in 10^{-6} sec^{-1}	2.5	1.5	4.0	
	max. exposure time, hours	115	19	7.2	

Table S.2 Summary of parameters for resuspension fitting. Maximum exposure time refers to the longest possible exposure period where resuspension accounts for loss of less than 5% of the deposited mass.

Recommendations

In the future work, the following are recommended to evaluate use of the aerodynamic surface for routine monitoring :

- To develop some measures to protect the aerodynamic surface from contamination by rain, birds, and insects.
- To use with different kinds of surface material to study the deposition of other species like nitric acid and sulfur dioxide.
- To explore the mechanisms responsible for variations in flux with exposure time. This will probably involve both wind tunnel studies and field work.
- To compare the deposition to Teflon plates with deposition to other kinds of vegetation in more detailed studies.

Chapter 1
Introduction

Dry deposition of atmospheric contaminants is known to be an important removal mechanism, of comparable importance to wet deposition in many cases. For example, Shannon [1981] has used budget studies of sulfur emissions in eastern U.S. and Canada to estimate that dry removal, wet removal, and transport out of the region are of similar magnitude during summer months. Dry deposition is roughly half as large as the other terms during the winter. Lindberg et al. [1986] have found that dry deposition represents more than half of the total annual input of SO_4^{2-}, NO_3^-, Ca, K, and acidity to an oak forest in Tennessee. Other studies [e.g. Galloway et al., 1984] suggest that dry deposition is less important than precipitation scavenging in eastern U.S., although still significant on an annual basis. Young et al. [1987] estimate that dry and wet deposition of atmospheric acidity are roughly equal in magnitude in mountainous regions of western U.S. ; dry deposition may be dominant in arid regions of the West.

1.1. The Process of Dry Deposition

Dry deposition may be broadly defined as the transport of particulate and gaseous contaminants from the atmosphere onto surfaces in the absence of precipitation. It is worthwhile to consider dry deposition as part of an overall atmosphere-surface exchange: gases are sometimes reversibly adsorbed onto surfaces only to be re-emitted, while particles may be deposited and subsequently resuspended. We often refer to *net* dry deposition as the resulting balance between downward and upward fluxes.

The key factors influencing dry deposition can be categorized into characteristics of the atmosphere, the nature of the surface, and properties of the depositing species [Sehmel, 1980]. Atmospheric properties influence the rate at which contaminants are delivered to the surface. Especially important is the state of the atmosphere close to the ground. The nature of the surface can have a marked effect on deposition. Of primary importance is the way in which the surface interacts with the atmosphere by exchanging momentum, heat, and mass. For example, a smooth, relatively nonreactive surface may result in rapid bounceoff of particles, and may not permit absorption or adsorption of certain vapors. A rougher, more

reactive surface favors greater deposition rates. Natural surfaces such as vegetation are highly variable in their characteristics; fluxes are often strong functions of the status of the vegetation during the growth cycle. Finally, properties of the depositing species will influence their transport to the surface and their ultimate fate after reaching the surface. For example, particles larger than a few micrometers are dominated by sedimentation, while diffusion is a more important mechanism for small particles and vapor deposition. Large particles are resuspended more easily than small particles [Garland, 1983].

The processes of deposition from the atmosphere to surfaces are divided into three steps [Sehmel and Hodgson, 1978; Hosker et al., 1982]. First is the transfer from the atmosphere to the boundary layer immediately surrounding the deposition surface, known as the quasi-laminar sublayer. This step is called aerodynamic transport, and it occurs by eddy diffusion and sedimentation. The second step, called boundary layer transport, occurs when contaminants are carried across the quasi-laminar sublayer. The key mechanisms for this step include diffusion, interception, inertial impaction and sedimentation. The final step in the deposition process occurs as contaminants reach the surface. Particles may simply adhere to the surface, or may react chemically producing irreversible changes in the deposited material. Vapors similarly may adsorb reversibly onto a surface or may undergo chemical reaction. Interactions with the surface may also involve resuspension of a fraction of deposited particles or re-emission of adsorbing vapors.

The dry deposition process is generally quantified by the deposition velocity V_d, which is defined as [Chamberlain,1953] :

$$V_d = -\frac{F}{C(z)}$$

where F is the deposition flux, or deposition per unit time per unit area, and $C(z)$ is the airborne concentration of the contaminant at a reference height, z. The minus sign is needed since downward flux has a negative value but the deposition velocity is defined as a positive quantity. F is assumed to be constant over the appropriate range of heights.

The dry deposition processes are also modeled by analogy between contaminant transport and the flow of electrons in an electrical circuit. The concentration is analogous to voltage, while the deposition flux is represented as an electrical current. Ohm's law can then be used to determine a resistance to transport as shown in Figure 1.1, analogous to an electrical resistance. The resistance to transport is merely the inverse of the deposition velocity and is typically divided into components representing the three steps in the deposition process, as discussed above.

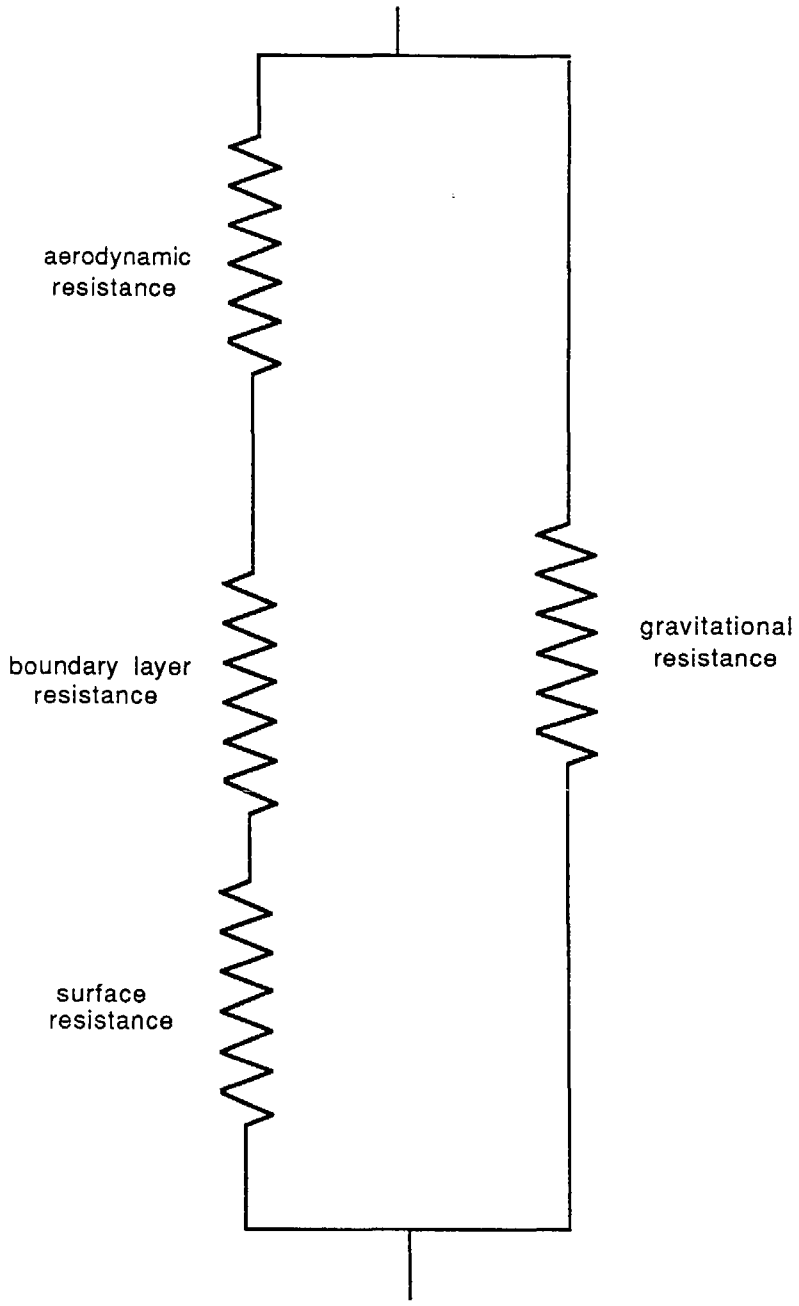

Figure 1.1 Schematic diagram showing the resistance model.

1.2. Measurement Methods for Dry Deposition

Over the years, several techniques have been developed for measuring dry deposition. These can be divided conveniently into two categories. The first category, surface analysis methods, includes all types of measurements which examine contaminant accumulation on surfaces of interest. The second category, atmospheric flux methods, involves measurements of contaminants in the atmosphere from which one may estimate the flux [Hicks et al., 1986]. Two methods, aerodynamic surrogate surfaces and foliar extraction, are both in the first category and have been used in this study.

Various kinds of surrogate surfaces have been used to estimate dry deposition because of their convenience, low cost, and reasonable control over the experiment. Surrogate surfaces which have been used in dry deposition studies include open buckets, petri dishes, Teflon disks, coated and uncoated glass, filter paper, plastic nets and artificial foliage. For each of these surrogate surfaces, the processes responsible for deposition may be affected by the particle attraction and capture characteristics of the surface material, and by the local turbulence induced by the surrogate surface size and shape [Munn and Bolin, 1971; Davidson et al., 1985]. In spite of the difficulty in correlating deposition on surrogate and natural surfaces, the former can provide an estimate of fluxes with controlled aerodynamic characteristics not currently obtainable from natural surfaces [Vandenberg and Knoerr, 1985].

In this study, a new aerodynamically designed surface is used to measure the deposition rate. It is a Teflon-coated solid aluminum frisbee-shaped symmetrical airfoil. A deposition plate with any surface characteristics can fit snugly into the recessed airfoil [Gamble, 1986]. The key features of the surface are :

1. Predictive air flow pattern : The boundary layer flow around the airfoil can be computed theoretically. Therefore, the boundary layer resistance can be predicted if the wind speed is known.
2. Independence of wind direction : The airfoil is designed to be radially symmetric.
3. Easy control of surface characteristics : The deposition surface is placed onto the top of the airfoil. Various kinds of surfaces can be used for any specific purpose. For example, Teflon-coated aluminum plates are used to measure the deposition to inert surfaces.

Besides use of the symmetric airfoil, foliar extraction has been used in these experiments. This method directly measures the amount of contaminant deposited on plants by washing the leaves with water. However, the uptake of contaminant during exposure, the complex flow patterns around plants, and the leaching from plants during washing, make data interpretation difficult.

1.3. Purpose of This Study

Dry deposition measurements to the aerodynamic surfaces and vegetation have been conducted simultaneously in Los Angeles Basin during June, July, August and September, 1987. The surrogate surfaces put onto the airfoils include Teflon-coated aluminum plates and nylasorb filter paper. The Teflon-coated surfaces are used to measure the deposition rate of particles without interference from gases because the surface material is inert. Nylasorb filter paper has very high reactivity with nitric acid gas and it will capture nitric acid in addition to nitrate particles. Deposition to vegetation is measured by washing the leaves of Ligustrum japonicum texanum (Waxleaf Privet), Pinus canariensis (Canary Island Pine) and Ligustrum japonicum (Japanese Privet). Comparing the deposition rates to the surrogate surfaces with those to the plants will illustrate the extent to which the airfoil deposition can be used to represent deposition to the vegetation. Such a comparison will also enhance our understanding of those complex factors influencing deposition onto both types of surfaces. Comparing fluxes of different exposure times on each surface type will indicate if exposure period is a important factor in determining dry deposition rate. Some additional limited measurements of deposition to surrogate surfaces have been conducted at Emerald Lake in Sequoia National Park. These experiments have provided deposition data for a remote area, in contrast to the deposition in the urban Los Angeles Basin. Note that this is the first time that the aerodynamic surfaces have been used in the field, although preliminary wind tunnel tests have been conducted previously.

Chapter 2

Dry Deposition onto Aerodynamic Surfaces and Vegetation in Los Angeles Basin

During the Southern California Air Quality Study (SCAQS) in June and July of 1987, the dry deposition fluxes to aerodynamic surfaces and vegetation were measured at Claremont, which is about 65 miles east of Los Angeles International Airport. Two different kinds of surrogate surfaces, Teflon plates and nylasorb filter paper, were put onto the top of the airfoils. At the same time, three different kinds of vegetation were used for comparison. As discussed earlier, this is the first time that the aerodynamic surrogate surfaces were used to measured the dry deposition rate in the field, although some wind tunnel studies were conducted previously. Preliminary results suggested that sedimentation dominates particle deposition onto the airfoils, so that the total mass deposition is mostly influenced by the concentration of large particles in the atmosphere [Davidson et al.,1985].

2.1. Experimental Methods

(A). Aerodynamic Surrogate Surfaces

The aerodynamic surrogate surface is composed of a Teflon-coated solid aluminum airfoil, which is shown in Figure 2.1, and a deposition plate. Both the airfoil and the plate are symmetrical with respective to their vertical axes so that wind direction does not have any effect on the air flow pattern. The deposition plate can have any kind of surface characteristics and is put on the top of the airfoil. The airfoils are mounted on the top of tripods to avoid soil contamination, such that the deposition plates are about 2.5 meters above ground. Teflon-coated aluminum plates and nylasorb filter paper are used as deposition surfaces in this study. Teflon-coated surfaces are inert to most chemical reactions, so that only particles deposit. In contrast, nylasorb filter paper is very reactive to nitric acid, so that both particles and nitric acid gas deposit. A total of ten airfoils are used in the study, eight with Teflon-coated aluminum plates and two with nylasorb filter paper.

In order to get fully developed air flow, the aerodynamic surfaces have to be set up at a location with enough upwind fetch. The location should be as far as possible from local sources such as traffic and other human activities to provide concentrations representative of

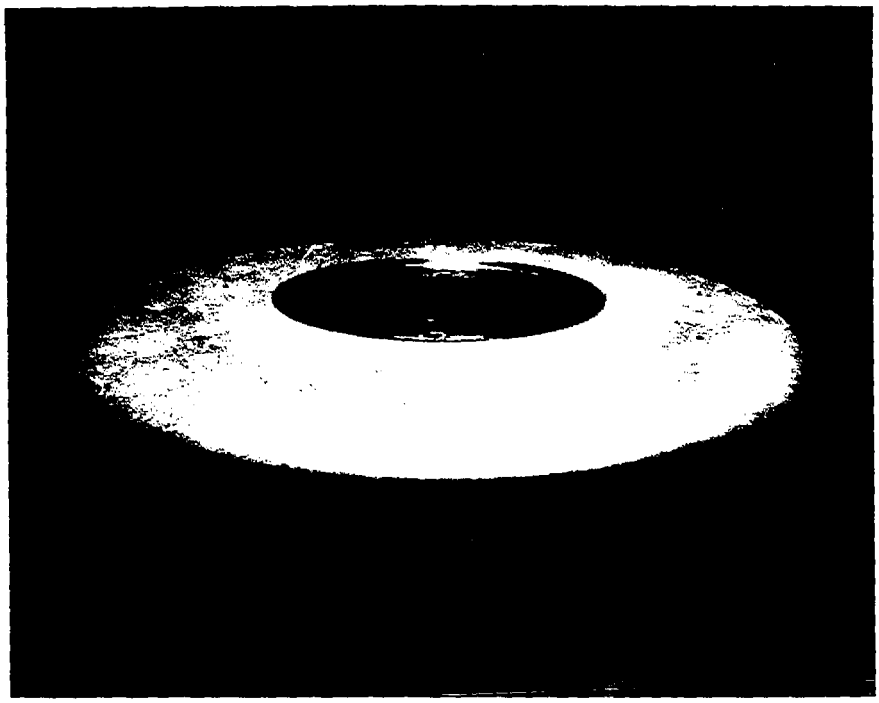

Figure 2.1 Aerodynamic airfoil without deposition surface.

the region. Many of the SCAQS experiments involving real-time continuous sampling were set up in a parking lot at the Claremont Colleges where electric power was available, known as the Claremont A Site. Possible local contamination over short time periods can be readily identified in the real-time data resulting from these experiments. Such contamination is a more serious problem for the airfoils, however, which integrate deposition over several hours. Furthermore, the airfoils do not require electricity, allowing greater flexibility in choosing sampling locations. For these reasons, the experiments were set up at Robert J. Bernard Biological Station instead of the Claremont A Site. This deposition field site, which is shown in Figure 2.2, is about 500 meters north of Foothill Boulevard and 250 meters west of Mills Avenue, roughly 800 meters NNW of the Claremont A Site. The Biological Station is a nature reserve area with fence around it, representing a typical background environment in Southern California. With the control of access to the area, there was minimal risk of vandalism. In order to compare the results with other SCAQS data, two of the ten aerodynamic surfaces were put on top of the trailer of the GM group at the Claremont A Site. The other eight airfoils were set up at the Biological Station.

Four Teflon-coated surfaces, two at the Claremont A Site and two at the Biological Station, collected samples for 12-hour or 24-hour exposure periods on nonintensive days. During intensive days, the two at the Biological Station were run according to the ARB intensive day schedule. That is, samples were collected at 1 am, 6 am, 10 am, 2 pm and 6 pm. An additional two airfoils were used with nylasorb filter paper to measure the dry deposition rate of nitric acid gas. The other Teflon-coated surfaces were originally assigned for longer exposure times such as two days, four days and eight days. Because of contamination from birds, we obtained only limited data with exposure times longer than two days.

After each exposure, the surface was removed from the airfoil and immediately washed using the TFE Teflon digestion vessel [Davidson et al., 1985] with 8 ml of distilled/deionized water. The vessel containing the plate was then shaken for three minutes to extract the pollutants, and the solution was poured into a polyethylene tube. Some primary studies done in Pittsburgh found that a three-minute extraction obtained the same results as five-minute, ten-minute and fifteen-minute extractions. Similar experiments run in Los Angeles also showed the same results. The nylasorb filter paper was put into polyethylene tubes and then placed in a freezer until analysis. The contaminants were extracted from the nylasorb filter paper by placing the tube with 16 ml of distilled/deionized water in an ultrasonic bath for one hour, then putting the tube on a hot plate at 65°C for 3 hours, and finally putting the tubes back in the ultrasonic bath for 5 hours.

To insure the quality of the data, every sample was duplicated. That is, two samples with the same kind of surface and the same exposure period were collected simultaneously. The

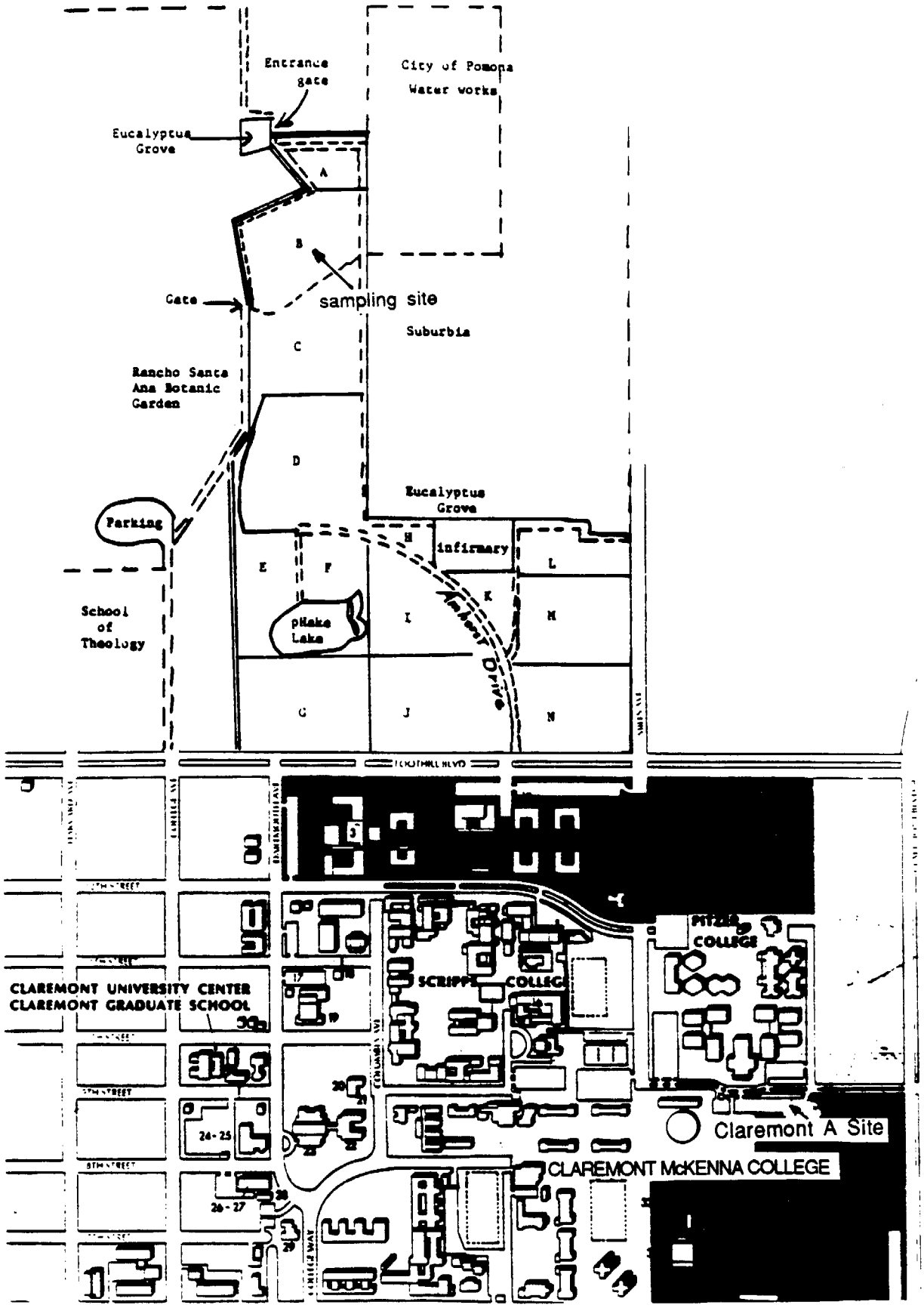

Figure 2.2 Location of experimental sites: the Biological Station and the Claremont A Site.

blanks for the Teflon plates were made in two different ways. First, clean Teflon plates were extracted in the laboratory using the same procedures performed in the field. These represented the possible contamination from the Teflon plates themselves and from the distilled/deionized water used to extract the deposited pollutants. Second, field blanks were made at the site in the same way as samples except that the exposure time on top of the airfoil was only about 5 minutes. These represented the possible contamination from handling in the field in addition to contamination of the blanks in the laboratory. The comparisons of the second type of blanks with the corresponding 12-hour exposure samples are shown in Figure 2.3. The Julian date of each comparison is listed in Table 2.1. One field blank was made for every five samples.

The concentrations of the lab blanks in ng/cm^2 are 11.8 ± 7.0 for nitrate, 1.39 ± 2.09 for sulfate, 0.09 ± 0.03 for lead and 1.76 ± 1.05 for calcium. The field blanks have concentrations of 14.6 ± 9.7, 2.78 ± 2.09, 0.09 ± 0.02 and 2.04 ± 1.32 ng/cm^2 for nitrate, sulfate, lead and calcium, respectively. Compared with the concentrations of the samples, the concentrations of the blanks are very low. Note that the blanks made in the field are all slightly greater than those made in the laboratory, but the differences are small. This suggests that the contamination from handling is not significant. The final net concentration in each sample has been computed as the difference between total concentration in the sample and the mean value of the field blanks.

(B). Vegetation

The plants that we used for most of the vegetation experiments in this study were Ligustrum japonicum texanum (Waxleaf Privet) and Pinus canariensis (Canary Island Pine). The former is the same as that used by John et al. [1985] in their study of dry deposition of nitrate and sulfate in West Los Angeles and Tanbark Flats. In addition to these two species of plants, we also used Ligustrum japonicum (Japanese Privet). Note that Ligustrum japonicum may be called Waxleaf Privet or Japanese Privet; to avoid confusion, the latter name is used here. L. texanum has larger and waxier leaves than L. japonicum. L. texanum, commonly found in nurseries throughout Los Angeles, is also more popular than L. japonicum. Both of these plants are about 1 meter high. P. canariensis with a height of 1.3 meters is also popular in Southern California. All of the plants were fixed onto a wooden table, which is 1.5 meters above the ground, at the Biological Station site. Thus the plants were at about the same height as the surrogate surfaces. Before the plants were put on-site, they were washed with pressurized distilled water twice for about 10-15 minutes each time. The concentrations of sulfate and nitrate in this distilled water were lower than 0.05 and 0.5 ppm, respectively. The plants were then washed leaf by leaf using a squeeze bottle with distilled/deionized water. The concentrations of nitrate, sulfate, lead and calcium in the distilled/deionized water were below the detectable level, which was about 1 ppb. After being exposed for some periods

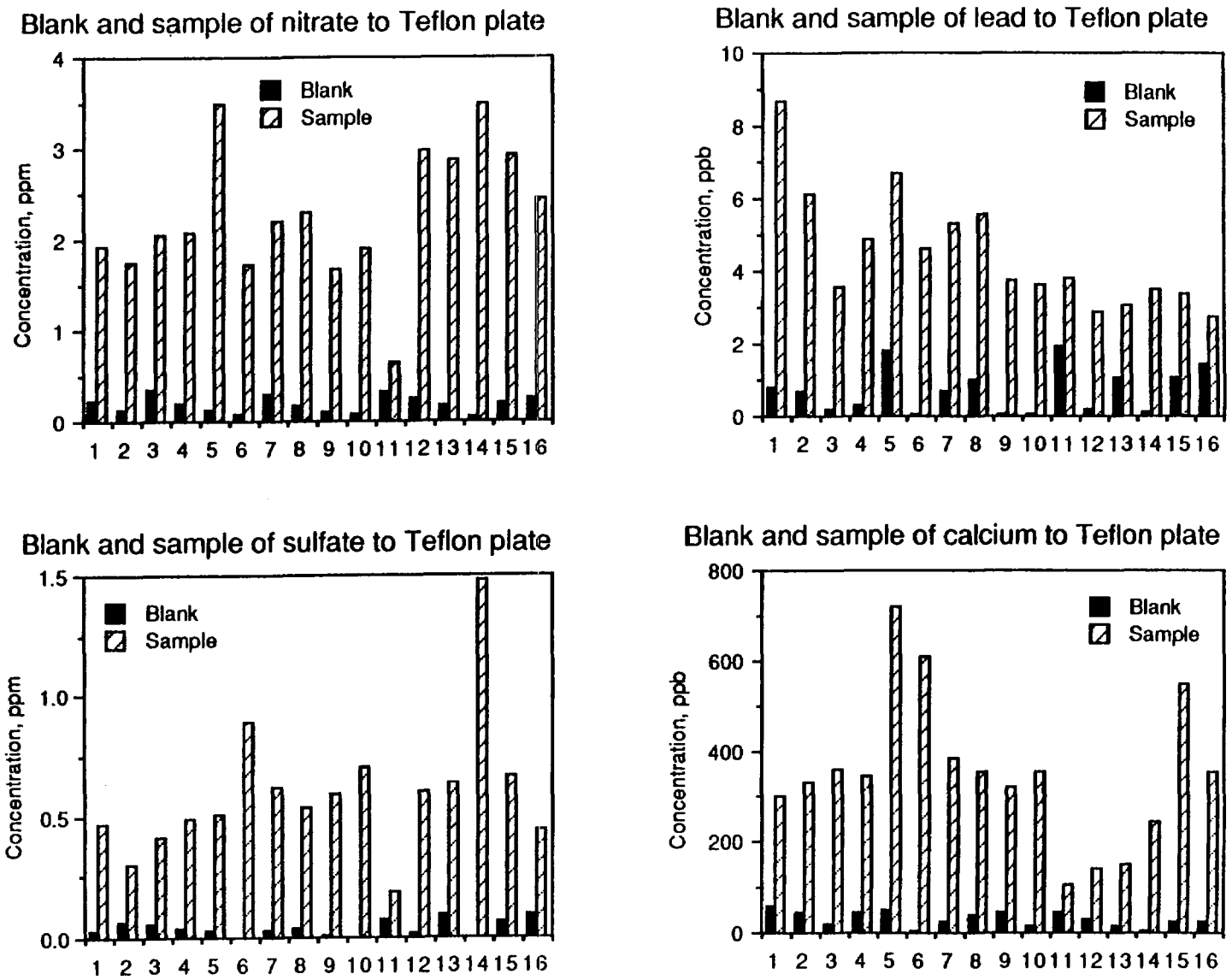

Figure 2.3 Comparison of samples and blanks from Teflon plates.

sample number	1	2	3	4	5	6	7	8	9	10
airfoil	#1	#2	#9	#10	#9	#2	#1	#2	#9	#10
date	171	171	171	171	172	173	178	178	178	178

sample number	11	12	13	14	15	16
airfoil	#1	#9	#10	#1	#2	#10
date	183	183	183	187	191	191

Table 2.1 The sampling dates and the airfoil numbers for the samples in Figure 2.3.

sample number	1	2	3	4	5	6	7	8
plant	#1	#2	#3	#4	#4	#7	#3	#5
date	176	176	176	176	184	184	188	188

Table 2.2 The sampling dates and plant numbers for the samples in Figure 2.4.

which ranged from 4 to 17 days, the leaves were harvested from the plants and were washed immediately with 50 ml of distilled/deionized water using ten leaves in each sample. Lindberg et al. [1984] have found that the kinetics of dissolution of calcium and nitrate from leaves were similar to dissolution from inert surfaces, with stable levels reached within 3 minutes. Thus the leaves harvested from the plants were also shaken in distilled/deionized water for three minutes. In order to have a better comparison between results of the foliar extraction and those of the surrogate surfaces, we chose leaves to the extent possible that were up-facing and were not shadowed by other leaves. Note that all of the plants were watered every day so that the plants were always in a state without water stress.

Because of the variation and complexity of dry deposition to vegetation, 2 to 4 samples consisting of ten leaves each with the same exposure time were collected simultaneously from the same plant or different plants. Field blanks were obtained by washing a set of ten cleaned leaves at the beginning of each exposure period. Only one such blank was obtained for each experiment. Comparing the concentrations of samples with those of blanks, we find that the blanks had much lower concentrations. Using Waxleaf Privet as an example, the average concentrations of nitrate, sulfate, lead and calcium in the blanks are 9.6 ± 12.6, 33.0 ± 34.3, 0.37 ± 0.10 and 45.9 ± 21.1 ng/cm^2, respectively. The blanks from vegetation have higher concentrations than those from the Teflon plates, but they are still much lower than samples. The comparisons of nitrate, sulfate, lead and calcium are shown in Figure 2.4 for each blank and the corresponding four-day exposure sample from Waxleaf Privet. The exposure time of each comparison is listed in Table 2.2. The higher concentrations in the vegetation blanks are believed to be caused by difficulties in washing the plants. Because of the longer exposure times for the vegetation, the blank/sample ratios are lower than those for the Teflon plates. The net concentration in each vegetation sample is taken as the total amount of contaminant in the sample minus the amount of contaminant in the one blank corresponding to that experiment. The final concentration for each experiment is computed as the average of the 2 to 4 samples collected at the same time.

Both surrogate surface and foliar extraction samples were refrigerated until they were analyzed. Analyses were conducted by ion chromatography for sulfate and nitrate and by flameless atomic absorption spectrophotometry for lead and calcium. The ion chromatography analyses were conducted using a Dionex IC 2010 at the California Air Resources Board Laboratory at El Monte. The procedures for quality control of the ARB were followed. The standards were recalibrated every 30 samples. The atomic absorption analyses for lead and calcium were run at the AA laboratory at Carnegie Mellon University, using quality assurance procedures established for prior National Science Foundation projects.

The numbers of samples and blanks are shown in Tables 2.3 and 2.4. In total there are 201 samples for the aerodynamic surfaces and 43 samples for foliar extraction.

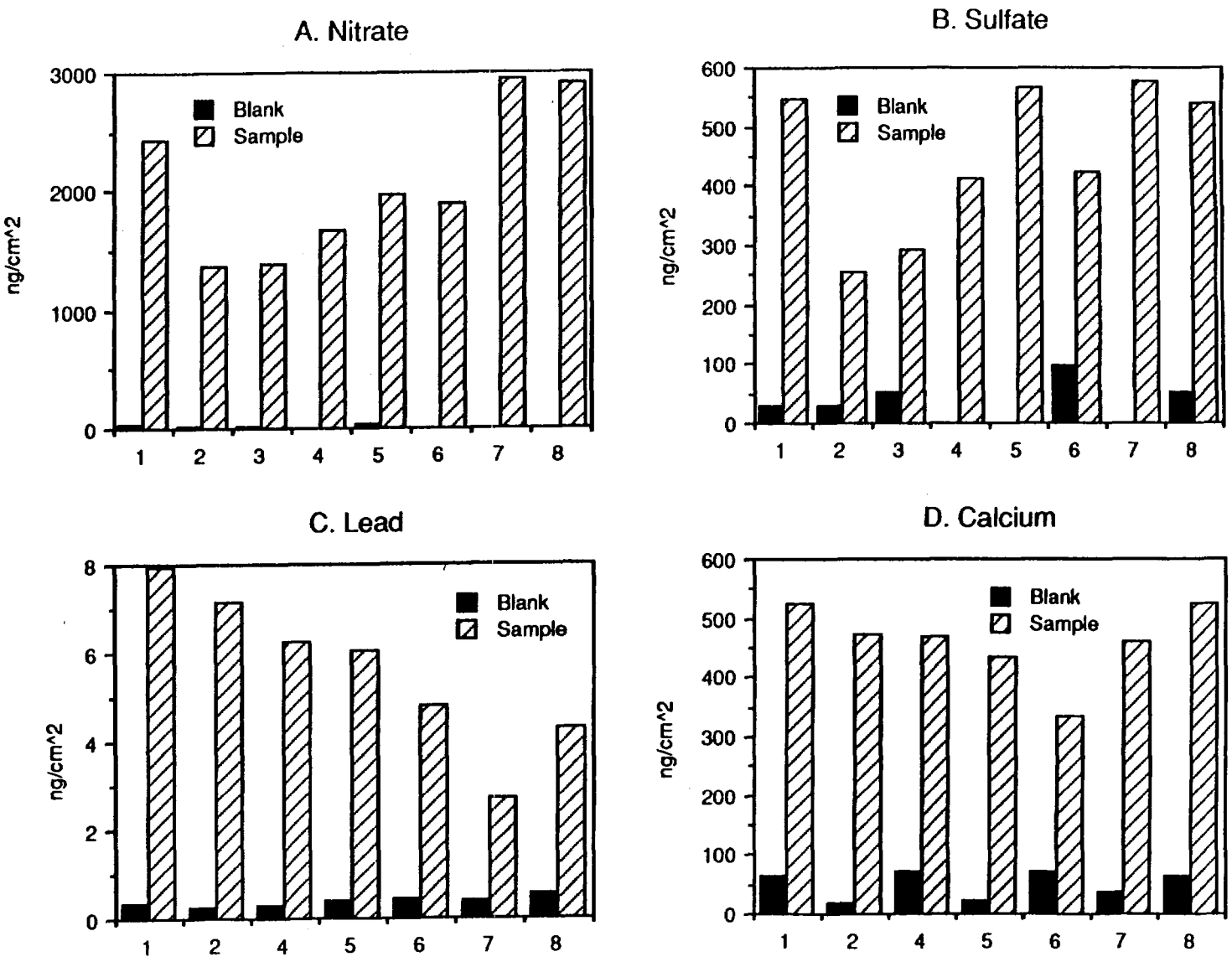

Figure 2.4 Comparison of samples and blanks from Waxleaf Privet.

Type of surfaces	Exposure time	Number
Teflon surface	12 hours	73(42)
	one day	39(19)
	two days	7(4)
	intensive days	52
	others	16(4)
nylon filters	12 hours	12
	4 days	2
blanks		44(6)

Table 2.3 : Total number of samples, and total number of blanks, for aerodynamic surrogate surfaces at both the Biological Station and the Claremont A Site. The number of samples or blanks at the Claremont A Site is shown in parantheses.

Plants	Exposure time	Number
L. Texanum	4 days	11
	8 days	7
	others	4
P. Canariensis	4 days	6
	8 days	4
	others	3
L. Japonicum		8
blanks		16

Table 2.4 : Numbers of samples and blanks for foliar extraction.

2.2. Results

(A) Aerodynamic Surrogate Surfaces - Teflon Plates

The results of dry deposition to Teflon plates are presented in four categories.

- The first category involves comparisons between identical deposition plates located side-by-side, sampling simultaneously. These comparisons illustrate experimental uncertainties associated with the sampling method. Note that all of the deposition fluxes measured during June and July are included in this comparison, since every experiment involved two simultaneously exposed samplers.
- In the second category, the fluxes from the two co-located samplers have been averaged to yield a single flux for that time period. The results may be used to compare fluxes at different times throughout the SCAQS program. Results are presented separately for the Biological Station and for the Claremont A Site.
- In the third category, the average fluxes from category 2, computed separately for each of the two sites, have been plotted on a single graph. This allows a comparison of the fluxes at the two sites. Separate graphs are plotted for nitrate, sulfate, lead and calcium.
- In the fourth and final category, the deposition fluxes for 12-hour runs and for the 4 to 6-hour SCAQS intensive runs are presented. These results illustrate the diurnal variation and the effect of exposure time on dry deposition rate.

Because the airborne concentrations needed to calculate deposition velocities are not yet available, the data are presented as fluxes in units of ng/sec m^2.

Category 1

Two Teflon plates with the same exposure period were set side-by-side at the Biological Station. Meanwhile, another two were set up in the same way at the Claremont A Site. The plates at the Biological Station were exposed 12 hours or 24 hours on non-intensive days and were run according to the SCAQS schedule on intensive days. For those at the Claremont A Site, the exposure time was always 12 hours or 24 hours. Contamination by bird excrement invalidated some of the samples, however. For all of the valid sample pairs, comparisons of the duplication are shown in Figures 2.5 and 2.6. Figure 2.5 shows the difference in fluxes of nitrate, sulfate, lead and calcium to simultaneously exposed Teflon plates at the Biological Station, while Figure 2.6 shows the difference in fluxes of these species for the Claremont A Site. The data are plotted as the percentage of the mean values for the Julian date representing the beginning of the exposure period.

The agreement between co-located samples is generally good. The values of the root mean square difference for nitrate, sulfate, lead and calcium at the Biological Station are 9.0%, 23.0%, 23.7%, and 15.6%, respectively. The values of root mean square difference for nitrate, sulfate, lead and calcium at the Claremont A Site are 6.8%, 10.2%, 12.8%, and 9.0%,

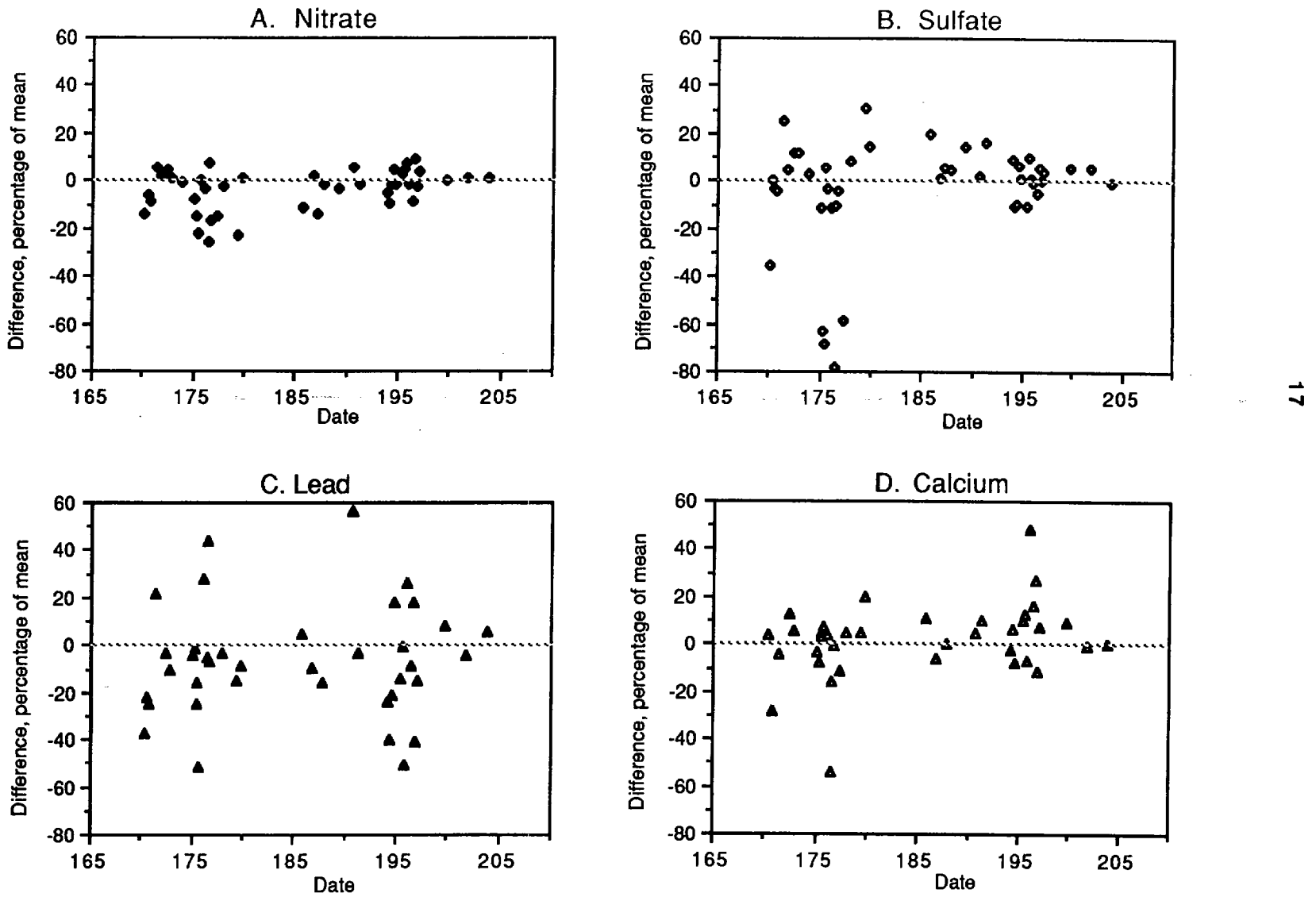

Figure 2.5 Comparison of duplications at the Biological Station.

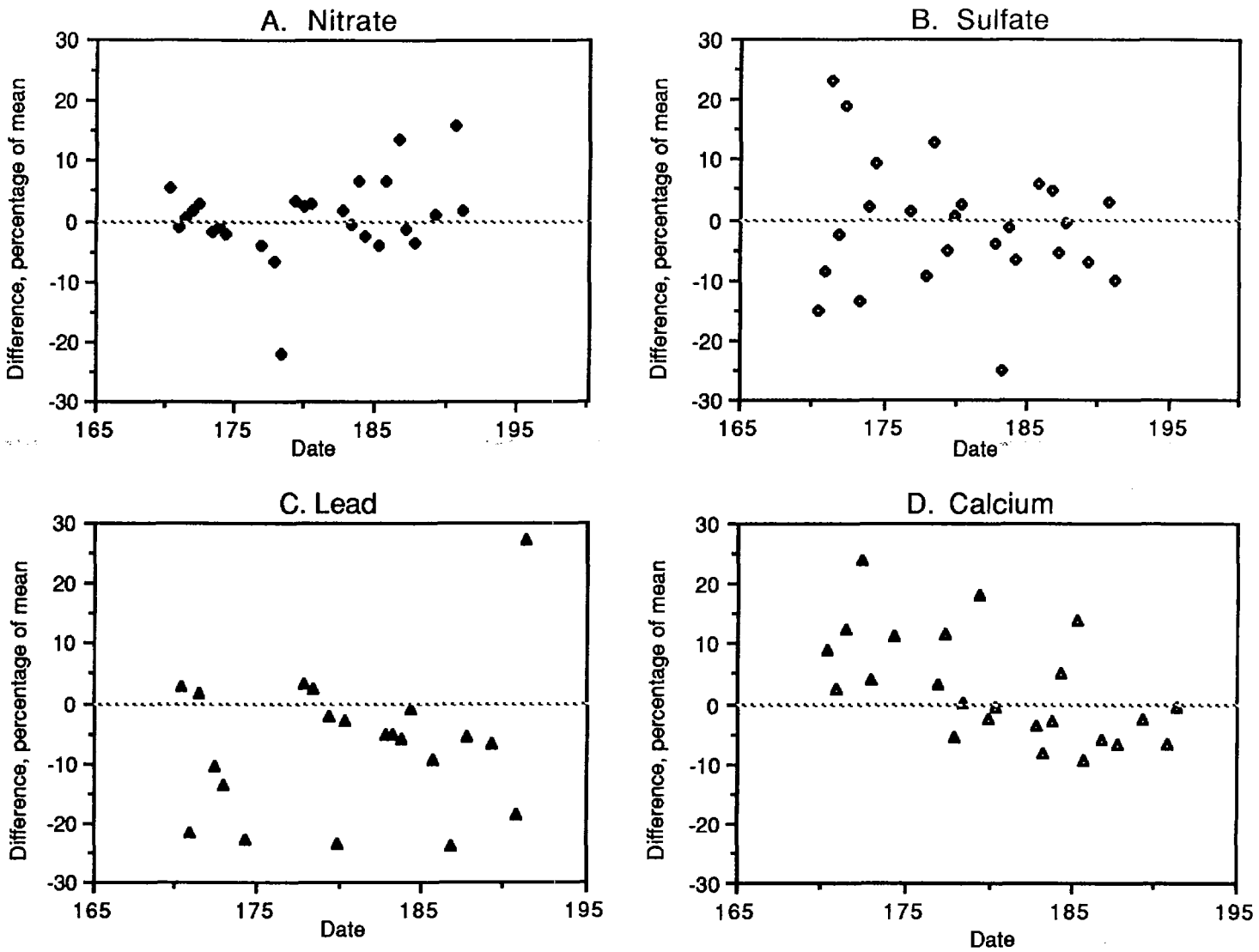

Figure 2.6 Comparison of duplications at the Claremont A Site.

respectively. Note that the agreement is better at the Claremont A Site than that at the Biological Station. Nitrate, whose fluxes are the greatest among the various species, shows the best agreement. Lead, whose fluxes are the lowest, shows the poorest agreement. The difference between conjugate samples comes from both actual variation in the fluxes and experimental error.

Category 2

For each sampling experiment, the two deposition fluxes (i.e., pair of conjugate values) have been averaged to provide a single flux for that time period. These average fluxes are plotted in Figures 2.7 and 2.8. The fluxes of nitrate are in the range of 7 - 213 ng/sec m^2 at the Biological Station and 24 - 131 ng/sec m^2 at the Claremont A Site. The fluxes of sulfate are in the range of 2 - 64 ng/sec m^2 and 4 - 19 ng/sec m^2 at the two sites, respectively. The fluxes of lead are in the range of 0.035 - 0.46 ng/sec m^2 at the Biological Station and 0.019 - 0.17 ng/sec m^2 at the Claremont A Site. The fluxes of calcium are in the range of 1.2 - 20.7 ng/sec m^2 and 1.4 - 9.1 ng/sec m^2 at the two sites, respectively.

The highest fluxes at the Biological Station are much higher than those at the Claremont A Site. For fluxes at the Biological Station, i.e. Figure 2.7, there are peaks around date 175 and date 195 in each plot. All of the peak fluxes are associated with intensive runs, that is, high airborne concentrations and short exposure times. Note that only the plates at the Biological Station were run on the SCAQS intensive day schedule. The high observed fluxes on the intensive run days are due in part to the high airborne concentrations on those days, although the effect of short exposure time may also have been important. The latter effect cannot be quantified until airborne concentration data are obtained. More details regarding the effect of exposure time on deposition rate will be discussed in the final category. For the four species analyzed, the order of fluxes from high to low is nitrate, sulfate, calcium and lead at both sites. The large nitrate fluxes result from both high airborne concentrations [Appel et al.,1980; John et al.,1985; Bytnerowicz et al.,1987] and high deposition velocities relative to sulfate [John et al.,1985,1986; Voldner et al., 1986; Bytnerowicz et al.,1987; Milford and Davidson, 1987]. Note that there is substantial variation in the fluxes for all four species. This is probably the result of variations in airborne concentration and in characteristics of the atmosphere which influence deposition velocity. The relative importance of each of these factors cannot be discussed until the airborne concentration data are obtained.

Category 3

In order to compare fluxes at the Biological Station with those at the Claremont A Site, the difference in values for each run involving simultaneous exposures have been plotted in Figure 2.9. The style of graphing is the same as that in Figures 2.5 and 2.6.

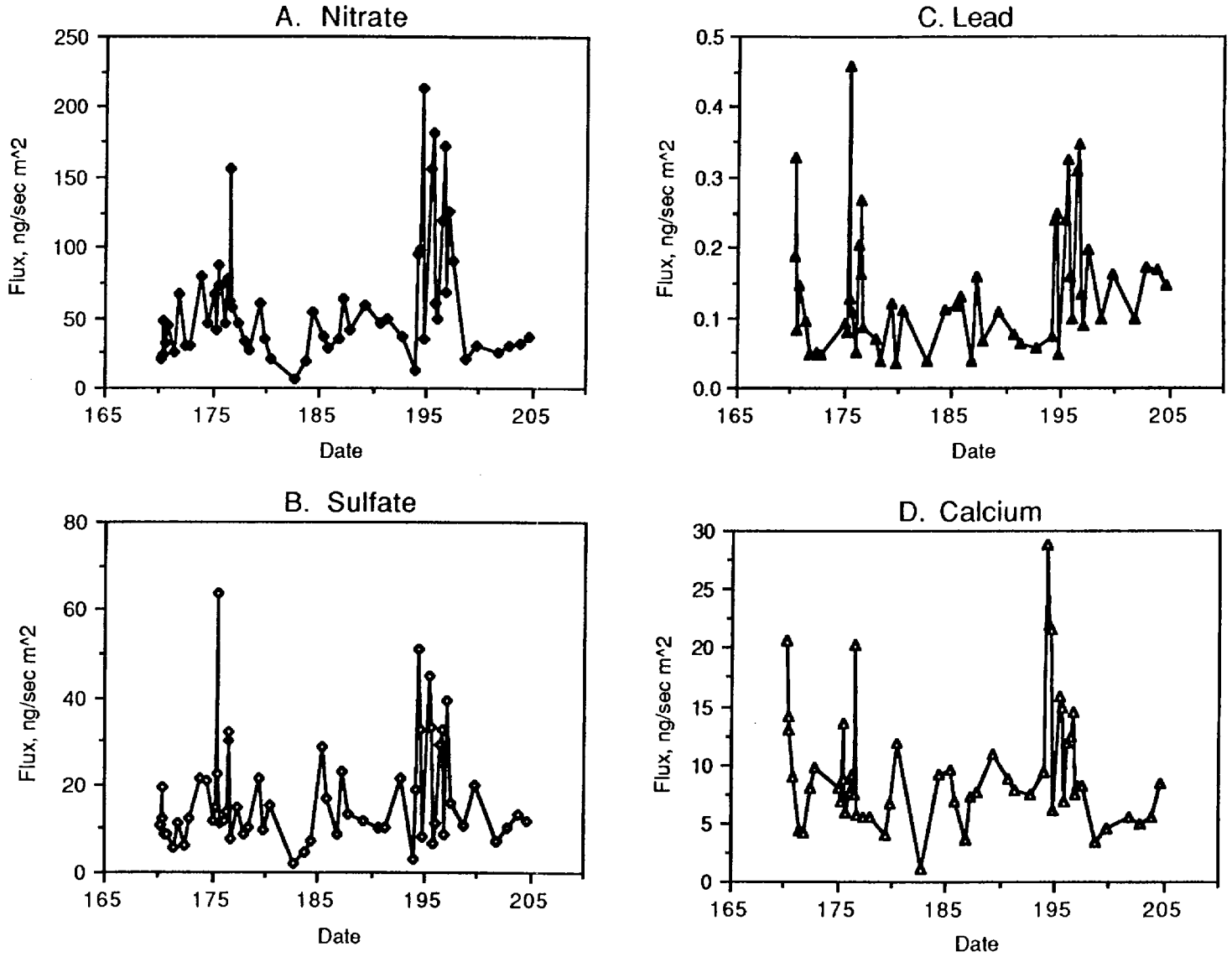

Figure 2.7 Deposition fluxes at the Biological Station.

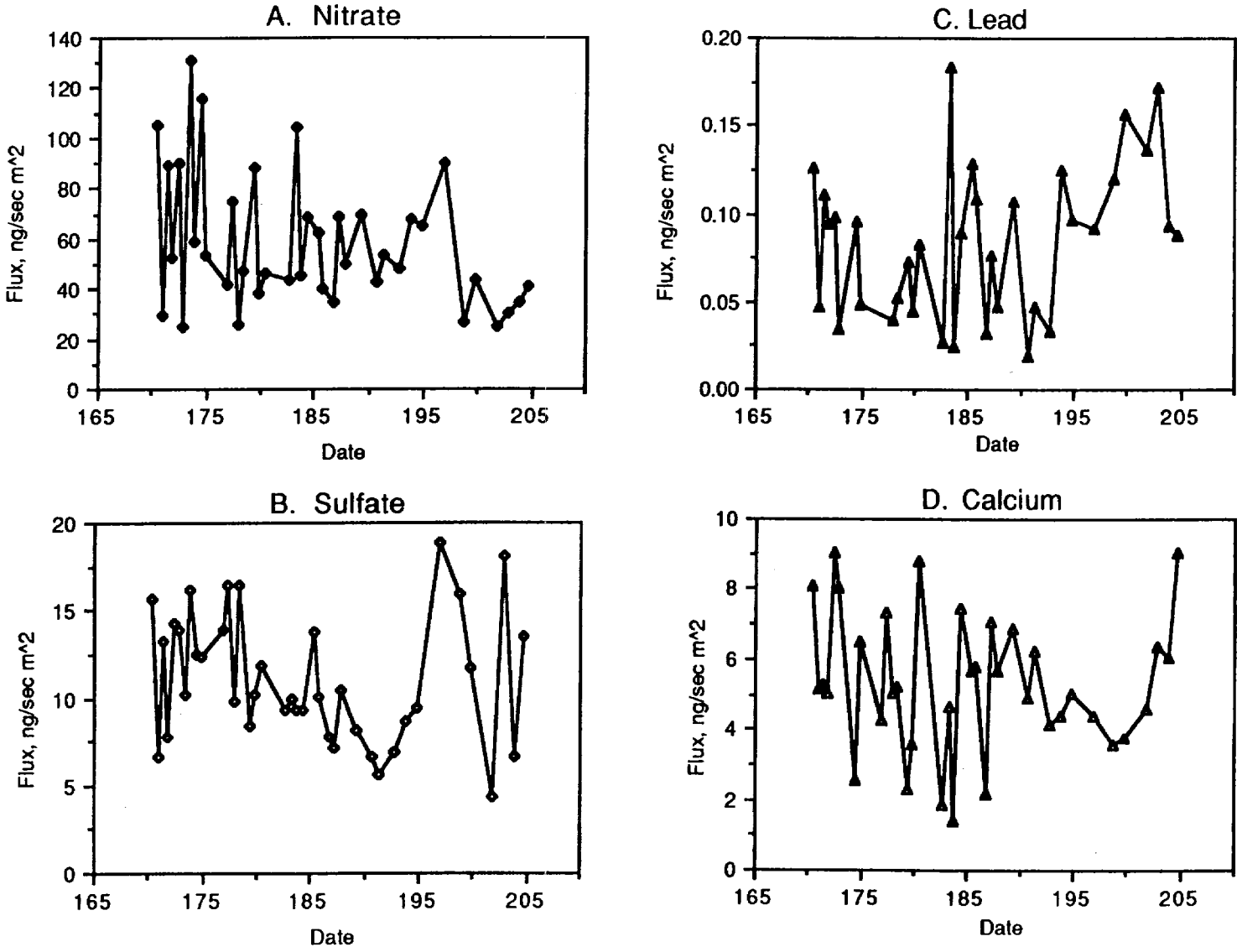

Figure 2.8 Deposition fluxes at the Claremont A Site.

The data in Figure 2.9 provide information on which of the two sites shows the greater fluxes. For example, 6 out of the 29 conjugate fluxes of nitrate are greater at the Biological Station. In contrast, 8 out of the 26 conjugate samples have greater fluxes of calcium at the Claremont A Site. In general, the fluxes at the Claremont A Site are greater than those at the Biological Station for nitrate, sulfate, and lead; the opposite is true for calcium. The ratios are 1.57 ± 1.09 for nitrate, 1.11 ± 0.80 for sulfate, 1.04 ± 0.75 for lead and 0.87 ± 0.26 for calcium. The greater activity at the Claremont A Site, both by SCAQS participants and by motor vehicles in nearby parking lots and streets, may be responsible for the higher observed fluxes of nitrate and sulfate. The water spray from an adjacent field at the Claremont A Site may be another source of contamination. The greater fluxes of calcium at the Biological Station are probably caused by soil resuspension because of greater dust levels there and because the Teflon plates are only 2.5 meters above ground. It should be noted, however, that the variability in fluxes from one experiment to the next is far greater than the differences between the two sites for all four contaminants.

Category 4

Figure 2.10 shows average fluxes plotted sequentially during a three-day intensive run period at the Biological Station. In each graph, the 4 to 6-hour exposures and 24-hour exposures are plotted together to be easily compared. Note that short-term SCAQS intensive sampling was not conducted at the Claremont A Site since the Biological Station was believed to be the better site, both from aerodynamic considerations and because of a greater distance from local sources. Strong diurnal variations are shown in all of the plots with greater fluxes during the daytime hours. Nitrate and lead have the highest fluxes during 2 pm to 6 pm, while sulfate has the highest fluxes during 10 am to 2 pm. The highest fluxes of calcium are not at the same time period throughout the three-day intensive runs. The greater fluxes during the day may be caused by both greater airborne concentrations and higher deposition velocities.

Comparing the short-term fluxes with 24-hour exposures, it is found that the 4 to 6-hour exposures generally yield higher deposition fluxes. Comparing 12-hour exposures with 2-day and 4-day exposures, we obtain the same results; the short-term exposures generally yield higher deposition fluxes. This is an important finding: the measured deposition flux, and presumably also the deposition velocity, are functions of exposure time. More quantitative discussion about the effect of exposure time on deposition rate is presented in the final section.

(B). Aerodynamic Surrogate Surfaces - Nylasorb Filters

Because of contamination from bird excrement, the sampling time of nylasorb filter paper was changed to intensive days only. In order to have a significant amount of pollutants relative to the background level of the paper itself, the exposure time was chosen to be 12 hours. The

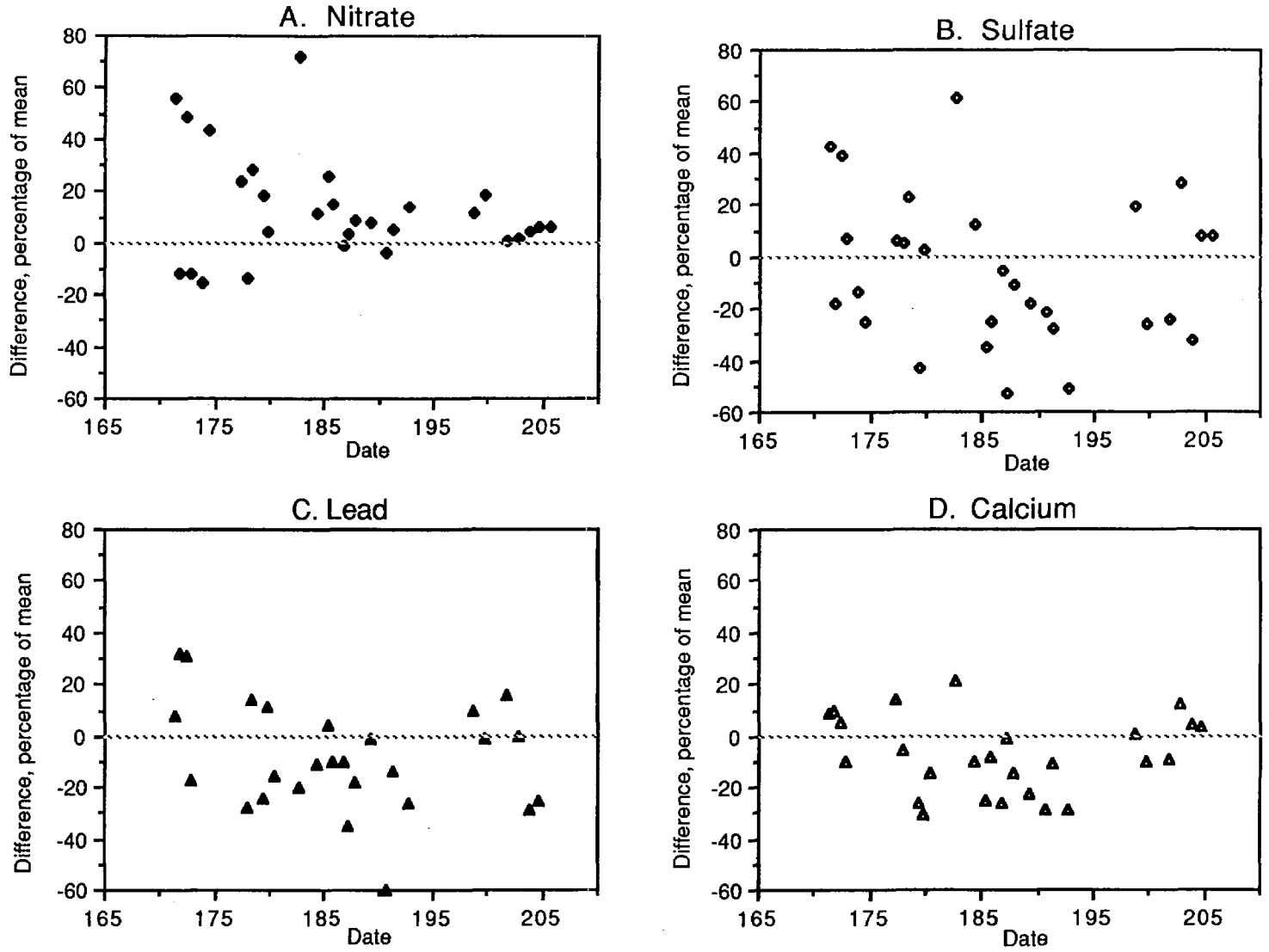

Figure 2.9 Comparison of fluxes at the two sites. Values greater than zero imply higher fluxes at the Claremont A Site; values less than zero imply higher fluxes at the Biological Station.

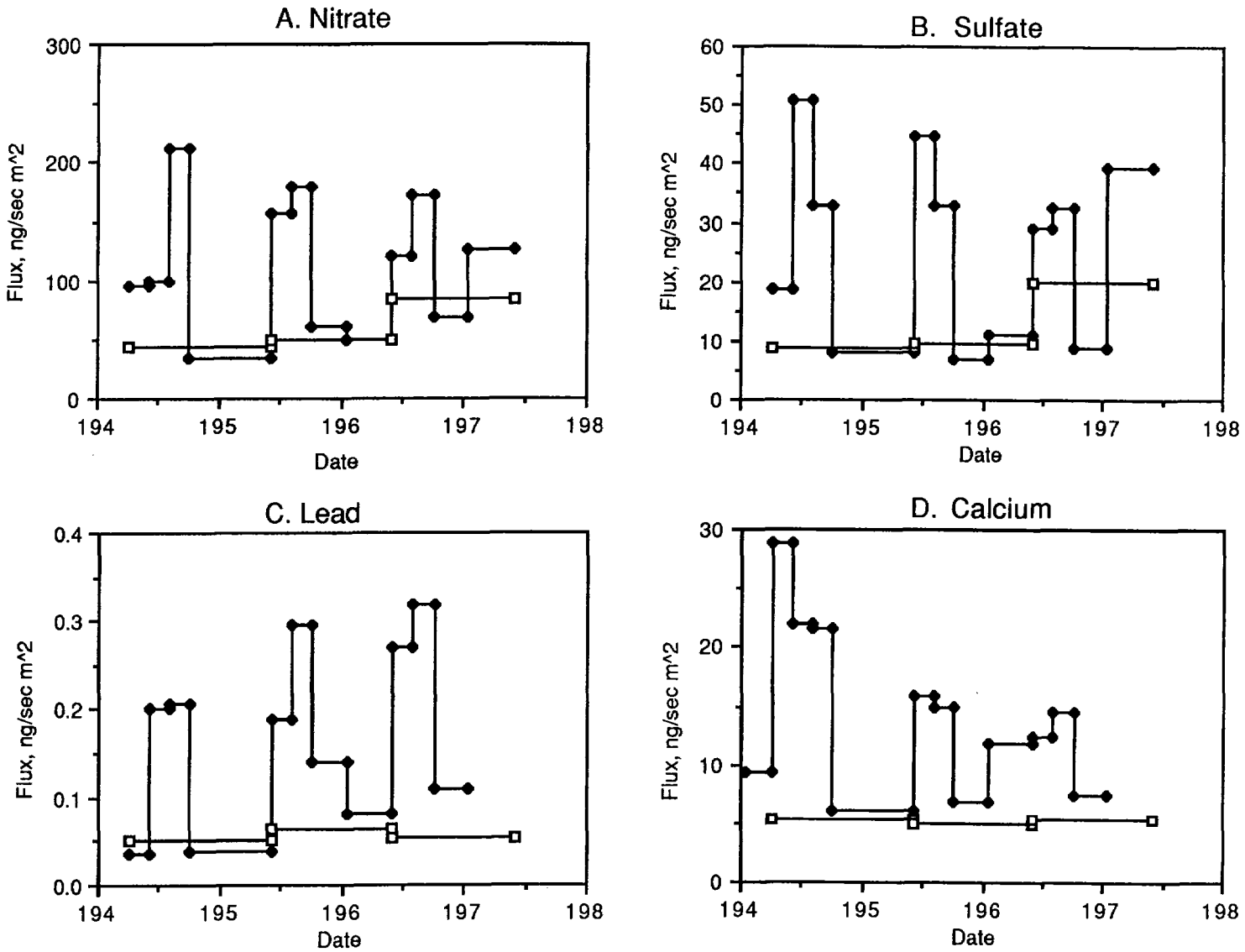

Figure 2.10 Deposition fluxes on intensive days. Diamonds are for exposure times according to the ARB schedule on intensive days and squares are for exposure times of 24 hours.

deposition fluxes of nitrate and sulfate are shown in Figure 2.11. Note that the exposure times of the Teflon plates were either 4 to 6 hours or 24 hours on intensive days. It is found that the 12-hour deposition fluxes for the nylasorb filter paper are greater than the 24-hour deposition fluxes on the Teflon plates but are smaller than the 4 to 6-hour exposures on the plates. More information will be provided when airborne concentrations are available to compute the deposition velocities. Because the effect of exposure time is so significant, it is difficult to compare the results of these different exposure times.

(C). Vegetation

All three species of plants were set up at the Biological Station. The deposition fluxes plotted separately for Waxleaf Privet, Canary Island Pine and Japanese Privet are shown in Figures 2.12 - 2.14. The data are plotted as horizontal lines connecting the starting and ending times of each sampling run. Different symbols are used to represent the various exposure times; square boxes with dots are for 4 days, solid diamonds are for 8 days, and crosses are for longer exposure times. Because of the natural variability of both deposition rate and leaf surface characteristics, all of the samples with the same exposure period were averaged to represent the deposition flux during that period. Thus, each line represents the average of two to four samples taken from the same or different plants at the same time.

In each graph, fluxes of several different exposure times are plotted together to be easily compared. The variations of fluxes to Waxleaf Privet are in the range of 16.7 - 67.5 ng/sec m^2 for nitrate, 3.3 -12.9 ng/sec m^2 for sulfate, 0.022 - 0.20 ng/sec m^2 for lead and 3.9 - 14.0 ng/sec m^2 for calcium. The variations of fluxes to Canary Island Pine are in the range of 74.7 - 116 ng/sec m^2 for nitrate, 10.4 - 32.5 ng/sec m^2 for sulfate, 0.057 - 0.23 ng/sec m^2 for lead and 7.4 - 26.1 ng/sec m^2 for calcium. For Japanese Privet, the fluxes vary from 25.9 to 77.1 ng/sec m^2 for nitrate, 7.5 to 41.2 ng/sec m^2 for sulfate, 0.036 to 0.33 ng/sec m^2 for lead and 7.9 to 23.2 ng/sec m^2 for calcium. Among the various species, the order of the fluxes to the vegetation is the same as that to the Teflon plates, decreasing in the order nitrate, sulfate, calcium and lead.

Comparison between the Teflon plate fluxes and the vegetation fluxes can be made only for the four-day exposures. Results show that deposition rates onto the vegetation are generally greater. The average deposition fluxes are shown in Table 2.5 while values of the average deposited mass per unit area are shown in Table 2.6. Among the different kinds of vegetation, the deposition fluxes to Canary Island Pine are the greatest while those to Waxleaf Privet are the smallest. The differences are statistically significant over 95 percent confidence level except for lead to Japanese Privet which is about 60 percent and lead to Canary Island Pine and nitrate to Japanese Privet which are both about 85 percent. The fluxes to Canary Island Pine exceed those to Waxleaf Privet by an average factor of 3.0 for nitrate, 2.3 for sulfate, 1.3 for lead and 2.0 for calcium. The Japanese Privet fluxes exceed those to the

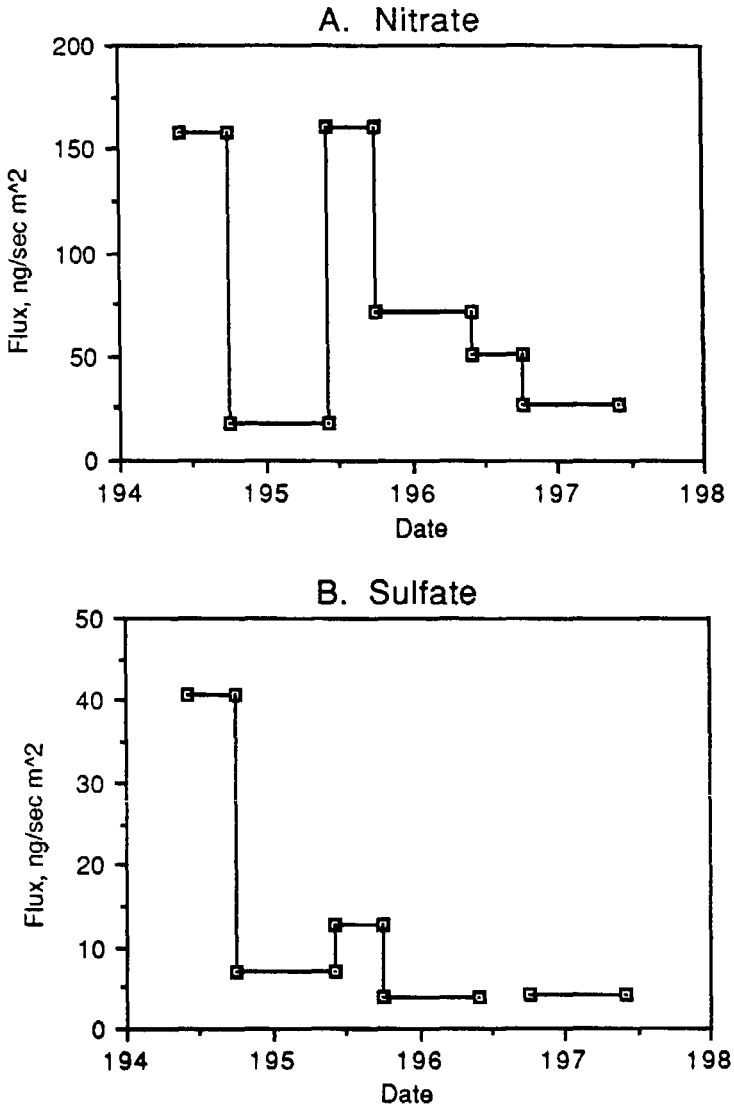

Figure 2.11 Deposition fluxes to nylasorb filter paper.

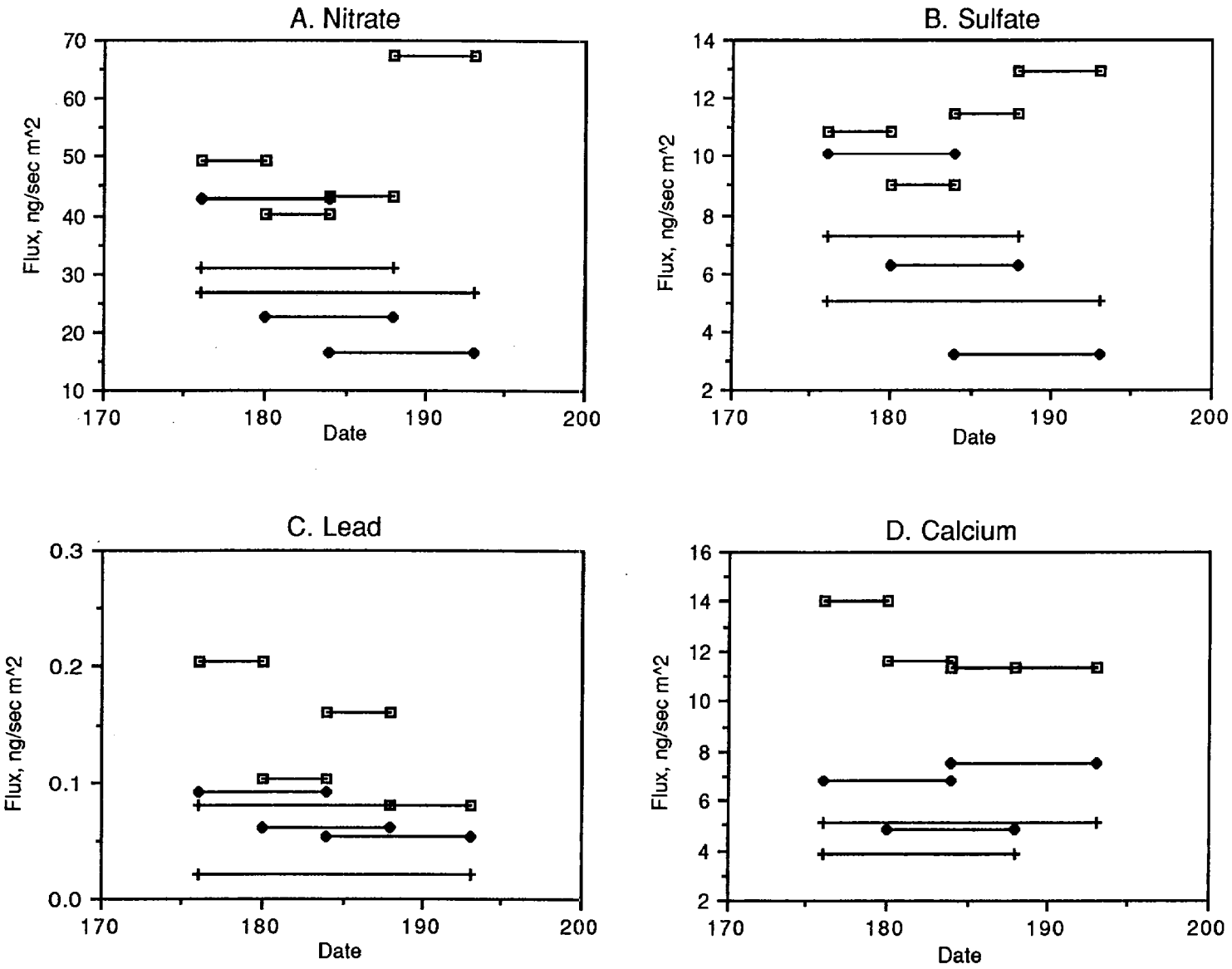

Figure 2.12 Deposition fluxes to Waxleaf Privet. Different symbols are used for various exposure times, namely squares for 4 days, diamonds for 8 days, and crosses for longer time periods.

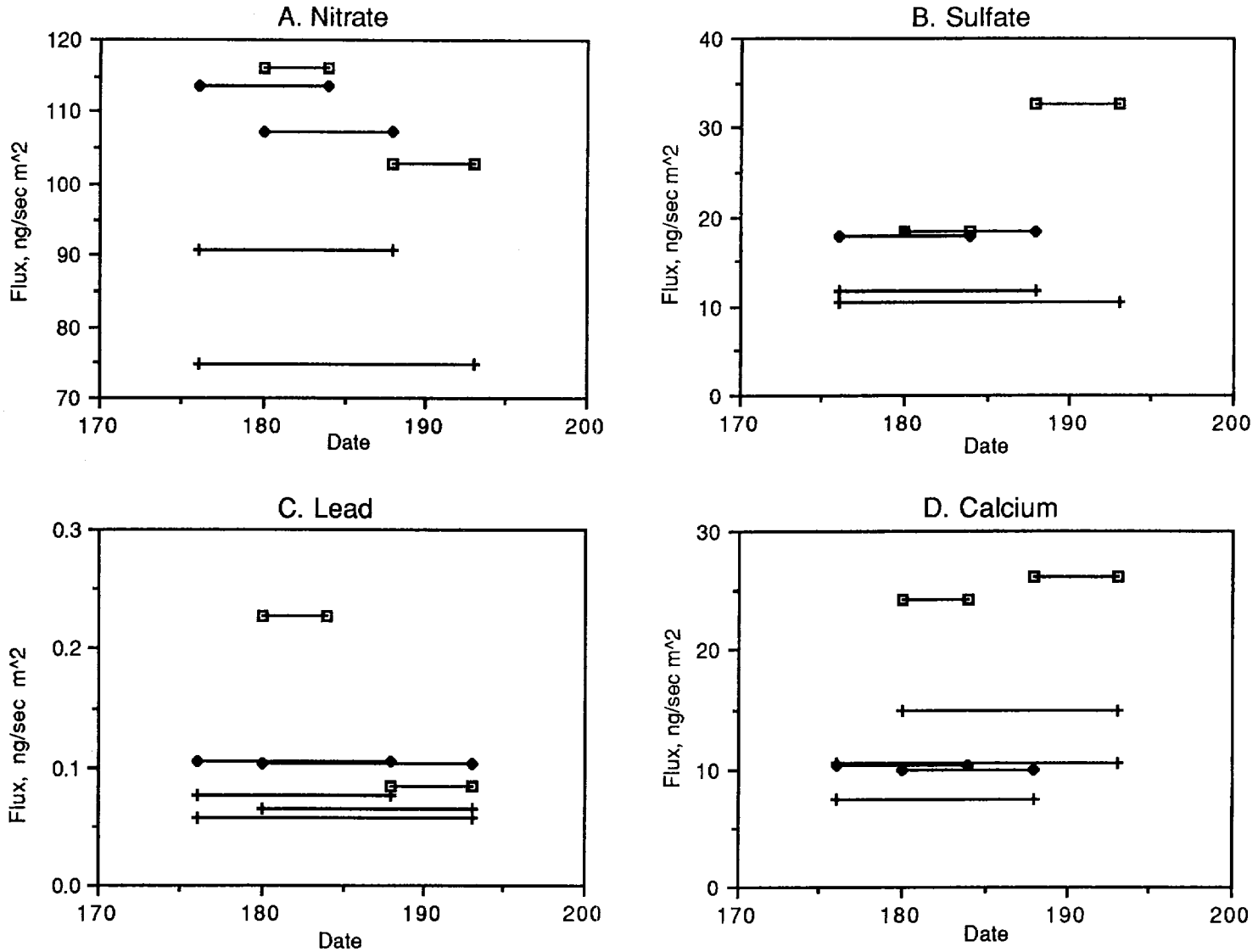

Figure 2.13 Deposition fluxes to Canary Island Pine. Different symbols are used for various exposure times, namely squares for 4 days, diamonds for 8 days, and crosses for longer time periods.

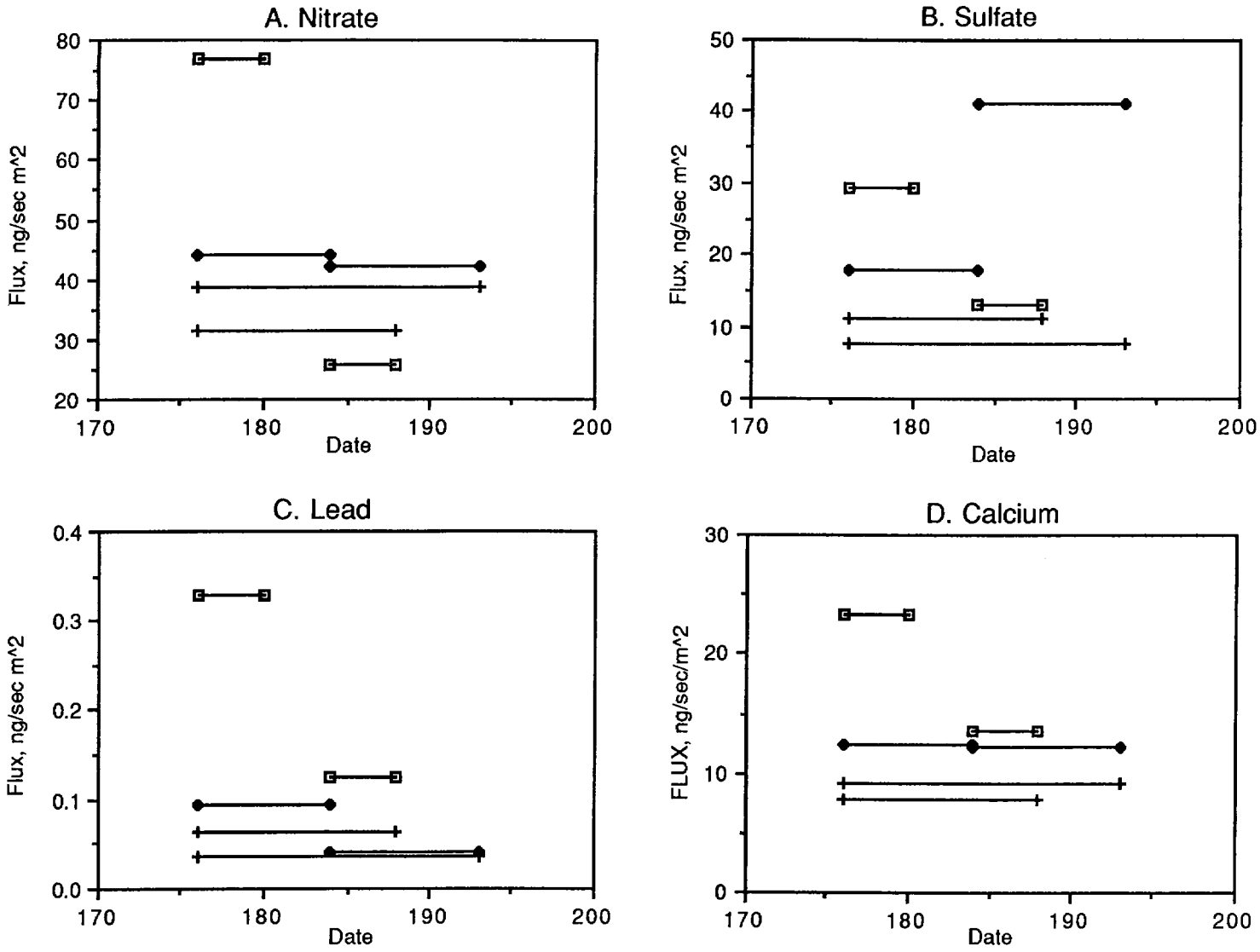

Figure 2.14 Deposition fluxes to Japanese Privet. Different symbols are used for various exposure times, namely squares for 4 days, diamonds for 8 days, and crosses for longer time periods.

	0.5 day	1 day	1.5 days	2 days	4 days
nitrate	56.8±29.1	40.6±17.0	53.7±9.4	41.7±14.6	24.0±5.1
sulfate	11.7±5.6	12.3±4.8	9.9±2.8	12.9±1.7	7.7±2.2
lead	0.072±0.043	0.112±0.041	0.070±0.027	0.082±0.026	0.079±0.026
calcium	5.4±2.5	5.7±1.6	7.2±1.5	9.0±2.2	6.5±2.9

A. Teflon plate

	4 days	8 days	12 days	16 days
nitrate	49.8±14.7	33.6±13.8	30.8±24.9	26.8±20.8
sulfate	11.0±3.5	7.7±3.8	7.2±3.9	5.0±3.7
lead	0.145±0.056	0.072±0.021	0.081±0.014	0.022
calcium	12.3±1.6	6.5±1.4	3.9	5.1

B. Waxleaf Privet

	4 days	8 days	12 days	16 days
nitrate	111.8±43.9	109.4±57.3	85.3±15.9	145.3
sulfate	23.1±8.7	11.4±13.9	11.2±1.5	22.1
lead	0.180±0.083	0.104±0.004	0.063±0.006	0.084
calcium	24.9±2.4	10.1±0.3	10.8±4.0	7.2

C. Canary Island Pine

	4 days	8 days	12 days	16 days
nitrate	51.5±36.2	43.2±1.2	31.3	38.7
sulfate	21.3±11.5	29.5±16.5	11.1	7.5
lead	0.227±0.144	0.068±0.036	0.064	0.036
calcium	18.4±6.8	12.3±0.2	7.9	9.2

D. Japanese Privet

Table 2.5 Summary of deposition fluxes to surfaces used in this study. All values are expressed in units of ng/sec m^2

	0.5 day	1 day	1.5 days	2 days	4 days
nitrate	157.9±133.4	386.7±149.9	694.1±116.1	695.7±254.6	821.9±138.0
sulfate	47.5±28.4	108.4±40.8	127.5±36.1	194.9±36.1	227.2±79.0
lead	0.24±0.19	0.94±0.33	1.03±0.37	1.30±0.61	2.37±1.13
calcium	22.9±10.4	37.4±18.0	93.4±19.6	168.3±46.1	179.8±56.2

A. Teflon plate

	4 days	8 days	12 days	16 days
nitrate	1827±705	2334±925	3180±2580	3930±3040
sulfate	401±145	530±264	748±402	736±544
lead	5.12±1.84	5.04±1.34	8.38±0.88	3.17
calcium	444.1±64.9	461.7±117.8	404.0	757.3

B. Waxleaf Privet

	4 days	8 days	12 days	16 days
nitrate	4109±1491	7470±3900	8989±1449	21217
sulfate	886±463	1238±620	1181±140	3223
lead	6.36±2.37	7.08±0.26	7.65±0.87	8.30
calcium	926±191	686.8±21.4	1046±544	1533

C. Canary Island Pine

	4 days	8 days	12 days	16 days
nitrate	1798±1302	3154±162	3237	5669
sulfate	742±417	2206±1380	1149	1104
lead	7.91±5.20	4.83±2.28	6.63	5.34
calcium	640±254	901±56	814	1340

D. Japanese Privet

Table 2.6 Summary of deposited mass per unit area to surfaces used in this study. All values are expressed in units of ng/cm^2.

Waxleaf Privet by an average factor of 1.3 for nitrate, 2.7 for sulfate, 1.2 for lead and 1.8 for calcium. These ratios represent averages of individual values of the ratio computed for each experiment. Differences in the values among the four pollutants and for the three plant species are probably due to differences in particle size distributions, vegetation surface characteristics, and transfer resistances around the plants. All of the data show that short-term exposures generally yield higher deposition fluxes, a phemonemon also found in deposition to the Teflon plates.

2.3. Discussion and Conclusions

Based on the results presented in the previous section, we reach the following conclusions :

(A). From the good agreement between conjugate samples, the uncertainties associated with co-located samplers is generally lower than 20%. These uncertainties include natural variation, sampling artifacts and limitations of instruments used for analyses. The difference between conjugate sample values is inversely proportionally to the amount of pollutant collected. Nitrate, with the greatest fluxes, has the best agreement. The fluxes of lead, which are smallest, differ most.

(B). The deposition fluxes at the Claremont A Site are generally greater than those at the Biological Station, except for calcium. The greater fluxes at the Claremont A Site may be caused by greater activity including SCAQS participants and automobiles there, as well as water spray at an adjacent field. The greater fluxes of calcium at the Biological Station are likely due to soil resuspension because of local dust at the site and the lower position of Teflon plates. Overall, the data show that the local sources at the Claremont A Site contribute slightly to the observed fluxes there.

(C). For both Teflon plates and vegetation, the fluxes decrease in the order nitrate-sulfate-calcium-lead. The short-term exposures generally have greater fluxes than longer experiments.

The differences in fluxes among the various species are caused by variations in airborne concentration and in deposition velocity; the latter is a function of particle characteristics, meteorological conditions, and surface conditions. From a recent literature review, the average deposition velocities for surrogate surfaces are 0.38 ± 0.28 cm/sec for nitrate, 0.26 ± 0.25 cm/sec for sulfate, 0.17 ± 0.16 cm/sec for lead and 2.46 ± 2.16 cm/sec for calcium [Davidson and Wu, 1988]. The large standard deviation associated with each deposition velocity implies great variability with the observed data. Generally, calcium has the greatest deposition velocity and lead has the smallest. For each contaminant, these deposition velocities are functions of atmospheric as well as surface conditions.

The greater fluxes for short-term exposures are also found in the study by John et al. [1986] for deposition to surrogate surfaces and vegetation. There are at least two possible processes responsible for this phenomenon in both the present study and that of John et al. : interactions between gaseous species and previously deposited particles, and resuspension of deposited particles. Thermodynamic equilibrium among ammonia, nitric acid and atmospheric aerosols is believed to be reached in the ambient environment [Hildemann et al.,1984; Stelson et al.,1984]. Unless a large fraction of the deposited particles is not from the atmosphere, such as local soil resuspension, the gas-particle interaction should not be significant. From the results for calcium, which is always in the form of solid particles in the ambient environment, it is likely that gas-solid interactions are not an important factor. Therefore, we assume that resuspension of deposited particles is the mechanism that causes the greater fluxes for short-term exposure.

It is of interest to consider this resuspension process theoretically. We begin with a mass balance on the deposition surface :

$$\frac{dM_i}{dt} = F_i - \beta_i M_i$$

where

M_i = deposited mass per unit area (ng/cm^2)

t = time (sec)

F_i = deposition flux (ng/sec cm^2)

β_i = resuspension rate of species i (1/sec)

Note that the resuspension rate is defined as the fraction of deposited mass resuspended per unit time [Sehmel, 1983]. Integrating the differential equation, we obtain a exponential form for deposited mass with respect to time :

$$M_i = \frac{F_i}{\beta_i}[1 - exp(-\beta_i t)]$$

$$= M_{if}[1 - exp(-\beta_i t)]$$

Here we assume the surface is clean at the beginning of sampling, that is, $M_i = 0$ at $t = 0$. Note that F_i / β_i ($= M_{if}$) represents the final and maximum amount of pollutant deposited by dry deposition per unit surface area.

The parameters are obtained by fitting the observed data with an exponential curve. The observed deposited mass and the exponential fitting are shown in Figures 2.15 - 2.17. The average deposition flux F_i and resuspension rate β_i for each species based on these plots are

summarized in Table 2.7. If the longest sampling period (i.e. 16 days for vegetation) is not represented by shorter exposures covering the entire period, then those data have not been used. For deposition to the Japanese Privet, there are only two measured data valid for the exponential fitting, preventing an exponential curve fit. Note that the intensive day sampling data are not included in the exponential fitting. There are two reasons for excluding these data. First, they represent a special case during the sampling period, that is, deposition at times of high airborne concentration. Second, the short-term exposures have variable time periods. Thus, the assumption of constant flux may not be good and the diurnal variation will bias the results.

Generally speaking, the exponential curve fits the observed data quite well. This implies that the assumed mechanism, resuspension of deposited particles, is indeed an important factor in the greater fluxes observed for short-term exposures. All the plots except for nitrate to Canary Island Pine show the effect of exposure times significantly. Many more samples are obtained for deposition to Teflon plates, resulting in better fitting for the exponential curve.

For the computed average fluxes, Canary Island Pine has the largest values for all four contaminants. It is of interest that the deposition fluxes to the Teflon plate are similar to those on the Waxleaf Privet. This is probably due to similar characteristics between both surfaces. All the resuspension rates except for nitrate to Canary Island Pine are on the order of 10^{-6} sec^{-1}.

The Teflon plate results in this study suggest that the resuspension rate is directly proportional to particle size. This is consistent with the findings of Garland [1983] in his study of resuspension of particles from soil and grass. In wind speeds from 3 to 10 m/sec, Garland [1983] has reported that the resuspension rate varies from 10^{-9} to 10^{-5} sec^{-1} for particle sizes ranging from < 1 to 5 μm. Our results lie at the upper end of the data of Garland. Future work with the SCAQS data will consider windspeeds during the experiments, enabling more meaningful comparisons with Garland's results.

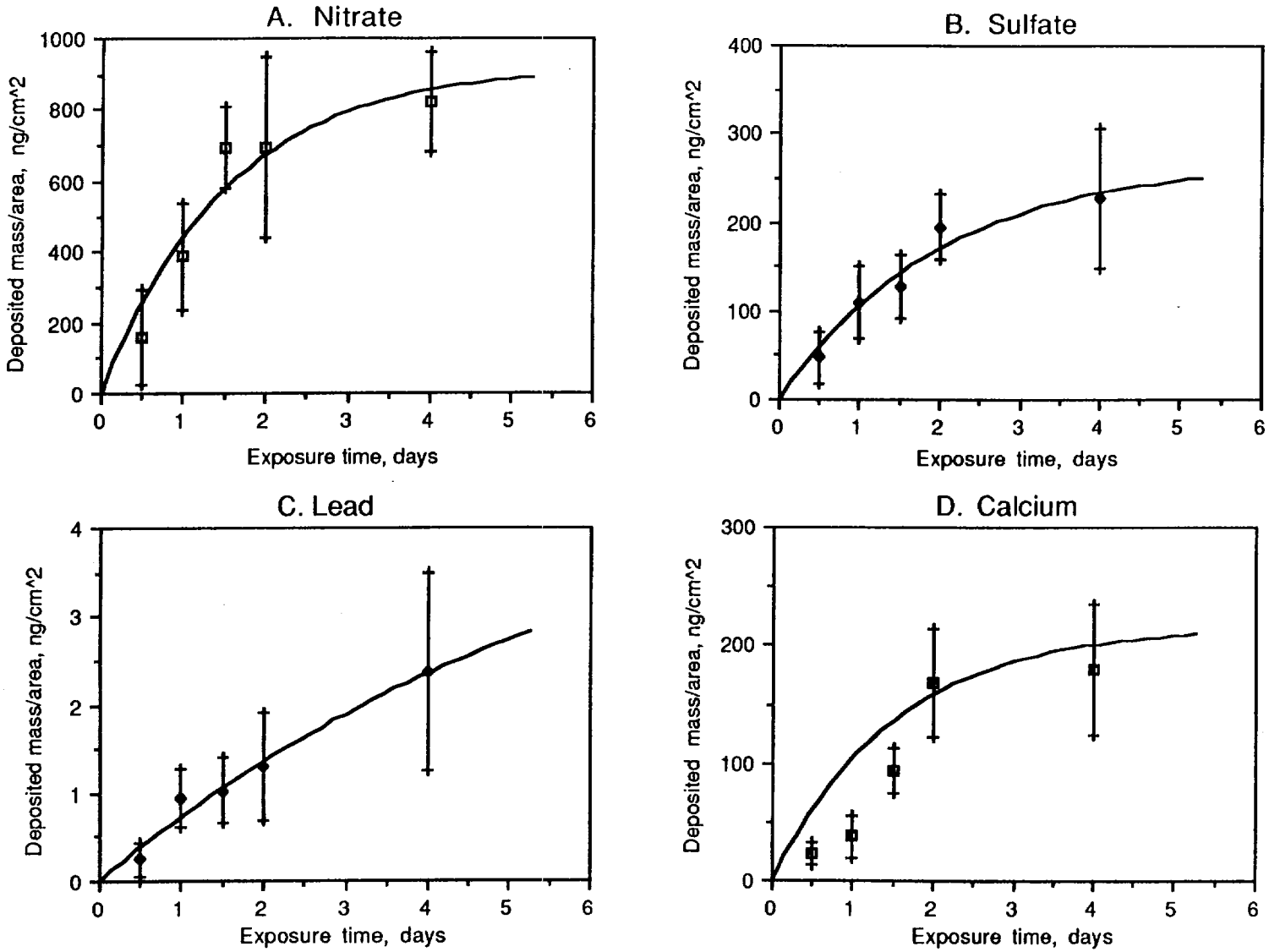

Figure 2.15 Effect of exposure time on deposition to Teflon plates.

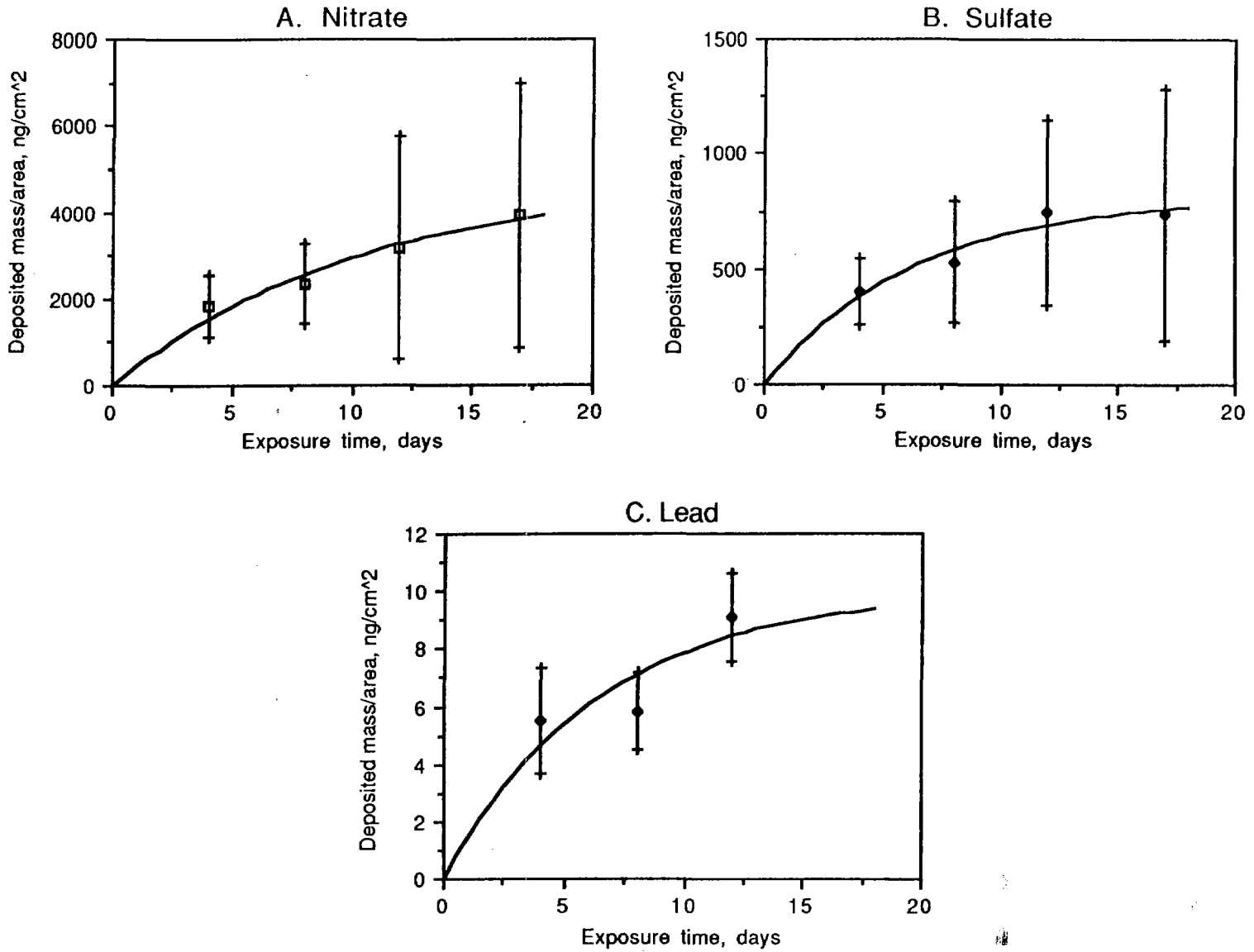

Figure 2.16 Effect of exposure time on deposition to Waxleaf Privet.

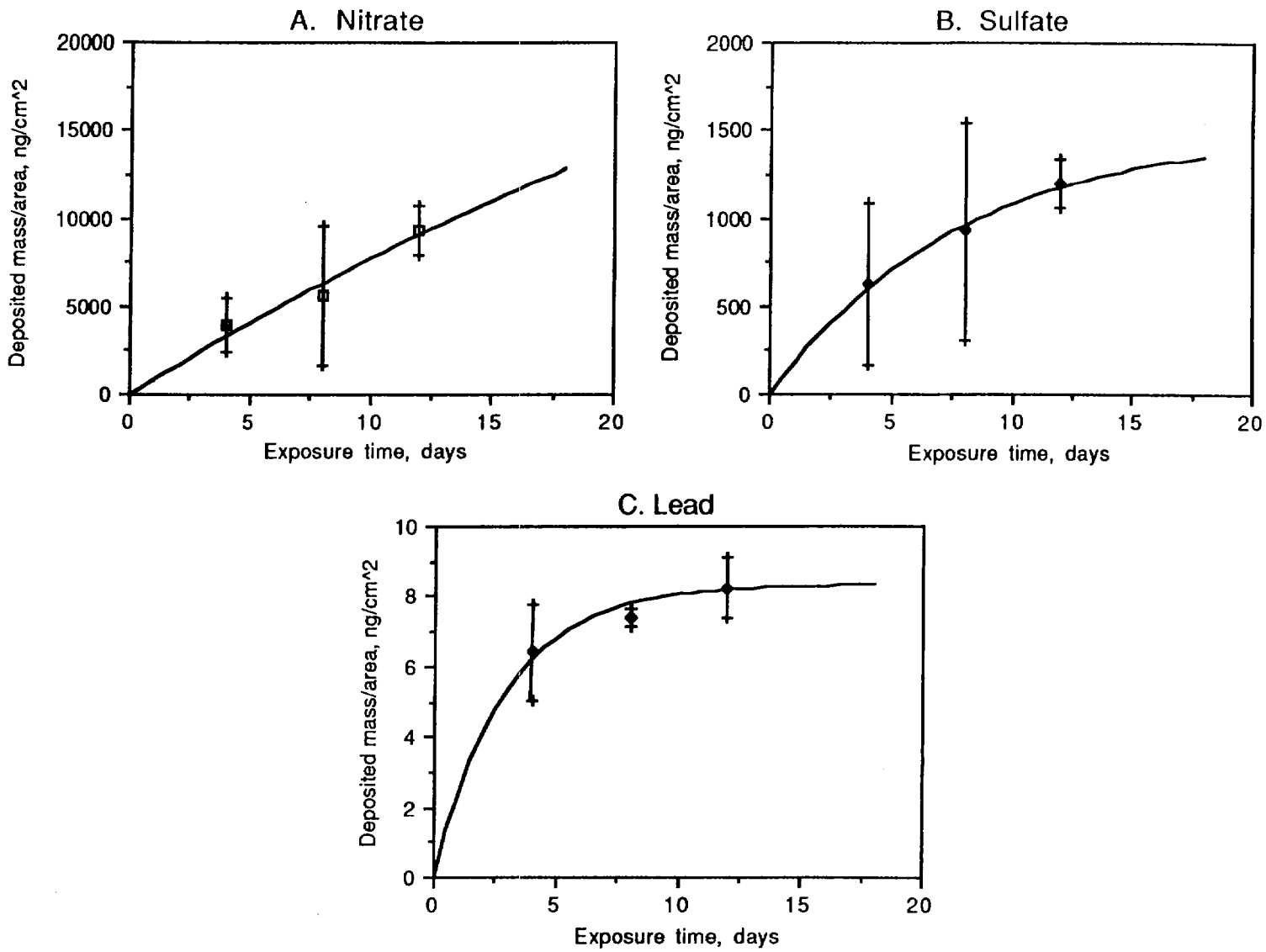

Figure 2.17 Effect of exposure time on deposition to Canary Island Pine.

surface	resuspension fitting	nitrate	sulfate	lead	calcium
Teflon plate	average flux ng/sec m^2	70.2	15.7	0.092	16.7
	resuspension rate in 10^{-6} sec^{-1}	7.6	5.8	1.8	7.7
	max. exposure time, hours	3.8	5.0	16	3.7
Waxleaf Privet	average flux ng/sec m^2	53.5	14.9	0.18	
	resuspension rate in 10^{-6} sec^{-1}	1.1	1.8	1.8	
	max. exposure time, hours	26	16	16	
Canary Island Pine	average flux ng/sec m^2	99.0	22.1	0.33	
	resuspension rate in 10^{-6} sec^{-1}	2.5	1.5	4.0	
	max. exposure time, hours	115	19	7.2	

Table 2.7 Summary of parameters for resuspension fitting. Maximum exposure time refers to the longest possible exposure period where resuspension accounts for loss of less than 5% of the deposited mass.

Chapter 3
Extended Southern California Air Quality Study

The Southern California Air Quality Study was extended from August 26 to September 3 because there were fewer than 12 intensive runs during June and July due to low smog levels. The field work durinig this extended period was conducted by a student at the Claremont Colleges. There were four airfoils used in the extended study to measure the deposition of nitrate and sulfate; the other six airfoils were used at Emerald Lake at the same time (see Chapter 5). Two kinds of surrogate surfaces were used, Teflon plates and nylasorb filter paper. Note that no foliar extraction was done in the extended study.

3.1. Experiment Methods

The four airfoils were set up at the Biological Station; prior to August 28 two were set up with Teflon plates and the other two with nylasorb filter paper. All four airfoils were used with Teflon plates after August 28. All of the airfoils were run with the same schedule, 12 hours or 24 hours, providing duplicate samples of both types of surfaces. The collection procedures were the same as those described in Chapter 3. After collection, the samples were sent back to CMU and were kept frozen until they were analyzed. The analyses of nitrate and sulfate in all samples by IC were conducted at CMU.

One blank was made for every sample, including both Teflon plates and nylasorb filter paper samples. The blanks were made in the same way as the samples except that the exposure times of the blanks were very short. Both the Teflon plate blank and the sample were obtained from the same plate and airfoil. The Teflon plate was washed in the field immediately prior to extraction of the blank. The net amount of contaminant deposited on the plate was taken as the difference between sample and the corresponding blank. The nylasorb filter paper sample and blank were made from different sheets of filter paper, but we assume that all of the sheets have similar levels of contaminant since they are from the same batch. The net amount of contaminant deposited on the nylasorb filter was taken as the difference between the sample and the average of all nylasorb blanks.

3.2. Results

In total, there are 34 Teflon plate samples and 6 nylasorb filter paper samples. One of the Teflon plate samples was lost because of leakage during shipping. Five of the Teflon plate blanks were lost for the same reason. Thus, there are only 29 Teflon plate blanks, and 28 sets of sample/blank pairs.

The comparison of concentrations in the Teflon plate blanks and samples is shown in Figure 3.1. The Julian date for of each comparison is listed in Table 3.1. Data for airfoils #1 and #2 are plotted in one set of graphs, while data for airfoils #9 and #10 are plotted in a second set of graphs. The ratio of sample/blank varies from 0.43 to 14.5 for nitrate (average$\pm$standard deviation : 6.1$\pm$4.8) and from 0.11 to 27.1 for sulfate (average$\pm$standard deviation : 5.0$\pm$5.6). The average concentrations of blanks in units of ng/cm^2 are 118$\pm$104 for nitrate and 40$\pm$37 for sulfate. These blanks have much higher concentrations of contaminant than those made in June and July, 8.1 times greater for nitrate and 14.4 times greater for sulfate. Note that some of blanks have higher concentrations than the corresponding samples, leading to negative net sample values. These negative values, and those samples without corresponding blanks, are not included in the following analysis.

The concentrations in the nylasorb filter paper blanks are higher than those in the Teflon plate blanks. The averages are 310$\pm$41.6 for nitrate and 208$\pm$205 for sulfate. This yields sample/blank ratios for the nylasorb filter paper which are too small to allow meaningful data. The comparison of concentrations between blanks and samples is shown in Figure 3.2 and the exposure time of each sample number is shown in Table 3.2.

The deposition fluxes of nitrate and sulfate to the Teflon plates are plotted in Figure 3.3. The flux to each individual plate is plotted as a horizontal line connecting the starting and ending times for the particular run. For the first three runs, only fluxes from airfoils #1 and #2 are plotted because the surfaces placed on airfoils #9 and #10 were nylasorb filter paper during this period. The average difference between the simultaneous samples shown in Figure 3.3 is 22.4$\pm$19.3% for nitrate and 23.2$\pm$23.8% for sulfate. The average fluxes are plotted in Figure 3.4. The fluxes of nitrate are always greater than those of sulfate. Strong diurnal variation is found for nitrate with much greater fluxes during the day. The diurnal variation is also found for sulfate, although not as pronounced.

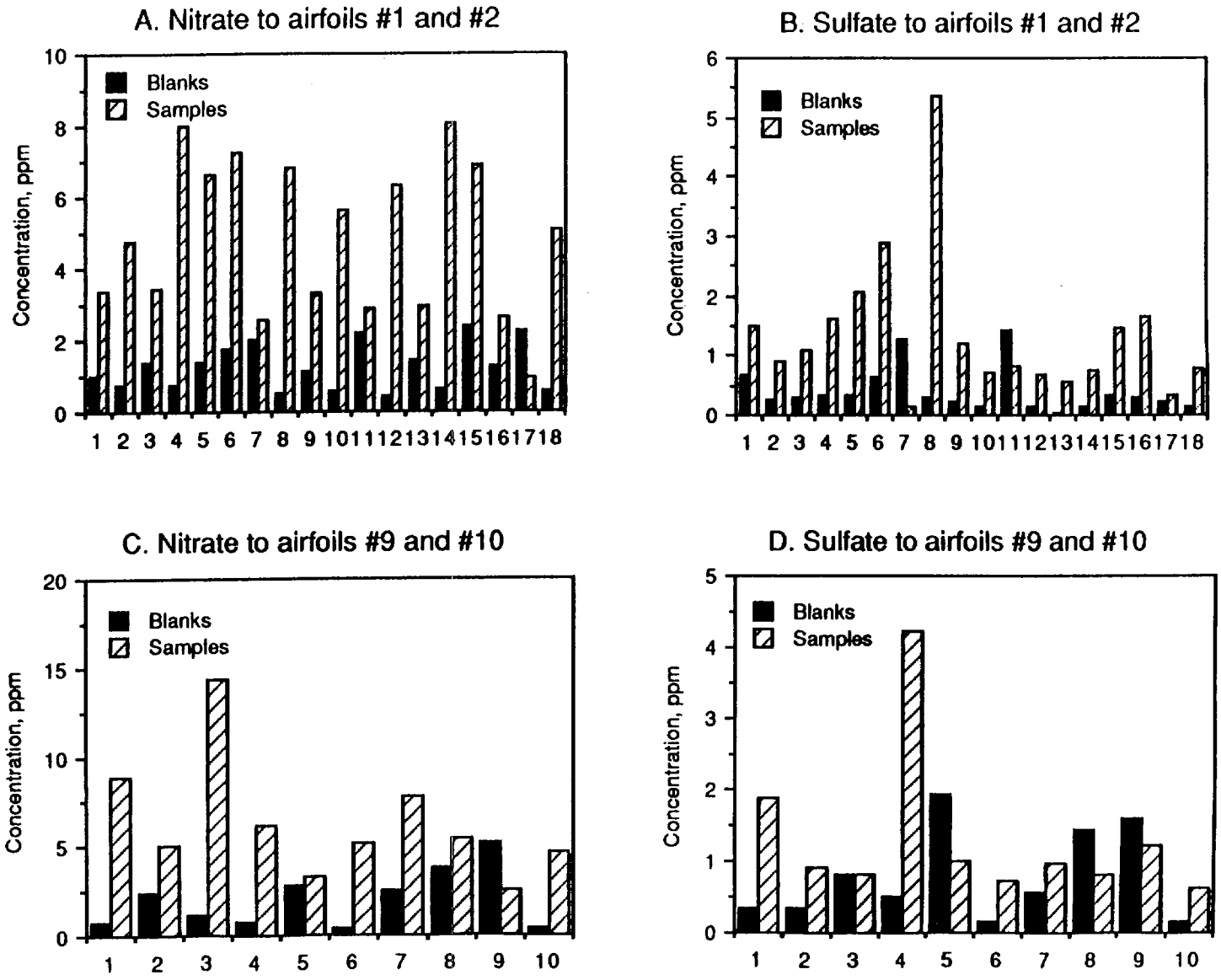

Figure 3.1 Comparison of samples and blanks from Teflon plates during extended sampling in August and September.

sample number	1	2	3	4	5	6	7
airfoil	#1	#1	#1	#1	#1	#1	#1
date	238.75	239.29	239.75	240.29	240.75	241.66	244.79
sample number	8	9	10	11	12	13	14
airfoil	#1	#1	#1	#2	#2	#2	#2
date	245.35	245.81	246.35	238.75	239.29	239.75	240.29
sample number	15	16	17	18			
airfoil	#2	#2	#2	#2			
date	240.75	244.79	245.81	246.35			

Table 3.1(a) The sampling dates and the airfoil numbers for the samples in parts A and B of Figure 3.1.

sample number	1	2	3	4	5	6	7
airfoil	#9	#9	#9	#9	#9	#9	p #10
date	240.29	240.75	241.66	245.35	245.81	246.35	240.29
sample number	8	9	10				
airfoil	#10	#10	#10				
date	241.66	244.79	246.35				

Table 3.1(b) The sampling dates and the airfoil numbers for the samples in parts C and D of Figure 3.1.

sample number	1	2	3	4	5	6
airfoil	#9	#9	#9	#10	#10	#10
date	238.75	239.29	239.75	238.75	239.29	239.75

Table 3.2 The sampling dates and the airfoil numbers for the samples in Figure 3.2.

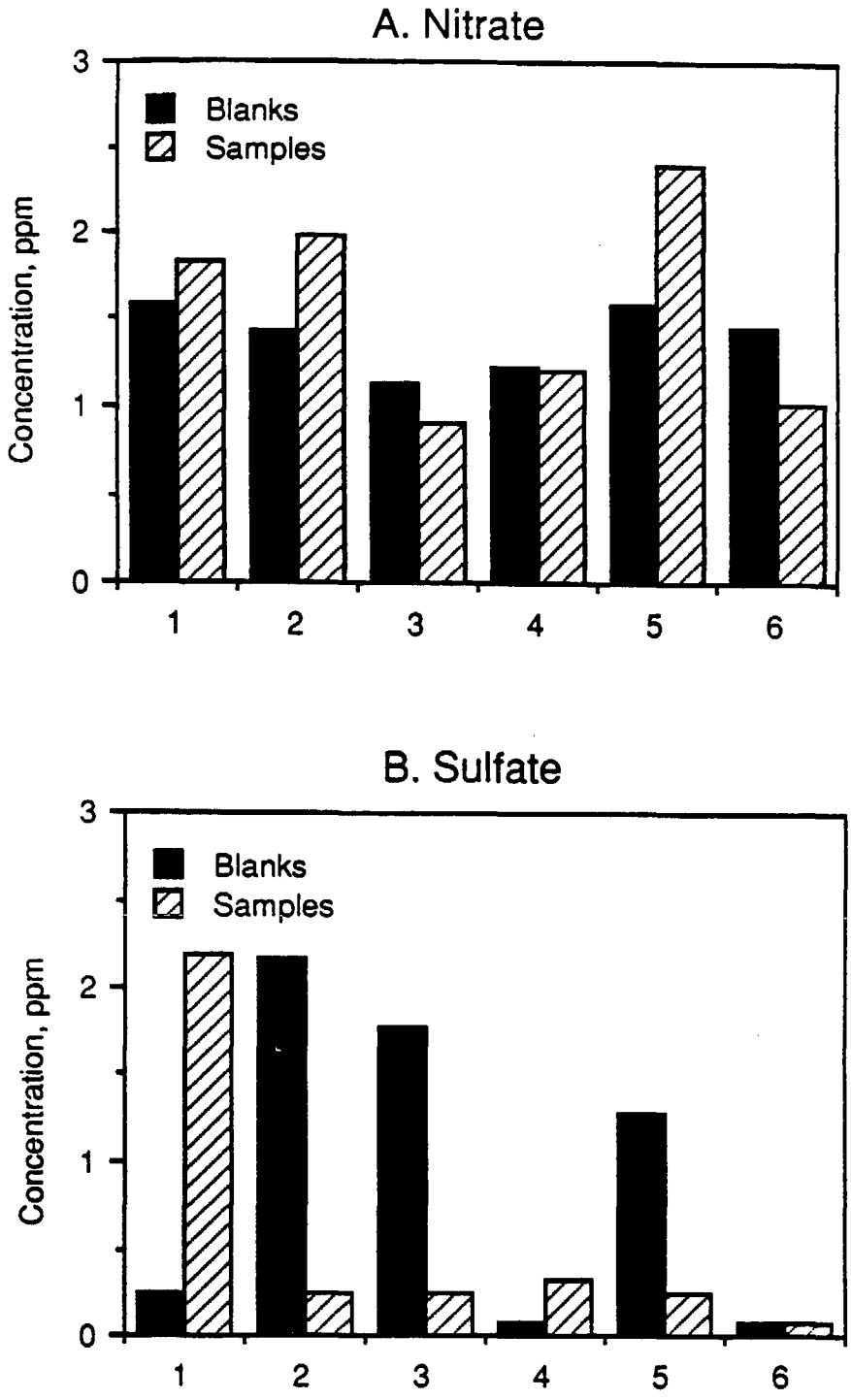

Figure 3.2 Comparison of samples and blanks from nylasorb filter paper extended sampling in August and September.

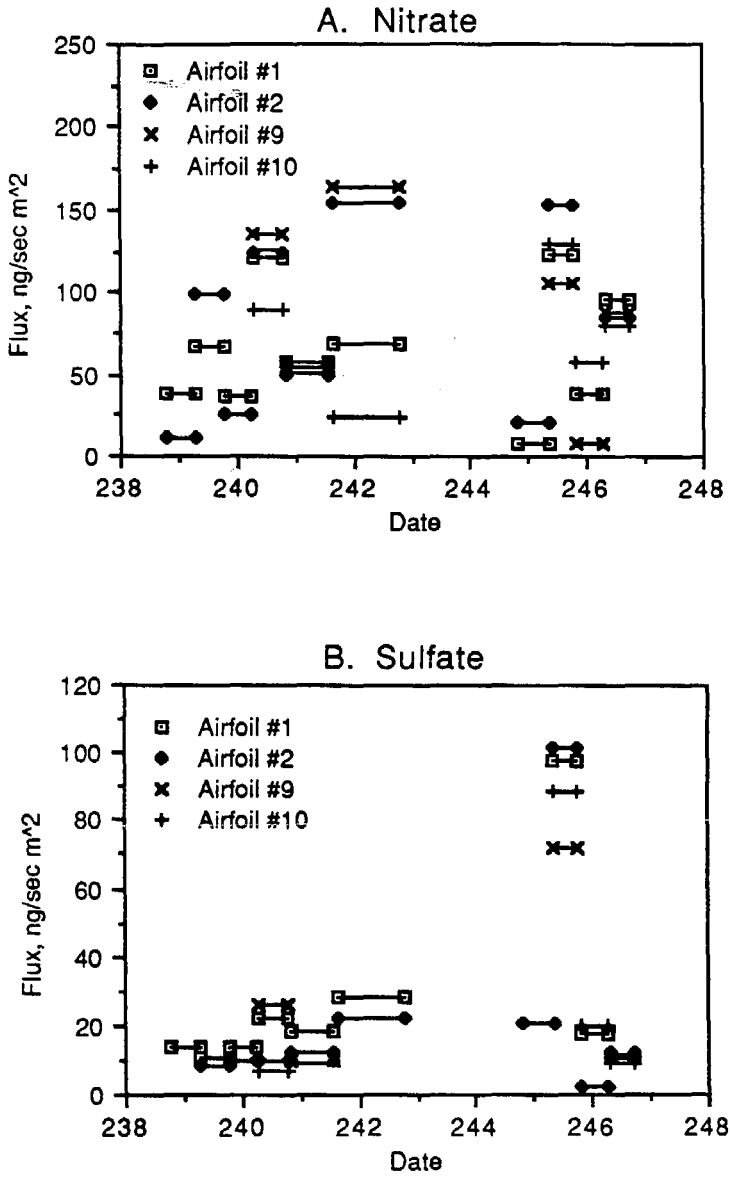

Figure 3.3 Comparison of simultaneous fluxes to Teflon plates during extended sampling in August and September.

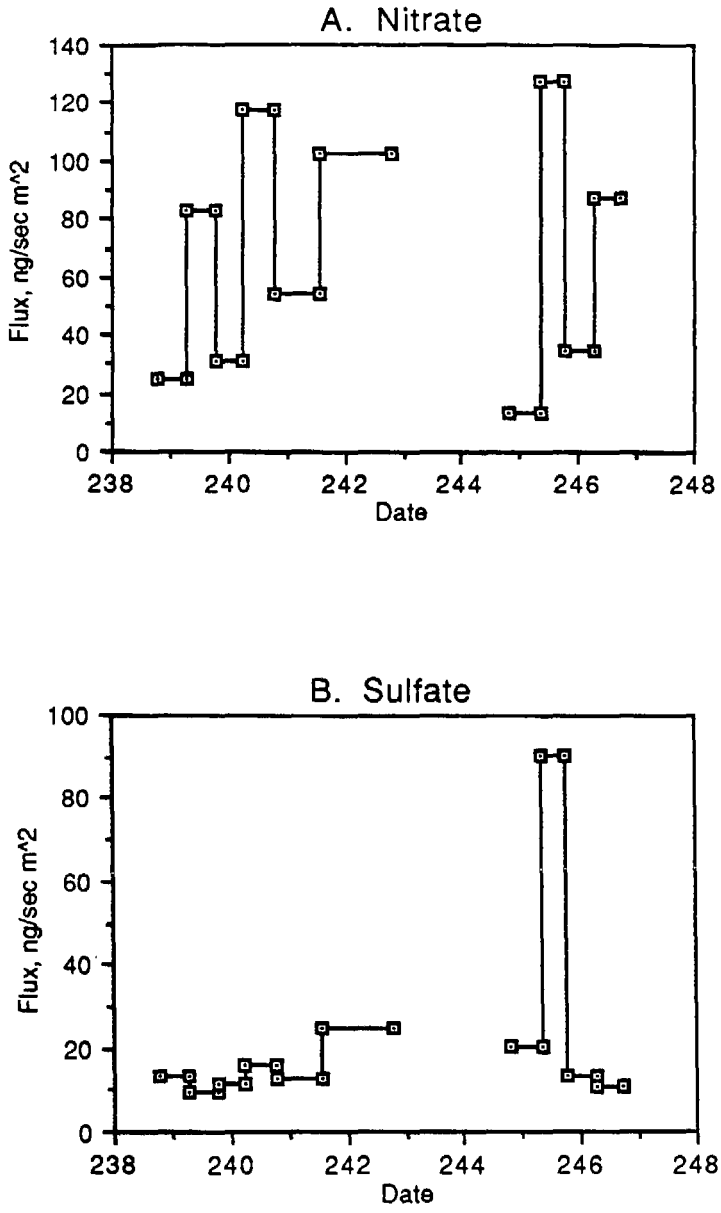

Figure 3.4 Deposition fluxes to Teflon plates during extended sampling in August and September.

3.3. Conclusions

The high concentrations of blanks, especially for the nylasorb filter paper, are responsible for the poor agreement among the simultaneous samples. The large amounts of contaminant in the blanks probably result from improper handling in the field. Despite these problems, the extended study data are consistent with values of the fluxes measured during June and July. Further comparison is difficult because airborne concentrations are not yet available.

Chapter 4

Dry Deposition onto Aerodynamic Surfaces at Emerald Lake in Sequoia National Park

After the June and July SCAQS experiments in Los Angeles, some of the airfoils were used at Emerald Lake in Sequoia National Park to measure the dry deposition of nitrate and sulfate. The field work was conducted from August 11 to September 30 by Air Resources Board contractors. Two different kinds of surfaces, Teflon plates and nylasorb filter paper, were mounted on top of airfoils to measure the deposition of nitrate, sulfate and nitric acid gas. Because of rain from mid-August to mid-September, only six runs were successful. This includes all four of the 2-day runs and another 2 runs with one-week exposure. The numbers of samples and blanks are listed in Table 4.1.

Type of surface	Exposure time	Number of samples	Number of blanks
Teflon surface	2 days	7	8
	7 days	4	2
nylon filter	2 days	8	8
	7 days	4	4

Table 4.1 Numbers of samples and blanks for deposition to aerodynamic surfaces at Emerald Lake.

4.1. Experimental Methods

Teflon-coated aluminum plates and nylasorb filter paper were used as deposition surfaces in this study. The experimental methods were similar to those used in SCAQS. The Teflon plate samples were digested with distilled/deionized water immediately after removal from the airfoils. The nylasorb filter paper samples were put into polyethylene tubes. Both were then shipped back to CMU and were kept refrigerated until analysis. All of the samples were analyzed by ion chromatography at CMU.

Like the sampling in SCAQS, two identical surfaces were set up side-by-side to duplicate the sampling. The comparison between the two simultaneous samples illustrates the

experimental uncertainties associated with the sampling method. Four two-day sampling experiments were run at the beginning of the study, then the exposure time was changed to one week for the duration of the project. One blank was made for every sample, including both Teflon plates and nylasorb filter paper. The blanks were made in the same way as the samples except that the exposure times of the blanks were less than 5 minutes. Because the Teflon plate blanks and samples were made from the same plate and airfoil, the concentration of each individual blank was subtracted from that of the corresponding sample. For nylasorb filter paper, the blank and sample were made from different pieces of filter paper. However, all the nylasorb filter paper samples were from the same batch. We have assumed that all the paper samples have similar background levels of each chemical species and that the contamination from handling is completely random. Thus the average of all of the blanks, instead of each individual blank, has been subtracted from the samples of nylasorb filter paper.

4.2. Results

The comparison of the concentrations in blanks and samples is shown in Figure 4.1 and the exposure time of each sample number is listed in Table 4.1. The concentrations of blanks from the Teflon plates have much greater variation than those from nylasorb filter paper. The average concentration in the Teflon plate blanks is 41.0 ± 24.3 for nitrate and 104 ± 127 ng/cm^2 for sulfate. For nylasorb filter paper, the average is 92.3 ± 30.8 for nitrate and 4.6 ± 7.8 ng/cm^2 for sulfate. Note that some of the blanks from the nylasorb filter paper have concentrations of sulfate below 5 ppb, the detectable level for the CMU ion chromatagraph.

The blanks from the Teflon plates in the Emerald Lake study are much higher than those made in SCAQS in June-July, averaging three times higher for nitrate and 38 times higher for sulfate. Note that some blanks have higher concentrations than the corresponding Teflon plate samples. There are many possible sources of contamination, including water used to digest the Teflon plate samples, unclean plates, and problems during handing; the exact sources of the contamination are unknown. The samples which have lower concentrations than the corresponding blanks are excluded from the following analysis.

The deposition fluxes of nitrate and sulfate to Teflon plates which were mounted in airfoils #7 and #8 are shown in Figure 4.2. The flux to each individual plate is plotted versus the exposure period which is expressed by Julian calendar date. The data are plotted as horizontal lines connecting the midpoints of triangles or X's. The midpoints represent the starting and ending times of a particular sampling run. The agreement between the samples which were exposed simultaneously is not as good for deposition to Teflon plates as during SCAQS; values differ by $53.9 \pm 10.8\%$ for nitrate and $23.1 \pm 8.6\%$ for sulfate. The results of deposition to nylasorb filter paper are plotted in the same way, shown in Figure 4.3. For these

sample number	1	2	3	4	5	6	7	8
airfoil	#7	#7	#7	#7	#7	#7	#8	#8
date	217	221	223	225	257	266	217	221

sample number	9	10	11	12
airfoil	#8	#8	#8	#8
date	223	225	257	266

Table 4.2(a) The sampling dates and airfoil numbers for the samples in parts A and B of Figure 4.1.

sample number	1	2	3	4	5	6	7	8
airfoil	#3	#3	#3	#3	#3	#3	#4	#4
date	217	221	223	225	257	266	217	221

sample number	9	10	11	12
airfoil	#4	#4	#4	#4
date	223	225	257	266

Table 4.2(b) The sampling dates and airfoil numbers for the samples in parts C and D of Figure 4.1.

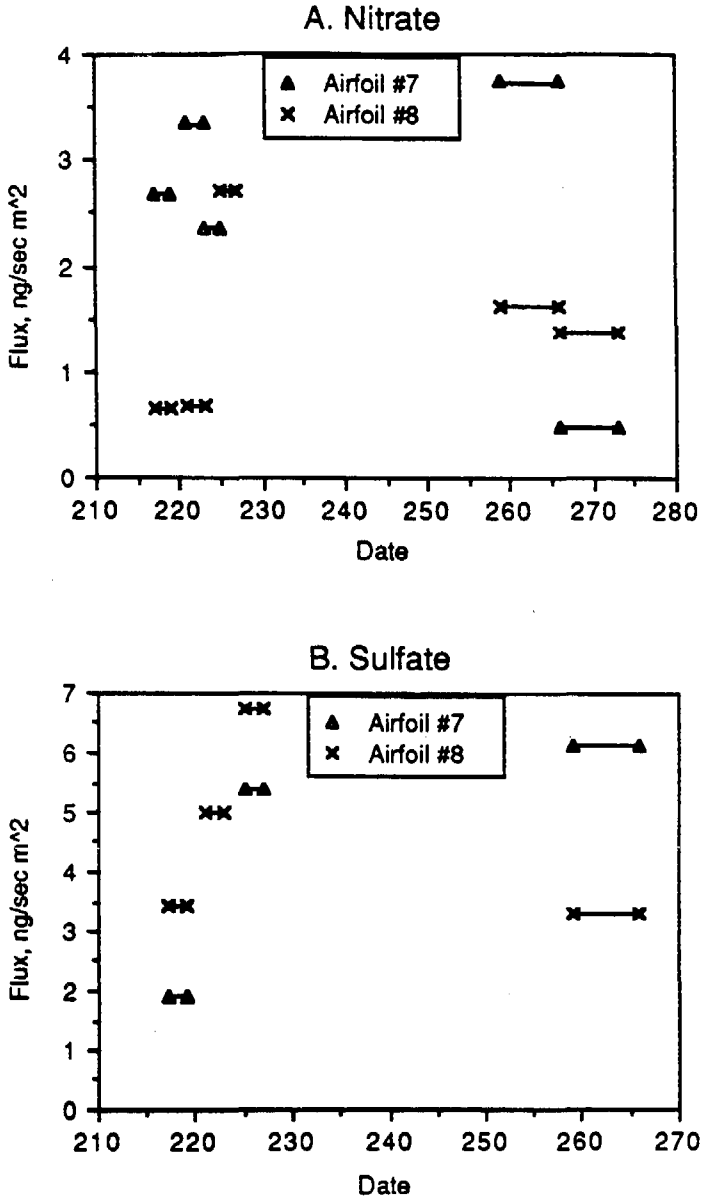

Figure 4.2 Deposition fluxes to Teflon plates at the Emerald Lake.

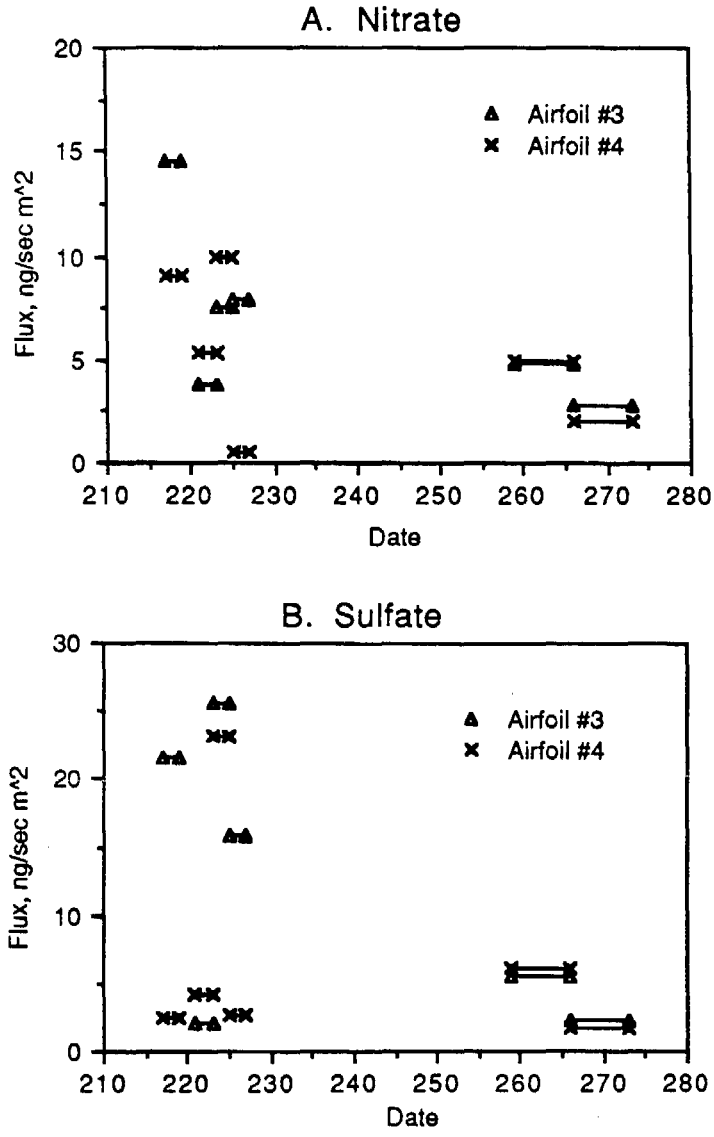

Figure 4.3 Deposition fluxes to nylasorb filter paper at Emerald Lake.

two airfoils, the triangles represent the deposition to airfoil #3 and the X's represent the deposition to airfoil #4. None of the blanks from nylasorb filter paper has a higher concentration than any of the samples, so all of the samples are included in the plots. The agreement between simultaneous samples is 26.7±28.5% for nitrate and 34.9±30.5% for sulfate.

The average fluxes to both surfaces are summarized in Table 4.2. Some of the data to the Teflon plates are the results of only one sample because the conjugate has been lost. The fluxes to the Teflon plates range from 0.93 to 2.7 ng/sec m^2 for nitrate (2.06±0.68) and from 2.7 to 6.1 ng/sec m^2 for sulfate (4.91±1.38). For each sample, the flux of sulfate is always greater than that of nitrate, by a ratio averaging 2.0±0.4. For the deposition to nylasorb filter paper, the fluxes of nitrate range from 2.5 to 11.8 ng/sec m^2 (6.10±3.45) and those of sulfate range from 1.9 to 24.4 ng/sec m^2 (9.45±8.23). Note that the deposition fluxes of nitrate to nylasorb filter paper are always greater than the corresponding fluxes to the Teflon plates for nitrate. In contrast, the fluxes of sulfate to the nylasorb filter paper are highly variable, sometimes greater and sometimes smaller than those to the Teflon plates. The greater fluxes of nitrate to the nylasorb filter paper are from the deposition of nitric acid gas; the difference is taken as the deposition flux of this gas. Values of the nitric acid fluxes are also shown in Table 4.2. The difference in the sulfate fluxes between both surfaces is caused by different surface characteristics influencing deposition of sulfate particles as well as some deposition of sulfur dioxide [Chen et al.,1986; Cadle and Mulawa,1987].

Bytnerowicz and Olszyk [1987] reported that the deposition fluxes to nylon filter paper in the units of ng/sec m^2 are 9.97±2.60 for nitrate and 0.92±1.08 for sulfate and those to Whatman 41 filter paper are 12.0±5.74 for nitrate and 2.09±1.17 for sulfate. Their mean fluxes of nitrate are greater than those in this study. In contrast, they found smaller fluxes of sulfate. The different materials and configurations used in both studies may be important factors for the differences. Vandenberg and Knoerr [1985] have found a wide range of deposition rates to various surrogate surfaces and Davidson et al. [1985] have shown the effect of collector geometry and material on deposition rate.

4.3. Conclusions

The high concentrations of blanks, imperfect agreement between simultaneous exposures and the small number of samples limit amount of data interpretation that can be conducted. The study still shows some consistent results which illustrate differences between dry deposition at Emerald Lake and in the Los Angeles area. A key difference is the much smaller deposition of nitrate at Emerald Lake than in LA. The deposition of sulfate, in contrast, appears to be only slightly smaller at Emerald Lake than in LA area. It is also of interest to compare nitrate and sulfate fluxes at the two sites: nitrate exceeds sulfate by a

exposure time,days	2	2	2	2	7	7
date	217-219	221-223	223-225	225-227	259-266	266-273
nitrate	1.67	2.01	2.36	2.71	2.69	0.93
sulfate	2.69	5.01		6.06	6.06	4.72

A. Teflon plate

exposure time,days	2	2	2	2	7	7
date	217-219	221-223	223-225	225-227	259-266	266-273
nitrate	11.76	4.55	8.73	4.19	4.91	2.46
sulfate	12.02	3.22	24.40	9.29	5.83	1.93

B. Nylasorb filter paper

exposure time,days	2	2	2	2	7	7
date	217-219	221-223	223-225	225-227	259-266	266-273
nitric acid	10.09	2.55	6.37	1.47	2.22	1.54

C. Flux of nitric acid gas

Table 4.3 Summary of fluxes to Teflon plates and nylasorb filter paper. All values are given in units of ng/sec m^2

significant margin in LA, but is actually slightly smaller than sulfate at Emerald Lake. These differences will be explored further when airborne concentration data are available.

Chapter 5
Summary

Aerodynamic surrogate surfaces employing Teflon plates and nylasorb filter paper were used to measure dry deposition in three sets of field experiments. The first set involved sampling at Claremont during the Southern California Air Quality Study (SCAQS) in June and July 1988. The second set involved sampling at the same location during an extension of SCAQS in August and September 1988. Finally, the third set included sampling at Emerald Lake in Sequoia National Park. Three species of vegetation (Waxleaf Privet, Canary Island Pine, and Japanese Privet) were also used to assess dry deposition during the first set of field experiments.

For the first field program, measurable dry deposition fluxes have been obtained for nitrate, sulfate, lead, and calcium. The Teflon plates yielded satisfactory results for sampling periods as short as four hours. The vegetation sampling yielded satisfactory results for periods as short as four days, although it is likely that good results can be obtained for even shorter periods such as 1 - 2 days.

The fluxes of all four contaminants on the Teflon plates are highly variable. Values (in ng/sec m^2) cover the following ranges: nitrate 7 - 213, sulfate 2 - 64, lead 0.035 - 0.46, and calcium 1.2 - 20.7. Results for the nylasorb filter paper and vegetation are roughly comparable. In general, deposition on the Canary Island Pine shows the greatest values, exceeding those on the Teflon plates and nylasorb filter paper by factors of 2 -3. Fluxes onto the Japanese Privet are only slightly lower than those onto Canary Island Pine, while fluxes onto the Waxleaf Privet are nearly the same as those on the Teflon plates and filter paper. These values are for experiments at the Biological Station; a smaller number of additional experiments with similar results using only Teflon plates were conducted at the SCAQS Claremont A Site at the Claremont Colleges.

One of the interesting findings in this study is the effect of exposure time on the observed deposition fluxes. Generally, short-term exposures yield greater deposition fluxes for both deposition to the Teflon plates and to vegetation. Resuspension of deposited particles is probably responsible for this phenomenon. Based on the assumed mechanism of resuspension from deposited particles, it is found that the resuspension rates of all four species from any surface are in the order of 10^{-6} sec^{-1}.

Only limited data are available from the second and third sets of field experiments. The results are generally consistent with the June - July SCAQS data, although nitrate fluxes are considerably smaller at Emerald Lake compared with Claremont. Sulfate fluxes at Emerald Lake are only slightly smaller than in Claremont.

In the future work, the following are recommended to evaluate use of the aerodynamic surface for routine monitoring :

- To develop some measures to protect the aerodynamic surface from contamination by rain, birds, and insects.
- To use with different kinds of surface material to study the deposition of other species like nitric acid and sulfur dioxide.
- To explore the mechanisms responsible for the effect of exposure times. This will probably involve both wind tunnel studies and field work.
- To compare the deposition to Teflon plates with deposition to other kinds of vegetation in more detailed studies.

Finally, it should be noted that final conclusions from this study require the use of airborne concentration data so that deposition velocities can be computed. At the time of preparation of this report, such data were not available. We expect that a considerable amount of additional information will be obtained from this study when the airborne concentration data from other groups are used. This will result in preparation of additional manuscripts for publication in Conference Proceedings or Journals, copies of which will be forwarded to The California Air Resources Board.

References

Appel B. R., Kothny E. L., Hoffer E. M. and Wesolowksi J. J. (1980) Sulfate and nitrate data from the California aerosol characterization experiment (ACHEX), in The Character and Origins of Smog Aerosols, Advances in Environmental Science and Technology, vol. 9, p 315.

Bytnerowicz A., Miller P. R. and Olszyk D. M. (1987) Dry deposition of nitrate, ammonium and sulfate to a *Ceanothus crassifolius* canopy and surrogate surfaces, Atmospheric Environment 21 : 1749-1757.

Cadle S. H. and Mulawa P. A. (1987) The retention of SO_2 by nylon filters, Atmospheric Environment 21 : 599-603.

Cebeci T. and Bradshaw P. (1977) Momentum Transfer in Boundary Layer, Hemisphere Publishing Corp., Washington, DC.

Chan W. H., Orr D. B. and Chung D. H. S. (1986) An evaluation of artifact SO_4^{2-} formation on nylon filters under field conditions, Atmospheric Environment 20 : 2397-2401.

Chow C. Y. (1979) An Introduction to Computational Fluid Mechanics, pp 134-153.

Davidson C. I., Lindberg S. E., Schmidt J. A., Cartwright L. G. and Landis L. R. (1985) Dry deposition of sulfate onto surrogate surfaces, J. Geophysical Research 90 : 2123-2130.

Davidson C. I. and Wu Y. L. (1988) Dry deposition of particles and vapors, in : Acid Precipitation, Adriano D. C.(editor), Springer-Verlag, New York, NY (in press).

Evans H. L. (1968) Laminar boundary-layer theory, Addison-Wesley Publishing Company, Reading, MA.

Galloway J. N., Whelpdale D. M. and Wolff G. T. (1984) The flux of S and N eastward from North America, Atmospheric Environment 18 : 2595-2607.

Gamble J. S. (1986) M.S. Thesis, Carnegie Mellon University, Department of Civil Engineering.

Garland J. A. (1983) Some recent studies of the resuspension of deposited material from soil and grass, in : Precipitation Scavenging, Dry Deposition, and Resuspension, vol. 2, Pruppacher H. R., Semonin R. G. and Slinn W. G. N.(editors), Elsevier Science Publishing Co., Inc., New York, NY, pp 1087-1097.

Hess J. L. (1975) Review of integral-equation techniques for solving potential-flow problems with emphasis on the surface-source method, Computer Methods in Applied Mechanics and Engineering, 5 : 145-196.

Hicks B. B., Wesely M. L. and Lindberg S. E. (1986) Proceedings of the NAPAP Workshop on Dry Deposition, Harpers Ferry, WV., March 25-27.

Hosker R. P. and Lindberg S. E. (1982) Review: Atmospheric deposition and plant assimilation of gases and particles, Atmospheric Environment 16 : 889-910.

John W., Wall S. M. and Ondo J. L. (1985) Dry acid deposition on materials and vegetation : concentrations in ambient air, Final Report, CA/DOH/AIHL/SP-34.

John W., Wall S. M., Ondo J. L. and Wang H. C. (1986) Dry deposition of acidic gases and particles, Final Report, CA/DOH/AIHL/SP-40.

Hildemann L. M., Russell A. G. and Cass G. R. (1984) Ammonia and nitric acid concentrations in equilibrium with atmospheric aerosols: Experiment vs theory, Atmospheric Environment 18 : 1737-1750.

Lindberg S. E., Lovett G. M. and Coe J. M. (1984) Acid deposition/forest canopy interactions, Final report to the Electric Power Research Institute (Project RP 1907-1).

Lindberg S. E., Lovett G. M., Richter D. D. and Johnson D. W. (1986) Atmospheric deposition and canopy interactions of major ions in a forest, Science 231 : 141-145.

Merk H. J. (1959) Rapid calculations for boundary-layer transfer using wedge solutions and asymptotic expansions, Journal of Fluid Mechanics 5 : 460.

Milford J. B. and Davidson C. I. (1987) The sizes of particulate sulfate and nitrate in the atmosphere - A Review, Journal of Air Pollution Control Association 37 : 125-1134.

Munn R. E. and Bolin B. (1971) Review: global air pollution - meteorological aspects, Atmospheric Environment 5 : 363-402.

Patankar S. V. and Spalding D. B. (1966) A calculation procedure for heat transfer by forced convection through two-dimensional uniform-property turbulent boundary layers on smooth impermeable walls, Proc. of 3rd Internat. Heat Transfer Conference, Chicago, IL, pp 50-63.

Patankar S. V. and Spalding D. B. (1967) A finite-difference procedure for solving the equations of the two-dimensional boundary layer, International Journal of Heat and Mass Transfer, 10 : 1389-1412.

Patankar S. V. and Spalding D. B. (1970) Heat and mass transfer in boundary layers : A general calculation procedure, Intertext Books, London.

Prandtl L. (1904) Uber Flussigkeitsbewegung bei sehr kleiner Reibung. Proc. 3rd Intern. Math. Congr. Heidelberg, pp 484-491.

Schlichting H. (1979) Boundary-Layer Theory, 7th ed., McGraw-Hill, Inc., New York, NY.

Sehmel G. A. (1980) Particle and gas dry deposition : A review, Atmospheric Environment 14 : 983-1009.

Sehmel G. A. (1983) Resuspension rates from aged inert-tracer sources, in : Precipitation Scavenging, Dry Deposition, and Resuspension, vol. 2, Pruppacher H. R., Semonin R. G. and Slinn W. G. N. (editors), Elsevier Science Publishing Co., Inc., New York, NY, pp 1073-1086.

Sehmel G. A. and Hodgson W. H. (1978) A model for predicting dry deposition of particles and gases to environmental surfaces, PNL-SA-6721 Battelle, Pacific Northwest Laboratory, Richland, WA.

Shannon J. D. (1981) A model of regional long-term average sulfur atmospheric pollution, surface removal, and net horizontal flux, Atmospheric Environment 15 : 689-701.

Spalding D. B. (1977) GENMIX : A general computer program for two-dimensional parabolic phenomena, William Clowes & Sons, London.

Stelson A. W., Bassett M. E. and Seinfeld J. H. (1984) Thermodynamic equilibrium properties of aqueous solutions of nitrate, sulfate and ammonium, in Chemistry of Particles, Fogs and Rain, edited by Jack C. Durham, Acid Precipitation Series, Vol. 2, Chap. 1, pp. 1-52, Ann Arbor Science Books, Ann Arbor, MI.

Vandenburg J. J. and Knoerr K. R. (1985) Comparison of surrogate surfaces techniques for estimation of sulfate dry deposition, Atmospheric Environment 19 : 627-635.

Volder E. C., Barrie L. A. and Sirois A. (1986) A literature review of dry deposition of oxides of sulfur and nitrogen with emphasis on long-range transport modelling in North America, Atmospheric Environment 20 : 2101-2123.

Young J. R., Ellis C. and Hidy G. M. (1987) Deposition of airborne acidifiers in the western environment, Journal of Environmental Quality 17 : 1-26.

Appendix A

Air Flow Patterns Around the Airfoil

The air flow past an airfoil is basically a three-dimensional, compressible flow. But in general, ambient windspeeds are less than 15 m/sec, so that the Mach number of the air flow is less than 0.05. Therefore, we can treat the air flow as incompressible [Schlichting, 1979]. For simplicity, we treat the problem as two dimensional flow and assume that the flow is in steady state.

L. Prandtl [1904] has proven that the flow around a solid body can be divided into two regions. One is a very thin layer in the neighborhood of the body where the influence of viscosity dominates. The other region is outside the thin layer where the frictional effect can be neglected. The thin region next to the surface is called the boundary layer and it contains a strong velocity gradient. Owing to the negligible frictional effect, air behaves like a perfect fluid in the other region where there is potential flow. Thus, to understand the air flow pattern around an airfoil, we may compute the velocity distribution in the potential flow region and in the boundary layer separately. From these, the boundary layer thickness, which is the distance from the surface where the airflow attains 99% of the potential velocity, can be determined.

The governing equations, in vector form, for air flow past an airfoil are the continuity equation :

$$\frac{\partial \rho}{\partial t} = -\nabla \cdot (\rho V)$$

and the Navier-Stokes equation :

$$\rho \frac{DV}{Dt} = -\nabla P + \nabla \cdot \tau$$

where ρ is the density of air, V is the velocity vector, P is pressure, τ is shear stress which is a tensor and $\frac{D}{Dt}$ is the substantial derivative which is equal to $\frac{\partial}{\partial t} + V\nabla$. For two-dimensional and incompressible flow, the continuity equation is simplified to :

$$\nabla \cdot V = 0$$

in vector form. In scalar form of Cartesian coordinates, the continuity equation becomes :

$$\frac{\partial u}{\partial x} + \frac{\partial v}{\partial y} = 0$$

where u and v are the x- and y- component of velocity vector V respectively.

Because of the nonlinear term in the substantial derivative, it is impossible to get an analytical solution except for some special cases. Fortunately, according to Prandtl's concept, these equations can be simplified for potential flow and boundary layer flow. Then the simplified equations are solved analytically or numerically.

A.1 Potential Flow Around the Airfoil

For potential flow, instead of solving the continuity equation and the Navier-Stokes equation for the velocity distribution, we solve for velocity potential ϕ which is defined as :

$$V = -\nabla\phi$$

Substituting the definition of velocity potential into the continuity equation, we obtain a Laplace equation for ϕ :

$$\nabla^2\phi = 0$$

A very important property of the Laplacian operator ∇^2 is linearity. That is, the solution of a linear combination of any variable which is governed by the Laplacian operator is just the linear combination of solutions of each variable. Thus a complicated flow pattern can be expressed as the sum of elementary flows like uniform flow, point source or sink, and so on. For example, the flow around a circular cylinder can be exactly expressed as the sum of uniform flow and dipole flow. This is the principle used to solve for potential flow around an airfoil. The procedure is called the panel method.

The panel method [Chow, 1979] is a powerful method used to solve for the potential flow around complex objects. It has been successfully applied not only to flow problems involving two- and three-dimensional bodies of complex geometry, but also to the problems concerning internal flows and nonuniform, unsteady flows [Hess, 1975]. In this method the surface is divided into a finite number of small areas called panels, each of which is a source distributed by an undetermined uniform density. The distributed sources are used to deflect the oncoming stream so that it will flow around the body. The requirement that the oncoming flow be tangent to every panel at a particular location gives a set of equations. These equations are used to compute the source densities on the panels.

For flow past a two-dimensional body as shown in Figure A.1, a finite number of points are selected on the surface. They are designated as the control points in the panel method. Through control points, lines tangent to the surface are drawn. The intersections of neighboring tangent lines are called the boundary points. Panels are defined by the line segments between a pair of neighboring boundary points. Another way to define panels is to select boundary points, instead of control points, on the surface. Panels are still the line segments between a pair of neighboring boundary points. The control point is then defined as the central point of each panel. These two different ways of defining of panels give the same

result and approach the real potential flow when the number of panels is large. It is the latter method used here. Therefore, the velocity potential of air flow around an airfoil is :

$$\phi(x_i, y_i) = Ux_i + \sum_{j=1}^{m} \frac{\lambda_j}{2\pi} \int_0^{S_j} \ln r_{ij}\, ds_j$$

where $\phi(x_i,y_i)$ is the velocity potential at point (x_i,y_i), i.e. the control point of panel i, U is the velocity of uniform flow which is the wind speed in our case, m is the number of panels, λ_j is the source strength per unit length of panel j, S_j is the length of panel j, and r_{ij} is the distance from the control point (x_i,y_i) to any arbitrary point on panel j.

In order to have flow around an airfoil, the normal velocity at any control point must be zero. That is, we only have tangential flow at the surface. With reference to Figure A.2, the resulting equation is :

$$\sum_{j=1}^{m} I_{ij}\lambda'_j = \sin\theta_i$$

where $I_{ij}=\pi$ when $i=j$; otherwise

$$I_{ij} = \int_0^{S_j} \frac{\partial}{\partial n_i}(\ln r_{ij})\, ds_j$$

and $\lambda'_j = \lambda_j / 2\pi U$ is the dimensionless source strength per unit length of panel j, where θ_i and n_i are defined in Figure A.2. Totally, there are m equations with m unknowns if I_{ij}'s are given since U and θ are known after specifying the panels.

With reference to Figure A.2, the integral is evaluated and after some manipulation the result for I_{ij} is

$$I_{ij} = \frac{1}{2}\sin(\theta_i - \theta_j)\ln\left[1 + \left(\frac{S_j^2 + 2AS_j}{B}\right)\right] - \cos(\theta_i - \theta_j)\left[\tan^{-1}\left(\frac{S_j + A}{E}\right) - \tan^{-1}\left(\frac{A}{E}\right)\right]$$

where

$$S_j = \sqrt{(X_{j+1} - X_j)^2 + (Y_{j+1} - Y_j)^2}$$

$$A = -(x_i - X_j)\cos\theta_j - (y_i - Y_j)\sin\theta_j$$

$$B = (x_i - X_j)^2 + (y_i - Y_j)^2$$

$$E = (x_i - X_j)\sin\theta_j - (y_i - Y_j)\cos\theta_j$$

and (x_i,y_i) are the coordinates of control point of panel i and (X_j,Y_j) are the coordinates of the first boundary point counted counterclockwise from panel j.

The number of panels selected for air flow around the airfoil is 396. Therefore we have to solve 396 equations simultaneously in order to find the dimensionless source strength per

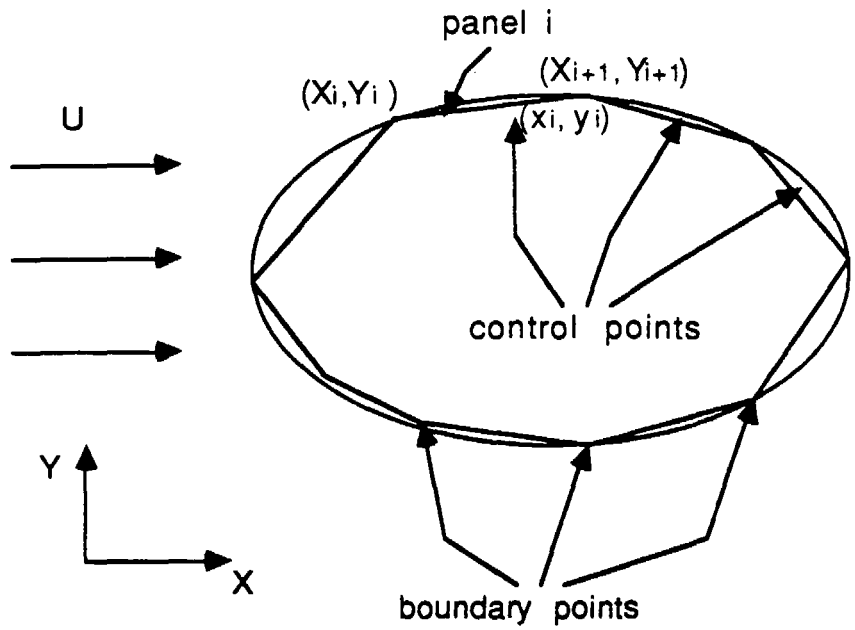

Figure A.1 Specification of panels, boundary points and control points on surface.

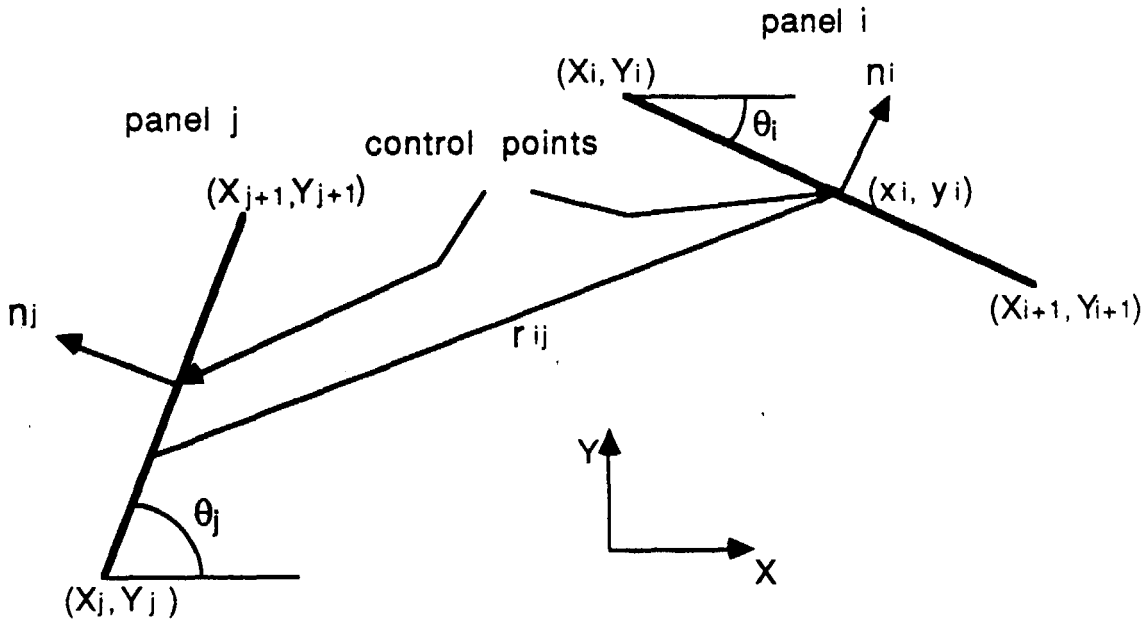

Figure A.2 Evaluation of integral I_{ij}

unit length, λ'_j. The Gauss-Jordan method (or augmented matrix method) is used here to solve these equations. Then the potential velocity at control point i is

$$\frac{u_i}{U} = \cos\theta_i + \sum_{j=1}^{m} \lambda'_j I'_{ij}$$

where u_i is velocity at control point i and I'_{ij} is the contribution to the tangential velocity at control point i by panel j. I'_{ij}=0 when i=j; otherwise

$$I'_{ij} = -\frac{1}{2}\cos(\theta_i - \theta_j)\ln[1 + (\frac{S_j^2 + 2AS_j}{B})] - \sin(\theta_i - \theta_j)[\tan^{-1}(\frac{S_j + A}{E})] - \tan^{-1}(\frac{A}{E})]$$

where S_j, A, B and E are defined as above.

The program, which is rewritten in Pascal, for computing potential flow around an airfoil is listed in Appendix B. In order to check its validity, it has been run for flow around a cylinder and the results are compared with the known solution for this shape. It is found that both are the same up to the fifth digit. A second method of checking the validity of the program is to calculate the sum of source strengths. Owing to the conservation of mass, the sum should be zero theoretically. The calculated sum is -4.46E-9 for the airfoil which is rounded off by the computer. Therefore, the program is good enough to be used to compute potential velocities of air flow around the airfoil.

The dimensionless potential velocities, defined as the ratio of potential velocity to oncoming velocity or wind speed, are shown in Figure A.3. They are plotted versus distance from the center of the airfoil. Thus, negative x-values are in front of the center and positive x-values are behind the center of the airfoil. The velocity distribution is symmetrical about the line x = 0 since airfoil is symmetrical to its center. Note that the stagnation point with velocity of zero is not at the exact front of the airfoil, but rather 0.148 cm from the front. This is because the airfoil is not symmetrical with respect to the x-axis.

The Teflon plate which is put onto the airfoil is a circle with diameter of 13 cm. But the region that we collect samples from is a circle with diameter of 12.1 cm. The dimensionless velocity above this area is almost constant with a value of about 1.1. The potential velocities which are obtained by multiplying the dimensionless potential velocities by wind speed are used to compute the boundary-layer thickness and the velocity distribution in the boundary layer.

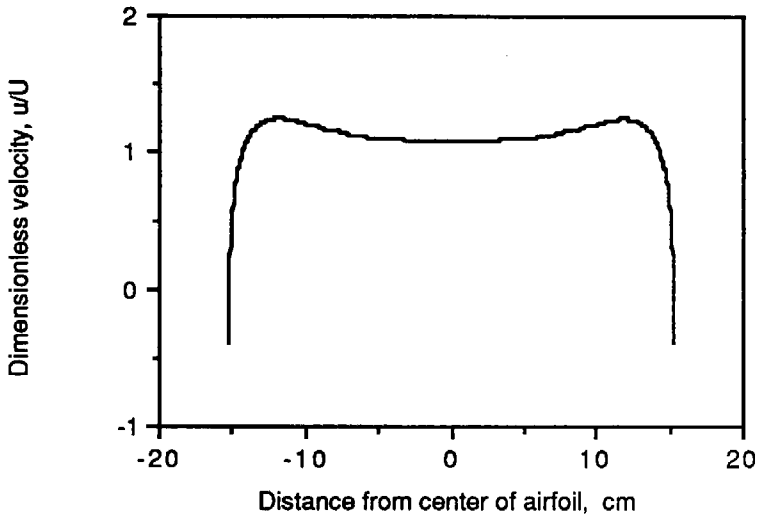

Figure A.3 Dimensionless potential velocity distribution around the airfoil.

A.2 Boundary Layer Flow Around the Airfoil

For two-dimensional and incompressible flow at steady state, the Navier-Stokes equation is simplified to [Schlichting, 1979] :

$$\rho\left(u\frac{\partial u}{\partial x}+v\frac{\partial u}{\partial y}\right)=-\frac{dP}{dx}+\frac{\partial}{\partial y}\left(\mu\frac{\partial u}{\partial y}\right)$$

in Cartesian coordinates. This equation coupled with the continuity equation determines the velocity distribution in the boundary layer. Note that the x-axis is the distance from the stagnation point along the surface. It is not the same as the x-axis that is generally used in Cartesian coordinates. The difference is shown in Figure A.4 where the y-axis is also defined. The x-axis is actually defined along the surface but it is drawn slightly above the surface in Figure A.4 in order to show it clearly. This expression is good only when the curvature of surface is much greater than the thickness of boundary layer.

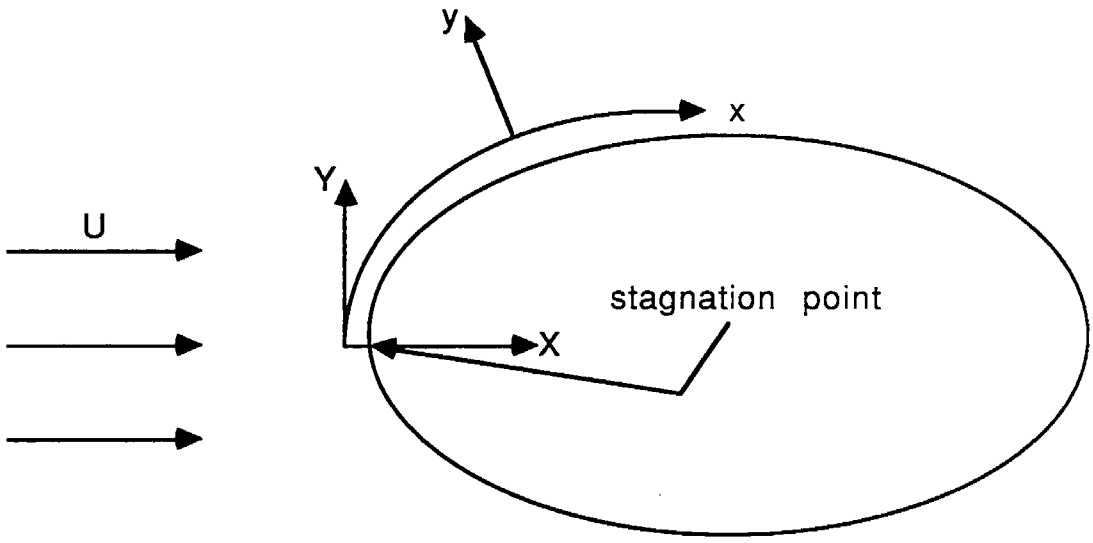

Figure A.4 Comparison between Cartensian coordinates (X,Y) and coundary layer coordinates (x,y). The boundary layer coordinates follow the contour of the airfoil.

There have been many efforts to solve the boundary layer flow for various situations. For example, Blasius used the similarity method to transform the partial differential equation of boundary layer flow over flat plate to an ordinary differential equation. Then he used a series expansion to solve the ordinary differential equation. Evans [1968] modified the method proposed by Merk [1959] which includes a Mangler transformation to transform the differential equation for general laminar boundary layer flow. Evans also used a series expansion to solve the differential equation. In addition to the differential form of the boundary layer equation, von Karman developed an integral form for boundary layer flow. This equation is valid for both laminar and turbulent flow, and in Cartesian coordinates it is :

$$\rho\frac{d}{dx}\int_0^{\delta}(u_0-u)u\,dy+\rho\frac{du_0}{dx}\int_0^{\delta}(u_0-u)\,dy=\tau_0$$

where δ is the boundary layer thickness, u_0 is the potential velocity which is obtained by the panel method and τ_0 is the shear stress at the internal boundary. Note that the velocity at the edge boundary of the boundary layer is equal to 0.99 of the potential velocity defined previously. Then an approximate boundary layer thickness is obtained by assuming a reasonable velocity distribution, e.g. a second or third degree polynomial velocity distribution.

The method used here was developed by Patankar and Spalding [1966,1967,1970,1977]. This method can be used for laminar and turbulent flow. Some key features of the method are :

1. Entrainment rate [Head,1958], the rate of fluid transferred across a boundary, is used to determine the boundaries of the region to be considered. Note that the thickness of the boundary layer grows in the downstream direction, that is, the amount of fluid in the boundary layer increases along the surface.
2. x ~ ω coordinates are used instead of Cartesian coordinates. ω is the dimensionless stream function and is defined as

$$\omega = \frac{\psi - \psi_I}{\psi_E - \psi_I}$$

where ψ is the stream function which is defined as $d\psi = \rho u dy$, and ψ_I and ψ_E are the stream functions at internal and external boundaries, respectively. Because of the increasing boundary layer thickness in downstream direction, the grid spacing which is good upstream is excessively fine and wasteful downstream. Similarly, the spacing chosen for downstream is too big for upstream locations and the accuracy is poor. Instead of using geometrical distance, the fraction of fluid in the boundary layer, which is the definition of ω, is used. Thus there are always the same number of grid points for the region of interest in the x ~ ω coordinate system.

3. The method is not self-starting, and we need initial conditions which give the boundary layer thickness and velocity distribution to begin the computation.

The initial conditions are obtained here by using the von Karman integral method. Several ways of approximation can be used with slightly different results at the beginning of the computation. The final results are virtually identical, however, showing a lack of sensitivity to initial conditions. Based on an assumed cubic velocity distribution at the beginning, the following equations are used to compute the initial conditions :

$$\delta_i = 2.4\sqrt{\nu / A_i U}$$

$$pei_i = 0.625\,\rho u_i \delta_i$$

$$6(\frac{y}{\delta_i})^2 - (\frac{y}{\delta_i})^4 - 5\omega = 0$$

$$u = \frac{u_i}{2}[3(\frac{y}{\delta_i}) - (\frac{y}{\delta_i})^3]$$

where

$$A_i = \frac{1}{U}\frac{du_i}{dx}$$

and A_i = 2.11 for air flow around the airfoil. U is the oncoming velocity of fluid or wind speed in our case, u_i is the initial potential velocity, δ_i is the initial boundary layer thickness, pei_i is the initial amount of air in the boundary layer and ν is kinematic viscosity of air. Note that the boundary layer thickness is not zero at the stagnation point.

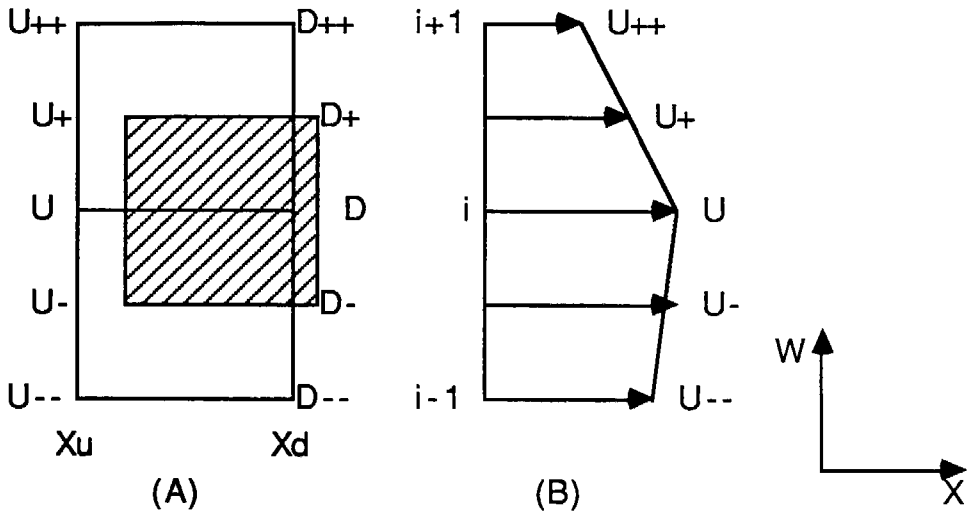

Figure A.5 The control volume (A) and the assumed velocity profile (B) used for derivation of micro-integral equation.

The boundary layer equation is transformed in the x ~ ω coordinate system to be

$$\frac{\partial u}{\partial x} + (a + b\omega)\frac{\partial u}{\partial \omega} = \frac{\partial}{\partial \omega}\left(c\frac{\partial u}{\partial \omega}\right) + d$$

where

$$a = \frac{-1}{\psi_E - \psi_I}\frac{d\psi_I}{dx}$$

$$b = \frac{-1}{\psi_E - \psi_I}\frac{d}{dx}(\psi_E - \psi_I)$$

$$c = \frac{\rho u \mu_{eff}}{(\psi_E - \psi_I)^2}$$

$$d = -\frac{1}{\rho u}\frac{dP}{dx}$$

This equation is integrated over the control volume as shown in Figure A.5 with the assumption of a local linear profile of velocity. After some manipulation and rearrangement, the resulting equation is

$$u = Au_{++} + Bu_{--} + C$$

where

$$A = A'/D; \quad B = B'/D; \quad C = C'/D;$$

$$A' = 2T_+' - L_+ - 0.25(P+G)\Omega_+;$$

$$B' = 2T_-' + L_- - 0.25(P+G)\Omega_-;$$

$$C' = 0.25P(3u\Omega + u_{++}\Omega_+ + u_{--}\Omega_-) + 2S_u;$$

$$D = 2(T_+' + T_-') + L_+ - L_- + 0.75(P+G)\Omega - 2S_d;$$

$$P = (\psi_E - \psi_I)/(x_d - x_u); \quad G = -(\psi_E - \psi_I)b;$$

$$L_+ = (\psi_E - \psi_I)(a + b\omega_+); \quad L_- = (\psi_E - \psi_I)(a + b\omega_-);$$

$$T_+ = (\mu_{eff})_+/(y_{++} - y); \quad T_- = (\mu_{eff})_-/(y - y_{--});$$

$$T_+' = 0.5[T_+ + |0.5L_+| + |T_+ - |0.5L_+||]; \quad T_-' = 0.5[T_- + |0.5L_-| + |T_- - |0.5L_-||];$$

$$\Omega = \omega_{++} - \omega_{--}; \quad \Omega_+ = \omega_{++} - \omega; \quad \Omega_- = \omega - \omega_{--};$$

$$S_u = -\left(\frac{dP}{dx}\right)\left(\frac{y_{++} - y_{--}}{2}\right); \quad S_d = 0;$$

and subscript ++ is at grid point (i+1), -- is at (i–1), + is at the midpoint of (i+1) and i, - is at the midpoint of i and (i–1), and the subscript for grid point i is omitted for convenience.

Thus, the velocity at each grid point is a linear combination of velocities at surrounding points. The coefficients are determined by velocities and y values at the previous step. But the equation is implicit since all the velocities at the current step are unknown. Because of the no slip condition on the surface, the assumed local linear profile of velocity is not good for the grid point next to the surface. Some other measures are taken which are included in procedure wf (a subroutine in the program; see Appendix C). The set of finite difference equations can be solved by matrix-inversion techniques like the one used for solving potential velocity. But another simpler successive-substitution method called the tri-diagonal matrix algorithm (TDMA) is used for this special case.

All the equations which have to be solved for obtaining velocity can be rewritten as

$$\begin{aligned}
u_2 - A_2u_3 &= C_2 + B_2u_1 \\
-B_3u_2 + u_3 - A_3u_4 &= C_3 \\
-B_4u_3 + u_4 - A_4u_5 &= C_4 \\
&\cdots \\
&\cdots \\
-B_{n-2}u_{n-3} + u_{n-2} - A_{n-2}u_{n-1} &= C_{n-2} \\
-B_{n-1}u_{n-2} + u_{n-1} &= C_{n-1} + A_{n-1}u_n
\end{aligned}$$

where n is the number of grid points cross the boundary layer. Note that on the left hand side the coefficients are nonzero only along the diagonal and the two adjacent lines on either side, and on the right hand side all terms are known. u_1 is the velocity at the internal boundary which is on the surface and is equal to zero under the no-slip assumption. u_n is the velocity at the external boundary, i.e., u_o or 0.99 of potential velocity. By algebraic substitution, the equations are converted into :

$$u_i = \alpha_i u_{i+1} + \beta_i$$

where $\alpha_i = A_i/(1 - B_i\alpha_{i-1})$ and $\beta_i = (B_i\beta_{i-1} + C_i)/(1 - B_i\alpha_{i-1})$ with $\alpha_2 = A_2$ and $\beta_2 = (B_2u_1 + C_2)$. With known boundary conditions at ω = 0 and ω = 1, the velocity at every grid point is computed by the above equation.

From the definitions of stream function, $d\psi=\rho u dy$, and ω which is $(\psi - \psi_I)/(\psi_E - \psi_I)$, we have $\rho u dy=(\psi_E-\psi_I)d\omega$. Therefore :

$$y = (\psi_E - \psi_I)\int_0^{\omega} \frac{1}{\rho u} d\omega$$

Knowing the velocity distribution, we can compute the thickness of the boundary layer which is the y value at ω = 1.

Entrainment rate is expressed mathematically as :

$$m_I = -\frac{d\psi_I}{dx}; \qquad m_E = -\frac{d\psi_E}{dx}$$

where m_I and m_E are entrainment rates at internal and external boundaries, respectively. At the internal boundary which is a solid surface, there is no fluid flow across the surface. Therefore, the entrainment rate is zero at the internal boundary and the rate of increasing fluid flow in the boundary layer is equivalent to the entrainment rate at the external boundary. At the external boundary the velocity gradient in the cross-stream direction is negligible and the boundary layer equation is reduced to :

$$\frac{du}{dx} = d$$

Substituting this result back into the boundary layer equation and combining with the definition of entrainment and the expression for y, we obtain the result :

$$m_E = \frac{-2\mu_{eff}}{(y_{n-1} - y_{n-2})}$$

The program which is also written in Pascal for computating the boundary thickness and velocity distribution is listed in Appendix C. The computation procedures and the associated procedures (or subroutines) in the program for each step are summarized in Figure A.6. After specifying the problem and the properties of air, data which are computed by the panel

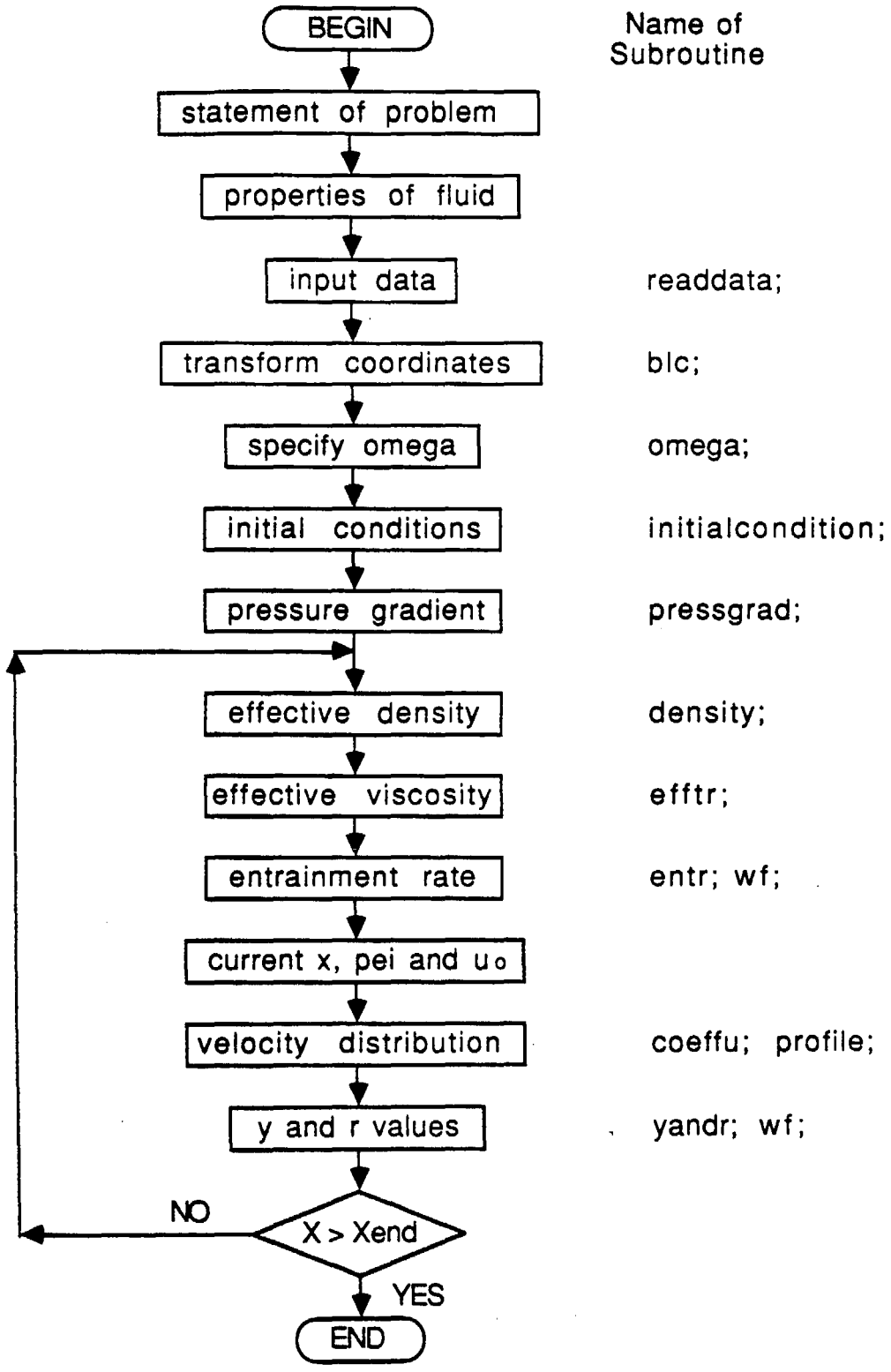

Figure A.6 Procedures for computing boundary layer thickness

method are input from the file. The x-axis values (which are defined as the distance from the stagnation point along the surface) and the pressure gradients are only computed at the points where potential velocities are calculated. The grid points are chosen to be uniformly distributed so that the interval of ω is bigger for grids near the external boundary because of the faster flow rate. After the initial conditons are computed, the velocity distribution and y values at each control point are calculated one by one until $X > X_{end}$. The effective viscosity for turbulent flow is calculated by using Prandtl's mixing length theory. This program can also be used for three-dimensional axisymmetric boundary layer flow. Air flow around the airfoil is treated as two-dimensional flow; thus the radius is set to unity. The program is checked by comparison of computed values and those in the literature for flow over flat plates and around circular cylinders. The comparisons are in good agreement. The velocity distributions in the boundary layer at x values of about 6, 10, 16 and 22 are plotted in Figure A.7

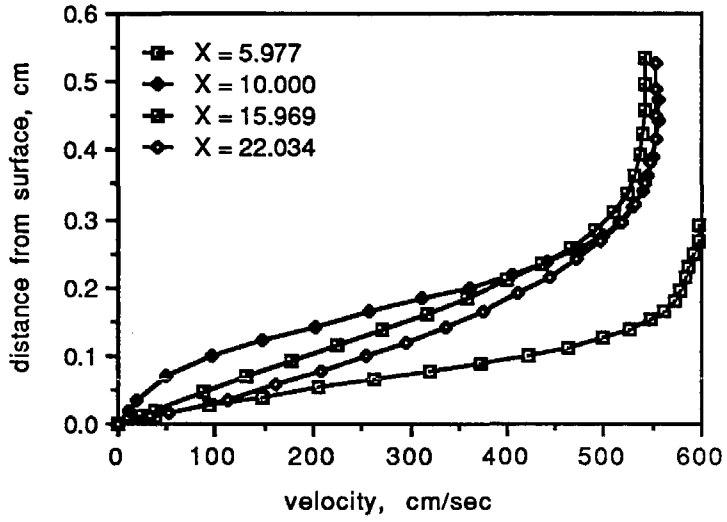

Figure A.7 Velocity distribution in the boundary layer around the airfoil.

The boundary layer thickness along the surface is plotted in Figure A.8 for wind speeds of 50, 100 and 500 cm/sec. The wind speed is assumed to be at the height of the airfoil which is about 2 meters above ground. The thickness of the boundary layer is almost constant in the region over the Teflon plate which ranges from X = 8.5 to X = 23.0 and it decreases with increasing wind speeds. It is about 1.7 cm over the Teflon plate for a wind speed of 50 cm/sec and is around 1.2 cm for a wind speed of 100 cm/sec; and at 500 cm/sec, it reduces to less than 0.5 cm.

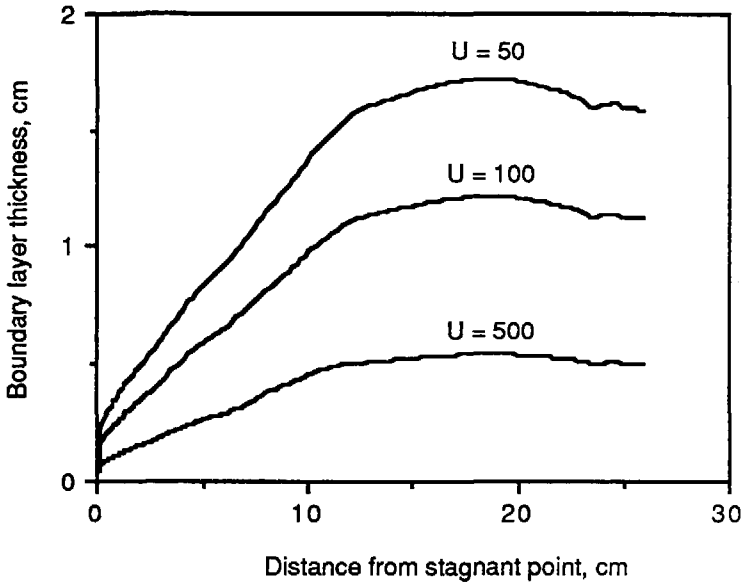

Figure A.8 Boundary layer thickness around the airfoil for different wind speeds.

Appendix B

Computation of the Potential Flow

```
{ * *  COMPUTATION OF FREE STREAM VELOCITY OF AIRFOIL BY PANEL METHOD  * * }

program panel4 (input,output);
  type
    subs1 = array [1..400] of real;
    subs2 = array [1..400,1..400] of real;
    subs3 = array [1..400,1..800] of real;
  var
    LOV,                      { Index for the meaning of ci }
    i,j,nm : integer;

    source1,source2 : text;

    pi,                       { Constant 3.14159 ..... }
    uf : real;                { Infinite uniform velocity }
    vel,                      { velocity at control points }
    lamda,                    { Unit-length source strength }
    cv,                       { Constant vector }
    cs,                       { Cosine theta, used to compute velocity }
    theta,                    { Angle of each element }
    cp,                       { Coefficient of pressure }
    bx,by,                    { Boundary points }
    cx,cy : subs1;            { Control points }
    ci : subs2;               { LOV = 0 : coefficient for solving lamda,
                                LOV = 1 : coefficient for computing velocity }
    miv : subs3;

  {  *  *  *  *   INPUT DATA FROM FILE -  aer.dat  *  *  *  *  }

  procedure readdata;
    var
      ir,kr,nr : integer;
    begin
      reset(source1,'aer.dat');
      for ir := 1 to 200 do                    { Input data }
        begin
          readln(source1,cx[ir],cy[ir]);
          cx[ir] := 2.54*cx[ir];
          cy[ir] := 2.54*cy[ir];
        end;

      for ir := 1 to 100 do            { Transfer data to boundary points }
        begin
          bx[ir] := -cx[ir];
          by[ir] := cy[ir];
          kr := 200-ir;
          bx[kr] := cx[ir];
          by[kr] := cy[ir];
        end;
      for ir := 101 to 200 do
        begin
          kr := 498-ir;
          bx[kr] := -cx[ir];
          by[kr] := -cy[ir];
          nr := 596-kr;
          bx[nr] := -bx[kr];
          by[nr] := by[kr];
        end;

      for ir := 1 to 396 do            { Compute control points }
        begin
          cx[ir] := 0.5*(bx[ir]+bx[ir+1]);
          cy[ir] := 0.5*(by[ir]+by[ir+1]);
        end;
    end;


    {  *  *  *  *  *   COMPUTE THE ANGLE OF EACH ELEMENT   *  *  *  *  *  }

  procedure angle;
    var
      ai,ak : integer;
    begin
      ak := 99;
      for ai := 1 to 396 do
        begin
          theta[ai] := (by[ai+1]-by[ai])/(bx[ai+1]-bx[ai]);
          theta[ai] := arctan(theta[ai]);
          if ( ai > (3*ak) ) then theta[ai] := theta[ai]+pi
                             else if ( ai > (2*ak) )
                                    then theta[ai] := theta[ai]-pi
                                    else;
        end;
    end;


    {  *  *  *  *  *   Procedure used to compute ci and cip   *  *  *  *  *  }

  procedure coeff (var ci : subs2; i,j : integer );
    var
      a,b,sj,e,is1,is2 : real;
    begin
      sj := sqrt(sqr(bx[j+1]-bx[j])+sqr(by[j+1]-by[j])); { Length of panel j }
      cv[i] := sin(theta[i]);                    { Constant vector used in
                                                   solving lamda }
      cs[i] := cos(theta[i]);
      a := -(cx[i]-bx[j])*cos(theta[j]);
      a := a-(cy[i]-by[j])*sin(theta[j]);
      b := sqr(cx[i]-bx[j])+sqr(cy[i]-by[j]);
      e := (cx[i]-bx[j])*sin(theta[j]);
      e := e-(cy[i]-by[j])*cos(theta[j]);
      is1 := (sj*sj+2*a*sj)/b;
      is1 := ln(1+is1);
      if ( e = 0 ) then is2 := 0
                   else
                     begin
                       is2 := (sj+a)/e;
                       is2 := arctan(is2)-arctan(a/e);
                     end;
      if ( LOV = 0 ) then
                       begin
                         if ( i = j ) then  ci[i,j] := 3.14159
                                      else
                                        begin
                                          is1 := 0.5*(sin(theta[i]-theta[j]))*is1;
                                          is2 := (cos(theta[i]-theta[j]))*is2;
```

```
                        ci[i,j] := is1-is2;
                              end;
                    end
                  else
                    begin
                      if ( i = j ) then ci[i,j] := 0
                                   else
                                     begin
                        is1 := 0.5*(cos(theta[i]-theta[j]))*is1;
                        is2 := (sin(theta[i]-theta[j]))*is2;
                        ci[i,j] := -is1-is2;
                                     end;
                    end;
  end;

{  *  *  *  *   Solving lamdas by Gauss-Jordan method   *  *  *  *  }

procedure gaujo ( var lamda : subs1 );
  var
    mi,mj,mk,ml : integer;
    int : real;
  begin
    for mi := 1 to nm do
      begin
        for mj := 1 to nm do
          begin
            miv[mi,mj] := ci[mi,mj];
            mk := nm+mj;
            if ( mi = mj ) then miv[mi,mk] := 1
                           else miv[mi,mk] := 0;
          end;
      end;
    for mi := 1 to nm do
      begin
        int := miv[mi,mi];
        if ( int = 0 ) then
                         begin
                           mk := mi;
                           repeat
                             mk := mk+1;
                             for ml := 1 to (2*nm) do
                             miv[mi,ml] := miv[mi,ml]+miv[mk,ml];
                             int := miv[mi,mi];
                           until ( int <> 0 );
                         end
                       else;
        for mj := 1 to (2*nm) do
        miv[mi,mj] := miv[mi,mj]/int;

        for mk := 1 to nm do
          begin
            if ( mk <> mi ) then
                            begin
                              int := miv[mk,mi];
                              for ml := 1 to (2*nm) do
                              miv[mk,ml] := miv[mk,ml]-int*miv[mi,ml];
                            end
                          else;
          end;
      end;

    for mi := 1 to nm do
      begin
        for mj := 1 to nm do
          begin
            mk := mj+nm;
            ci[mi,mj] := miv[mi,mk];
          end;
      end;

    for mi := 1 to nm do
      begin
        lamda[mi] := 0;
        for mj := 1 to nm do
        lamda[mi] := ci[mi,mj]*cv[mj]+lamda[mi];
      end;
  end;

  {  *  *  *  *   Computation of velocity at control points   *  *  *  *  }

procedure tvc ( var vel : subs1 );
  var
    ti,tj : integer;
    cigma : real;
  begin
    for ti := 1 to nm do
      begin
        cigma := 0;
        for tj := 1 to nm do
        cigma := cigma+(lamda[tj])*(ci[ti,tj]);
        vel[ti] := (cs[ti]+cigma);
      end;
  end;

procedure presscoef(var cp : subs1);
  var
    pi : integer;
  begin
    for pi := 1 to nm do
    cp[pi] := 1-vel[pi]*vel[pi];
  end;


  {  ------------------------------------------------------------------  }
  {  *   *   *   *   *     BEGINNING OF PROGRAM     *   *   *   *   *   }
  {  ------------------------------------------------------------------  }

begin

  nm := 396;
  pi := 3.14159265;
  uf := 1;

  readdata;

  angle;

  for i := 1 to nm do
  writeln(i,bx[i]:10:5,by[i]:12:5,cx[i]:12:5,cy[i]:12:5,theta[i]:16:7);

  writeln('COMPUTE COEFFICIENTS USED TO SOLVE LAMDAS.');

  LOV := 0;
  for i := 1 to nm do
    begin
      for j := 1 to nm do
      coeff (ci,i,j);
    end;
```

```
  writeln('COMPUTE LAMDAS.');

  gaujo (lamda);

  writeln('COMPUTE COEFFICIENTS USED TO SOLVE VELOCITYS.');

  LOV := 1;
  for i := 1 to nm do
    begin
      for j := 1 to nm do
      coeff (ci,i,j);
    end;

  writeln('COMPUTE VELOCITYS.');

  tvc (vel);

  presscoef (cp);

  rewrite (source2,'panel4.dat');

  for i := 1 to nm do
  writeln(source2,i,cx[i]:12:4,cy[i]:12:4,lamda[i]:12:4,vel[i]:12:4,
                  cp[i]:12:4);

  rewrite(source1,'conpot1.dat');
  writeln(source1,'n','     bx   ','     by   ','     cx   ','     cy   ',
                  '   lamda  ','   theta  ');
  writeln(source1);
   for i := 1 to nm do
  writeln(source1,i,bx[i]:10:4,by[i]:10:4,cx[i]:10:4,cy[i]:10:4,
                  lamda[i]:10:4,theta[i]:10:4);

  uf := 0;
  for i := 1 to nm do
  uf := lamda[i]+uf;
  writeln('Sum of lamda = ',uf);

end.
```

Appendix C

Computation of the Boundary Layer Flow

```
{    *   *   *   COMPUTATION OF BOUNDARY LAYER THICKNESS    *   *   *    }
{    *   *   *     MODIFIED FROM PATANKAR AND SPALKING      *   *   *    }

program blwsp2 (input,output);
  type
    subs1 = array [0..50] of real;
    subs2 = array [0..400] of real;
  var
    infile,outfile1,outfile2 : text;

    LORT,          { index : 0 for laminar flow, 1 for turbulent flow }
    KRAD,          { index : 0 for plane, 1 for axisymmetry }
    COMP,          { index of compressibility : 0 for incompressible fluid, }
                   {                            1 for compressible fluid }
    KIN,           { index of inner boundary : 1 for wall, 2 for free stream,}
                   {                         and 3 for symmetrical axis }
    KEX,           { index of outer boundary as KIN }
    TEST,          { index of printing : 0 for no, 1 for yes }
    DATAS,         { index of saving data : 0 for no, 1 for yes }
    SCR,           { index used to pause the appearance on the screen. }
                   { Hit any key to continue. }
    npl,np2,np3,   { slip points }
    istep,         { number to account for the forward integration }
    n,             { number of grid point }
    ind
            : integer;

    u,             { velocity }
    au,bu,cu,      { coefficients of equation of velocity }
    om,            { dimensionless stream function }
    r,             { radius }
    y,             { normal distance from the inner boundary }
    mueff,         { effective viscosity }
    emu,           { (product of mueff and r at midpoint)/(distance of y }
                   {                                    between grid points) }
    rho,           { density }
    rhou           { product of density and velocity at midpoint between }
                   {                                    grid points }
            : subs1;

    rmi,rme,       { entrainment rates at inner and outer boundaries }
    csalfa,        { cosine alfa }
    ri,            { radius at inner boundary }
    cx,cy,         { coordinates of control points }
    xb,            { boundary layer coordinate distance }
    uf,            { free stream velocity }
    dpdx           { pressure gradient in x-direction }
            : subs2;

    infvel,        { infinite velocity of coming flow }
    mu,            { laminar viscosity }
    rhoc,          { referent density }
    psii, psie,    { stream function at inner and outer boundaries }
    pei,           { difference of psie and psii }
    bpi,bpe,       { shape factor used to compute y near boundaries }
    omi,ome,       { omega's at the inner boundaries of the outer half- }
                   {                              intervals of the grid }
    t1,tnp3,       { diffusive flux near boundaries }
    taui,taue,     { shear stresses at internal and external boundaries }
    dx,            { forward distance in x-direction}
    xu,xd,         { x's at upsteam and downstream }
    y25,yn15,      { y's at om = (om(2)+om(3))/2 and om = (om(np1)+om(np2))/2 }
    r25,rn15,      { r's defined as y25 and yn15 }
    rhou3,rhoun1   { products of density and velocity at points 3 and np1 }
            : real;


  {    *   *   *    INPUT DATA FROM FILE - PANEL4.DAT    *   *   *    }

procedure readdata;
  var
    ri,rn : integer;
    rlamda,rtheta : real;
  begin
    reset(infile,'panel4.dat');
    for ri := 1 to 396 do
    readln(infile,rn,cx[ri],cy[ri],rlamda,uf[ri],rtheta);

    uf[0] := 0;                { Choose only nonegative velocity points }
    for ri := 1 to 200 do
    uf[ri] := infvel*uf[ri+4];
  end;

{    *    TRANSFORM INPUTTED DATA TO BOUNDARY LAYER COORDINATES    *    }

procedure blc;
  var
   bi : integer;
   dist,frac,stag : real;
 begin
   xb[0] := 0.0;
   cx[0] := -15.24; cy[0] := 0;
   for bi := 1 to 200 do
     begin
       dist := sqr(cx[bi]-cx[bi-1])+sqr(cy[bi]-cy[bi-1]);
       dist := sqrt(dist);
       xb[bi] := xb[bi-1]+dist;              { Boundary layer coordinate }
     end;

   for bi := 1 to 200 do
     begin
       cx[bi] := cx[bi+4];
       cy[bi] := cy[bi+4];
     end;

   frac := (0+0.0384)/(0.0635+0.0384);       { Stagnation point }
   stag := xb[4]+frac*(xb[5]-xb[4]);

   for bi := 1 to 196 do                     { BLC from stagnation point }
   xb[bi] := xb[bi+4]-stag;

   if ( TEST <> 0 ) then
      begin
        writeln('    cx    ','    cy    ','    xb    ','    vel    ');
```

```
        for bi := 1 to 195 do
        writeln(cx[bi]:10:4,cy[bi]:10:4,xb[bi]:12:4,uf[bi]:12:4);
        readln(SCR);
      end
                  else;
  end;

{    *   *   *    SPECIFY THE DIMENSIONLESS STREAM FUNCTION    *   *   *    }

procedure omega (var om : subs1);
  var
    io : integer;
  begin
    np1 := n+1;
    np2 := n+2;
    np3 := n+3;
    om[1] := 0;
    om[np3] := 1;
    for io := 2 to np2 do
    om[io] := sqr((io-2)/n);
    om[2] := 0; om[np2] := 1;
    omi := (om[2]+om[3])/2;
    ome := (om[np1]+om[np2])/2;

    if ( TEST <> 0 ) then
                    begin
                      for io := 1 to np3 do
                      writeln (' om(',io:2,') =   ',om[io]:10:8);
                      readln(SCR);
                    end
                   else;
  end;


{    *   *   *    SPECIFY THE INTERNAL RADIUS    *   *   *    }

procedure radi (var ri : subs2 );
  var
    ir : integer;
  begin
     for ir := 1 to 50 do
     begin
       ri[ir] := 0;                                { flat plane }
       csalfa[ir] := 1;
     end;
  end;


{    *   *   *    COMPUTE THE PRESSURE GRADIENT    *   *   *    }

procedure pressgrad (var dpdx : subs2 );
  var
    ip : integer;
    slop1,slop2 : real;
  begin
    for ip := 1 to 195 do
      begin
        slop1 := (uf[ip]-uf[ip-1])/(xb[ip]-xb[ip-1]);
        slop2 := (uf[ip+1]-uf[ip])/(xb[ip+1]-xb[ip]);
        dpdx[ip] := -rhoc*uf[ip]*0.5*(slop1+slop2);
      end;

    if ( TEST <> 0 ) then
      begin
        writeln(' ip',' dpdx ');
        for ip := 10 to 195 do
        writeln(ip:3,dpdx[ip]:12:5);
        readln(SCR);
      end;
  end;


{    *   *   *    COMPUTE THE DENSITY OF FLUID    *   *   *    }

procedure density (var rho :subs1 );
  var
    id : integer;
  begin
     if ( COMP = 0 ) then
       begin
         for id := 1 to np3 do
         rho[id] := rhoc;
       end
                   else;

     if ( TEST <> 0 ) then
                      begin
                        for id := 1 to np3 do
                        writeln('rho(',id:2,') = ',rho[id]:10:8);
                        readln(SCR);
                      end
                     else;
  end;


{    *   *   *    COMPUTE THE EFFECTIVE VISCOSITY    *   *   *    }

procedure efftr (var mueff :subs1 );
  var
    ie,ke : integer;
    fr,ak,almg,ufac,udif,hudif,dudymn,dudyl,ex,exl,udmin,
    el12,el34,el56,el23,el45,emut : real;
    dudy,yedge,el : subs1;
  begin
     if ( LORT = 0 ) then
       begin                                        { Laminar flow }
         for ie := 1 to np3 do
         mueff[ie] := mu;
       end
                   else
       begin                                         { Turbulent flow }
         fr := 0.033;
         ak := 0.435;
         almg := 0.09;
         ufac := 0.01;

         udif := u[np3]-u[1];
         hudif := 0.5*udif;
         dudymn := fr*udif/y[np3];

         for ie := 2 to np2 do
         dudy[ie] := abs((u[ie+1]-u[ie-1])/(y[ie+1]-y[ie-1]));
         ke := 1;
         ex := dudy[2]-dudymn;
         if ( ex >= 0 ) then yedge[ke] := 0
                        else;
         for ie := 3 to np2 do
           begin
```

```
          exl := ex;
          ex := dudy[ie]-dudymn;
          if ( (exl*ex) < 0 ) then
                              begin
                                ke := ke+1;
                                yedge[ke] := 0.5*(y[ie]+y[ie-1]);
                              end
                             else;
        end;
      if ( ke < 6 ) then
                    begin
                      for ie := (ke+1) to 6 do
                      yedge[ie] := y[np3];
                    end
                   else;
      el12 := (yedge[2]-yedge[1])*almg;
      el34 := (yedge[4]-yedge[3])*almg;
      el56 := (yedge[6]-yedge[5])*almg;
      el23 := 0.5*(el12+el34);
      el45 := 0.5*(el34+el56);

      for ie := 2 to np2 do
        begin
          dudyl := dudy[ie]*el[ie];
          udmin := ufac*u[ie];
          if ( dudyl < udmin ) then dudyl := udmin
                              else;
          emut := rho[ie]*el[ie]*dudyl;
          mueff[ie] := mu+emut;
        end;
    end;

  if ( TEST <> 0 ) then
                  begin
                    writeln(' ie','     mueff     ');
                    for ie := 1 to np3 do
                    writeln(ie:3,mueff[ie]:15:8);
                    readln(SCR);
                  end
                 else;
end;

{    *    SPECIFY THE INITIAL CONDITIONS OF Y, U, R AND PEI    *    }

procedure initialcondition;
  var
    ini : integer;
    delta,ufi,ls,rs,dum,f : real;
  begin
    ufi := 2.11E-4;               { free stream velocity at initial point }
    delta := 0.065443;            { boundary layer thickness }
    pei := 5*rhoc*ufi*delta/8;    { total flow amout interested }

    y[1] := 0; y[2] := 0;         { initail y's }
    y[np2] := delta; y[np3] := delta;
    ls := 0;
    for ini := 3 to npl do
      begin
        rs := 0;
        dum := 0;
        repeat
          ls := ls+0.01;
          dum := ls;
          f := exp(4*ln(dum))-6*dum*dum+5*om[ini];
          until ( f < 0 );
          repeat
            dum := 0.5*(ls+rs);
            f := exp(4*ln(dum))-6*dum*dum+5*om[ini];
            if ( f < 0 ) then ls := dum
                         else rs := dum;
          until ( abs(f) < 1E-8 );
          y[ini] := dum*delta;
        end;
      y25 := 0.5*(y[2]+y[3]);

      for ini := 1 to np3 do                    { initial u's and r's }
        begin
          dum := y[ini]/delta;
          u[ini] := ufi*(3*dum-dum*dum*dum)/2;
          r[ini] := 1;
        end;

       for ini := 1 to np3 do
       rhou[ini] := rhoc*u[ini];
       rhou3 := rhou[3];
       rhoun1 := rhou[np1];
       for ini := 2 to npl do
       rhou[ini] := (rhou[ini]+rhou[ini+1])/2;

      if ( TEST <> 0 ) then
        begin
          writeln(' The initial conditions ');
          writeln('ini','         y       ','       u       ',
                  '       r       ','       rhou     ');
          for ini := 1 to np3 do
          writeln(ini:3,y[ini]:15:8,u[ini]:15:8,r[ini]:15:8,rhou[ini]:15:8);
          readln(SCR);
        end
                    else;
  end;

   {    *    *    *    WALL FUNCION FOR WALL BOUNDARY    *    *    *    }

procedure wf (var out1,out2,out3 : real );
  var
    nit : integer;
    kwall,ewall,hwall,ss,shalf,shalf1,uref,rhoref,rref,vref,yref,
    re,rruref,er : real;
  begin
     kwall := 0.435;
     ewall := 9.0;
     hwall := 0.9;
     shalf := 0.04;
     uref := (u[2]+u[3])/2;
     rhoref := 0.5*rho[1]+0.25*(rho[2]+rho[3]);
     rref := 0.5*(r[2]+r[3]);
     yref := y25;
     vref := mueff[1];
     re := uref*rhoref*yref/vref;
     rruref := rref*rhou[2];

     if ( re < 120 ) then
                     begin
                       ss := 1/(re+1E-30);
                       out1 := 0.5;
                       emu[2] := vref*rref/(abs(y[3]-y[2]));
                     end
                    else
```

```
                    begin
                      er := re*ewall;
                      nit := 0;
                      repeat
                        shalf1 := shalf;
                        shalf := kwall/(ln(er*shalf));
                        nit := nit+1;
                        until ( ( abs(shalf-shalf1) < 0.0001 ) or
                                ( nit > 11 ) );
                        ss := sqr(shalf);
                        out1 := kwall/(kwall+shalf);
                        emu[2] := 0.25*rhoref*rref*(abs(u[3]-u[2]))*
                                  (sqr(kwall/out1));
                    end;
    out2 := ss*rruref;
    out3 := out2*uref/r[1];
  end;

{    *    CAMPUTE THE VERTICAL DISTANCE FROM INNER BOUNDARY, Y AND R    *    }

procedure yandr (var y,r : subs1 );
  var
    iy : integer;
    inte : subs1;
    inte25,inten15 :real;
  begin
     for iy := 1 to np3 do
     rhou[iy] := rho[iy]*u[iy];
     rhou3 := rhou[3];
     rhoun1 := rhou[np1];
     for iy := 2 to np1 do
     rhou[iy] := (rhou[iy]+rhou[iy+1])/2;

     { Calculation of bpi at internal boundary }

     if ( KIN = 1 ) then wf(bpi,t1,taui)
                    else
                      begin
                        if ( KRAD = 0 ) then
        bpi := (1+(2*rhou[1]/rhou[2]))/3
                                       else
        begin
          bpi := (2*r[1]/(r[2]+r[3]))*((5*rhou[1]/rhou[2])+1);
          bpi := bpi+3*((rhou[1]/rhou[2])+1);
          bpi := bpi/(6*((2*r[1]/(r[2]+r[3]))+1));
        end;
                      end;

     { Calculation of bpe at external boundary }

     if ( KEX = 1 ) then wf(bpe,tnp3,taue)
                    else
                      begin
                        if ( KRAD = 0 ) then
        bpe := (1+(2*rhou[np3]/rhou[np1]))/3
                                       else
        begin
          bpe := (2*r[np3]/(r[np1]+r[np2]))*((5*rhou[np3]/rhou[np1])+1);
          bpe := bpe+3*((rhou[np3]/rhou[np1])+1);
          bpe := bpe/(6*((2*r[np3]/(r[np1]+r[np2]))+1));
        end;
                      end;

     { Calculation of the I-integral }

     inte[1] := 0;
     inte25 := (omi*pei)/(bpi*rhou[2]);
     inte[3] := inte25+(om[3]-omi)*pei/(rhou[2]+rhou3);
     inte[2] := 2*inte25-inte[3];
     for iy := 4 to np1 do
     inte[iy] := inte[iy-1]+(om[iy]-om[iy-1])*(pei/rhou[iy-1]);
     inten15 := inte[np1]+2*(ome-om[np1])*pei/(rhou[np1]+rhoun1);
     inte[np3] := inten15+(1-ome)*pei/(bpe*rhou[np1]);
     inte[np2] := 2*inten15-inte[np3];

     { Calculation of y's and r's }

     if ( KRAD = 0 ) then
       begin
          for iy := 1 to np3 do  { For plane, r doesn't appear in the }
          r[iy] := 1;            { governing equations.  We set r = 1 to }
                                 { simplify equations. }
          r25 := 1;
          rn15 := 1;
          for iy := 1 to np3 do
          y[iy] := inte[iy];
          y25 := inte25;
          yn15 := inten15;
       end
                  else
       begin
          for iy := 1 to np3 do
          r[iy] := ri[istep]+y[iy]*csalfa[istep];
          for iy := 1 to np3 do
          y[iy] := 2*inte[iy]/(ri[istep]+sqrt(sqr(ri[istep])+2*inte[iy]*
                   csalfa[istep]));
          y25 := 2*inte25/(ri[istep]+sqrt(sqr(ri[istep])+2*inte25*
                 csalfa[istep]));
          yn15 := 2*inten15/(ri[istep]+sqrt(sqr(ri[istep])+2*inten15*
                  csalfa[istep]));
       end;
     if ( TEST <> 0 ) then
        begin
          writeln(' iy',' rhou ',' y ',' r ');
          for iy := 1 to np3 do
           writeln(iy:3,rhou[iy]:15:8,y[iy]:15:8,r[iy]:15:8);
           readln(SCR);
         end
                  else;
  end;

  {    *    *    COMPUTE THE ENTRAINMENT RATES AT BOUNDARIES    *    *    }

procedure entr (var rmi,rme :subs2 );
  var
    ien : integer;
    ulim,rat : real;
  begin
     ulim := 0.01;
     for ien := 2 to np1 do
     emu[ien] := (0.5*(r[ien]+r[ien+1])*mueff[ien])/(y[ien+1]-y[ien]);
     emu[np2] := (0.5*(r[np3]+r[np1])*mueff[np3])/(y[np3]-y[np1]);
     if ( KIN = 2 ) then
                      begin
                        rat := abs((u[3]-u[1])/(u[np3]-u[1]+1.0E-30));
                        if ( rat < ulim ) then
                           rmi[istep] := 2*emu[2]*rat/ulim
                                      else
```

```
                    rmi[istep] := 2*emu[2];
                  end
                else rmi[istep] := 0;
    if ( KEX = 2 ) then
                  begin
                    rat := abs((u[npl]-u[np3])/(u[np3]-u[1]+1.0E-30));
                    if ( rat < ulim ) then
                       rme[istep] := 2*emu[np2]*rat/ulim
                                  else
                       rme[istep] := 2*emu[np2];
                  end
                else rme[istep] := 0;
    if ( TEST <> 0 ) then
                    begin
                      writeln('rmi(',istep:3,') = ',rmi[istep]);
                      writeln('rme(',istep:3,') = ',rme[istep]);
                      readln(SCR);
                    end
                  else;
  end;

  {    *    *    *    COMPUTE THE COEFFICIENTS FOR VELOCITY    *    *    *    }

procedure coeffu (var au,bu,cu : subs1 );
  var
    ic : integer;
    pgd4,gd8,hlp,ahlp,thlp,tp,ttp,
            hlm,ahlm,thlm,tm,ttm,
            ad,bd,cd,du            : real;
  begin
     if ( KIN = 1 ) then wf(bpi,tl,taui)
                    else
                      begin
                        tl := 0;
                        if (KRAD = 0 ) then
       bpi := (1+(2*rhou[1]/rhou[2]))/3
                                       else
       begin
         bpi := (2*r[1]/(r[2]+r[3]))*((5*rhou[1]/rhou[2])+1);
         bpi := bpi+3*((rhou[1]/rhou[2])+1);
         bpi := bpi/(6*((2*r[1]/(r[2]+r[3]))+1));
       end;
                      end;
     pgd4 := ((pei/dx)+(rmi[istep]+rme[istep]))/4;
     gd8 := (rmi[istep]+rme[istep])/8;
     hlp := rmi[istep]/2 - 2*gd8*(om[2]+om[3]);
     ahlp := abs(hlp);
     thlp := 2*hlp;
     tp := emu[2];
     ttp := tp+ahlp+abs(tp-ahlp);
     ad := ttp-thlp-tl-pgd4*(om[3]-om[2]);
     bd := 2*(rmi[istep]+tl);
     cd := (pei/dx/4)*(om[3]-om[2])*(3*u[2]+u[3])
           -dpdx[istep]*r[2]*(y[3]-y[1]);
     du := ad+bd+(pei/dx)*(om[3]-om[2]);
     au[2] := ad/du;
     bu[2] := bd/du;
     cu[2] := cd/du;
     if ( KEX = 1 ) then wf(bpe,tnp3,taue)
                    else
                      begin
                        tnp3 := 0;
                        if ( KRAD = 0 ) then
       bpe := (1+(2*rhou[np3]/rhou[npl]))/3
                                       else
       begin
         bpe := (2*r[np3]/(r[npl]+r[np2]))*((5*rhou[np3]/rhou[npl])+1);
         bpe := bpe+3*((rhou[np3]/rhou[npl])+1);
         bpe := bpe/(6*((2*r[np3]/(r[npl]+r[np2]))+1));
       end;
                      end;
     hlm := (rmi[istep]/2)-2*gd8*(om[npl]+om[np2]);
     ahlm := abs(hlm);
     thlm := 2*hlm;
     tm := emu[npl];
     ttm := tm+ahlm+abs(tm-ahlm);
     ad := 2*(tnp3+rme[istep]);
     bd := ttm+thlm-tnp3-pgd4*(om[np2]-om[npl]);
     cd := (pei/dx/4)*(om[np2]-om[npl])*(3*u[np2]+u[npl])
           -dpdx[istep]*r[np2]*(y[np3]-0.5*(y[npl]+y[np2]));
     du := ad+bd+(pei/dx)*(om[np2]-om[npl]);
     au[np2] := ad/du;
     bu[np2] := bd/du;
     cu[np2] := cd/du;

     for ic := 3 to npl do
     begin
       hlp := (rmi[istep]/2)-2*gd8*(om[ic+1]+om[ic]);
       hlm := (rmi[istep]/2)-2*gd8*(om[ic]+om[ic-1]);
       thlp := 2*hlp;
       thlm := 2*hlm;
       ahlp := abs(hlp);
       ahlm := abs(hlm);
       tp := emu[ic];
       tm := emu[ic-1];
       ttp := tp+ahlp+abs(tp-ahlp);
       ttm := tm+ahlm+abs(tm-ahlm);
       ad := ttp-thlp-pgd4*(om[ic+1]-om[ic]);
       bd := ttm+thlm-pgd4*(om[ic]-om[ic-1]);
       cd := (pei/dx/4)*(3*u[ic]*(om[ic+1]-om[ic-1])+
             u[ic+1]*(om[ic+1]-om[ic])+u[ic-1]*(om[ic]-om[ic-1]))
             -dpdx[istep]*r[ic]*(y[ic+1]-y[ic-1]);
       du := ad+bd+(pei/dx)*(om[ic+1]-om[ic-1]);
       au[ic] := ad/du;
       bu[ic] := bd/du;
       cu[ic] := cd/du;
     end;
     if ( TEST <> 0 ) then
                      begin
                        writeln(' ic',' au ',' bu ',
                                ' cu ');
                        for ic := 2 to np2 do
                        writeln(ic:3,au[ic]:15:8,bu[ic]:15:8,cu[ic]:15:8);
                        readln(SCR);
                      end
                    else;
  end;

  {    *    *    COMPUTE THE VELOCITY FROM FROM COEFFICIENTS    *    *    }

procedure profile (var u : subs1 );
  var
    ip,idash : integer;
    tem : real;
    as,bs,cs,f : subs1;
  begin
    for ip := 1 to np3 do
       begin
```

```
        as[ip] := au[ip];
        bs[ip] := bu[ip];
        cs[ip] := cu[ip];
        f[ip] := u[ip];
      end;

    bs[2] := bs[2]*f[1]+cs[2];
    for ip := 3 to np2 do
       begin
         tem := 1-bs[ip]*as[ip-1];
         as[ip] := as[ip]/tem;
         bs[ip] := (bs[ip]*bs[ip-1]+cs[ip])/tem;
       end;
    for idash := 2 to np2 do
       begin
         ip := n+4-idash;
         f[ip] := as[ip]*f[ip+1]+bs[ip];
         if ( f[ip] < 0 ) then f[ip] := (ip/(ip+1))*f[ip+1]
                          else;
       end;
    for ip := 1 to np3 do
       u[ip] := f[ip];

    if ( TEST <> 0 ) then
      begin
        writeln(' ip','       u       ');
        for ip := 1 to np3 do
        writeln(ip,u[ip]:15:8);
        readln(SCR);
      end
                    else;
  end;

{ ------------------------------------------------------------------------ }
  {     *     *     *     BEGINNING OF MAIN PROGRAM     *     *     *     }
{ ------------------------------------------------------------------------ }

 begin

  { Statement of the Properties of Problem }
    LORT := 0;          { Laminar flow }
    COMP := 0;          { Incompressible fluid }
    KRAD := 0;          { Flat surface }
    KIN := 1;           { Internal boundary - wall surface }
    KEX := 2;           { External boundary - free stream }

  { Statement of the Properties of Fluid at Referent State }
    rhoc := 0.0011769;                          { unit : g/cm3 }
    mu := 0.00018464;                           { unit : g/s cm }
    infvel := 100;                              { unit : cm/sec }

  { Statement of the Control Index }
    TEST := 0;
    DATAS := 1;

    if ( DATAS = 1 ) then
      begin
        rewrite(outfile1,'blwsp1t.dat');
        rewrite(outfile2,'blwspt1t.dat');
        writeln(outfile1,'      x     ',',     y     ',',       u       ');
        writeln(outfile2,'       xd   ',',           y   ');
      end
                    else;
    n := 20;

    xu := 0.0001;
    xd := 0.0001;

    readdata;

    blc;

    omega (om);

    initialcondition;

    pressgrad (dpdx);

    for istep := 1 to 140 do
      begin

        density (rho);

        efftr (mueff);

        entr (rmi,rme);

        dx := xb[istep]-xb[istep-1];
        xd := xb[istep];

        pei := pei+rme[istep]*dx;

        u[np3] := 0.99*uf[istep];

        coeffu (au,bu,cu);

        profile (u);

        yandr (y,r);

        if ( DATAS = 1 ) then                    { PRINT RESULTS TO FILES }
          begin
            writeln(outfile1,xd:12:8);
            for  ind := 1 to np3 do
            writeln(outfile1,y[ind]:24:8,u[ind]:15:8);
            writeln(outfile2,xd:12:8,y[ind]:15:4);
          end
                        else;

        xu := xd;
      end;

end.
```